HUMAN BOCAVIRUS 1 GENOME ORGANIZATION AND REPLICATION MECHANISM

By

Weiran Shen

Submitted to the graduate degree program in Microbiology, Molecular Genetics and Immunology and the Graduate Faculty of the University of Kansas in partial fulfillment of the requirements for the degree of Doctor of Philosophy.

Dissertation Committee:

_____

Chairperson: Jianming Qiu, Ph.D.

_____

Edward Stephens, Ph.D.

_____

Hao Zhu, Ph.D.

_____

Joe Lutkenhaus, Ph.D.

_____

Severin Gudima, Ph.D.

_____

Thomas Yankee, Ph.D.

Date Defended: August 17th, 2016

The Dissertation Committee for Weiran Shen

certifies that this is the approved version of the following dissertation:

HUMAN BOCAVIRUS 1 GENOME ORGANIZATION AND REPLICATION MECHANISM

_____

Chairperson: Jianming Qiu

Date approved: August 17th, 2016

Abstract

Human bocavirus is a human pathogen that was identified in 2005. For the past decade, most of the studies about this virus were focused on clinical detection and its association-with diseases, while very little was known about the molecular virology.

The studies presented in this thesis are composed of three parts: 1) Identification of novel HBoV1 proteins by transfection of an HBoV1 infectious clone or during HBoV1 infection; 2) exploring the interactions between the viral genome and proteins to uncover the details underlying HBoV DNA replication; and 3) providing evidence of HBoV1 hairpin independent DNA replication.

In the first study, we identified three new non-structural proteins of human bocavirus 1 during infection of polarized human airway epithelium. Of the three newly identified proteins, we proved that one non-structural protein is critical for virus replication in the polarized human bronchial airway epithelium. The creation of a non-replicating infectious HBoV1 mutant may have particular utility in vaccine development for this virus.

In the second study, we identified both cis- and trans-acting proteins that are required for HBoV1 DNA replication at the right-end hairpin in HEK293 cells. We also localized the minimal replication origin to a 46-nt sequence in the right-end hairpin, which contains both NS1 nicking and binding sites. The identification of these essential elements of HBoV1 DNA replication acting both in cis and trans provides opportunities for developing antiviral strategies targeting HBoV1 DNA replication, and to design next generation recombinant HBoV1 vectors, a promising tool for gene therapy of lung diseases.

In the third study, we provided evidence that HBoV1 could replicate independent of hairpin sequence, which is quite different from other parvoviruses. Although the mechanisms are not fully understood, this study opened new directions for future studies of parvoviruses.

Acknowledgements

First of all, I would like to take this opportunity to thank my mentor, Dr. Jianming Qiu, for his guidance and support of my research in the past years. After struggling to conduct research while completing my master's degree, he taught me the skills necessary to become an excellent scientist. I received systematic training spanning how to do basic, simple technical skills all the way to developing and concluding a projects. His hard-working attitude, guidance, and patience always motivated me to go deeper into the field of parvoviruses. His gracious help was not only limited to scientific research but also extended to generous support in the difficulties of life, providing encouragement and lighting my passion. His profound knowledge, sharp mind, and sensitivity to scientific significance enriched my growth and honed my critical thinking. With his training, I am ready and excited for my future scientific endeavors.

I appreciate the help of all the colleagues that worked together with me. I would like to thank Fang Cheng, Peng Xu, Saieed Safder Fnu, Dr. Wei Zou, Dr. Xuefeng Deng and Dr. Zekun Wang in our lab. Fang taught me important technical details and the basic principles of performing experiments. Peng gladly provided helps whenever he could. Xuefeng, Wei, and Zekun were experts in helping with my bench work, and discussions with Safder helped generate good ideas. We were always a friendly group and helped each other to improve, to explore, and to enjoy our time in lab.

I am grateful to Dr. Edward Stephens, Dr. Hao Zhu, Dr. Joe Lutkenhaus, Dr. Severin Gudima, Dr. Thomas Yankee, and Dr. Wen-xing Ding. Your supervision of my research broadened my thinking and motivated me to become a better researcher. Your high scientific standards encouraged me to further challenge myself. I am also thankful to the department teachers and office staff. I appreciate the help of Miranda Machacek for the thesis proofreading.

Last but not least, I want to thank my parents and my wife Jizi Kuang. Your love makes me able to overcome any difficulties, to face up any challenges, and to find a way to my best future.

Table of Contents

Acceptance page ..... **ii**

Abstract ..... **iii**

Acknowledgements ..... **iv**

Table of Contents ..... **v**

Chapter I: Introduction 1

Chapter II: Identification and Functional Analysis of Novel Non-structural Proteins of Human Bocavirus 1

Abstract 20

Introduction 20

Materials and Methods 22

Results 27

Discussion 55

Chapter III: Analysis of the Cis and Trans Requirements for DNA Replication at the Right End Hairpin of the Human Bocavirus 1 Genome

Abstract 62

Introduction 62

Materials and Methods 65

Results 71

Discussion 101

Chapter IV: Hairpin-independent HBoV1 DNA replication

Abstract 108

Introduction 108

Materials and Methods 109

Results 111

Discussion 122

Chapter V: Conclusions 123

References 125

Chapter 1

Introduction

After the isolation of bovine parvovirus (BPV) in 1961, only canine minute virus (or minute virus of canines, MVC) was classified in the genus *Bocavirus* of the *Parvoviridae* family, until the discovery of human bocavirus 1 (HBoV1) in 2005 (1,3,28). Since then, more viruses were isolated and classified in the genus *Bocavirus*, including porcine bocavirus, gorilla bocavirus, feline bocavirus and sea lion bocavirus (18,77,86,91). In 2014, the International Committee on Taxonomy of Viruses (ICTV) reclassified the *Parvoviridae* family (28). All bocaviruses are now in the genus *Bocaparvovirus*.

Parvovirus is a non-enveloped icosahedral virus with linear single-stranded DNA (ssDNA) genome in a size range of ~4.7-5.7 kilobases (kb) (28). There are two subfamilies in the *Parvoviridae* family, which are *Parvovirinae* and *Densovirinae*. The former subfamily of viruses infect vertebrates, while the latter infect invertebrates. Eight genera are included within the *Parvovirinae* subfamily in the most updated classification, including *Amdoparvovirus, Aveparvovirus, Bocaparvovirus, Copiparvovirus, Dependoparvovirus*, *Erythroparvovirus*, *Protoparvovirus* and *tetraparvovirus* (28). Adeno-associated virus (AAV) in the genus *Dependoparvovirus*, parvovirus B19 in the genus *Erythroparvovirus,* and minute virus of mice (MVM) in the genus *Protoparvovirus* have been well studied. Both termini of their genomes contain partial double-stranded hairpin structures with mismatched nucleotides.

The terminal hairpin structures are critical to parvovirus replication. Parvoviruses that have unique terminal hairpin sequence are called heterotelomeric parvoviruses, while parvoviruses that have identical hairpin terminal sequence are called homotelomeric parvoviruses. The two terminal repeats of heterotelmoeric parvoviruses, e.g., MVM and MVC, are named the left-end hairpin (LEH) and the right-end hairpin (REH), which correspond to the 3’ end and 5’ end of the negative sense ssDNA viral genome, respectively. For homotelomeric

parvoviruses, e.g., AAV and B19, the terminal hairpins are called inverted terminal repeats (ITRs). Based on whether parvovirus replication relies on another helper virus, e,g., adenovirus, parvoviruses are referred as dependoparvovirus (AAV) or autonomous parvovirus (e.g., B19, MVM, and MVC).

This introduction summarizes the epidemiology, genome organization, transcription profile, functions of viral proteins, and infection life cycle of HBoV1 with discussions of other bocaparvoviruses. Additionally, the general models and mechanisms of parvovirus DNA replication are discussed.

Epidemiology of HBoV1

To date, four species of human bocaparvoviruses have been isolated. They are HBoV1, HBoV2, HBoV3, and HBoV4 in the order of their discovery. HBoV1 was first identified from nasopharyngeal aspirates of young children who had lower respiratory tract infections (3). It was also detected in blood and stool samples (154), whereas HBoV2, HBoV3 and HBoV4 were mainly found in stool samples (5,78,79). HBoV1 is found globally and associated with acute respiratory infections, such as acute wheezing, pneumonia, asthma, or bronchiolitis, especially, in infants under two years old (2,13,23,50,59,61,73,74,104,105,111,132). Death resulting from pure HBoV1 infection has been reported due to high tilters of HBoV1 (23,85,158). In most cases, HBoV1 was detected together with other respiratory pathogens, so the etiological role of HBoV1 in respiratory diseases is difficult to confirm. However, careful clinical studies applying more accurate markers (quantitative PCR, viral mRNA and antigen detection, and antiviral antibody detection), in addition to mere HBoV1 DNA detection by PCR have been done, providing accumulating evidence that HBoV1 is an important respiratory pathogen in children (2,12,21-23,43,50,52,58,76,80,85,98,103,107,108,111,132,139,158,160,162). Pneumonia, bronchiolitis, acute otitis media, common cold, and exacerbation of asthma are the most common clinical manifestations of HBoV1 respiratory tract infections, with symptoms of cough, fever, rhinitis, wheezing, and diarrhea (2,4,11,14,20,39,48-

50,58,82,96,98,102,109,111,114,117,124,127,131,132,149,157,158,162). Currently, there are no animal models available for HBoV1 in vivo infection. Nevertheless, in in vitro tissue culture, HBoV1 infection has been directly demonstrated to cause injuries to cultured human airway epithelia, including tight junction disruption, decreased cilia and cellular hypertrophy (42,45,69).

Genome organization of Bocaparvoviruses

Within the genus *Bocaparvovirus*, the full-length genomes of HBoV1, BPV and MVC have been sequenced, including both terminal hairpins (16,119,145). The genome of HBoV1 is 5,543 nucleotides in length with distinct hairpin sequences and structures at both ends (**Fig. 1**). HBoV1 LEH is 140-nt in length and is predicted to be 'Y' shaped with short axial ears, mismatches and unpaired bubbles (69). There are no detailed studies on the function of bocavirus LEH. In MVM, it has been shown that the MVM LEH is important for transcription initiation with the help of non-structural protein 1 (NS1) and plays a critical role in genome packaging (89). The bocaparvovirus REH of MVC and BPV, but not HBoV1, harbor sequences which have the potential to be folded into cruciform structure near the end tip, although it is less favorable thermodynamically for BPV (145). This cruciform structure also appears in MVM, and was proved to be required for MVM DNA replication (7,34,36). Bocaparvovirus REH is a perfect duplex structure without any mismatch. Notably, MVC LEH and HBoV1, BPV REH were isolated both in flip and flop forms, while the other termini of these three viruses were only found in one form (69,145).

The HBoV1 genome encodes two groups of genes encoding non-structural (NS) proteins and viral structural (capsid) proteins (VP). NS proteins function in virus replication and VP proteins function in packaging of the viral genome.

Figure 1-1. The model of negative sensed HBoV1 genome structure.

The structure of HBoV1 LEH and REH are modeled with 5’ end and 3’ end sequences being labeled. Dotted regions stand for the single stranded DNA region that encodes non-structural and structural proteins.

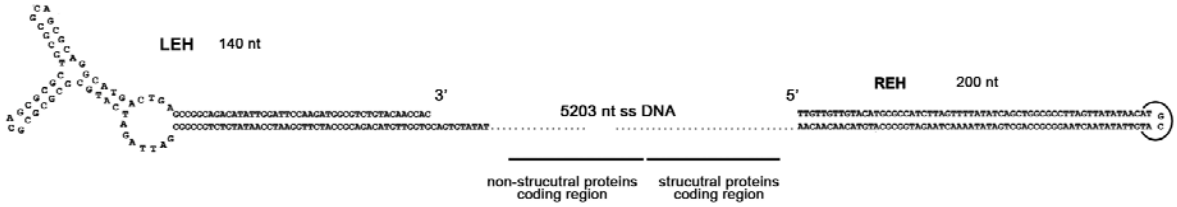
LEH
140 nt
3'
5203 nt ss DNA
5'
REH
200 nt
non-strucutral proteins coding region
strucutral proteins coding region

HBoV1 life cycle

After the construction of an HBoV1 infectious clone (pIHBoV1), more than 12 different cell lines were transfected by pIHBoV1, including HeLa, human embryonic kidney 293 (HEK293), A549, BEAS-2B cells. Only HEK293 cells were demonstrated to support an efficient DNA replication of HBoV1 (69). HEK293 cells were not infected by the virus, suggesting that HEK293 cells lack the virus receptor or are inefficient in the intracellular tracking of the virus. Notably, a high titer of HBoV1 virions is produced from HEK293 cells transfected with pIHBoV1 (~5,000 genome copies/cell) (69). The purified virions are infectious to differentiated human airway epithelial cells (HAE) cultured on an air-liquid interface (ALI) (45,69), which mimics virus infection of the natural host, the human airway epithelia.

HBoV1 directly infects primary HAE-ALI cultures through either the apical or the basolateral surface, suggesting that the virus receptor is expressed on both polarities of the airway epithelia (**Fig. 1-2**, steps 1-2). In general, parvoviruses are believed to enter the cells through receptor-mediated endocytosis, as blocking endosome acidification disrupts AAV2 and MVM infection (step 3) (8,47,125). Virions traffic to the cytoplasm along microtubules and are released from the endosome by an unknown mechanism (130,159). Accumulation of AAV2 virions were observed in a perinuclear localization, suggesting that nuclear translocation is a limiting step (8,165). Virions may also directly disrupt the nuclear envelop to translocate into the nucleus (step 4) (27,167). Within the nucleus, the viral genome is released and recognized by the cellular replication and repair machinery (step 5, 6). Then, the complementary strand of the viral ssDNA genome is synthesized before transcription (step 7), followed by expression of viral NS proteins. NS proteins are associated with the viral genome and are required for genome packaging (steps 16-18) (15,51,140). However, NS proteins are not packaged into the mature virions. The viral DNA replication process likely involves complex hairpin structure changes and protein-genome interactions, which produces viral DNA intermediates in different sizes and structures. HBoV1 transcription, protein expression and

Figure 1-2. The infection life cycle of HBoV1.

HBoV1 infection of HAE-ALI is illustrated based on studies of HBoV1 and speculation from other parvoviruses, which are explained in the text.

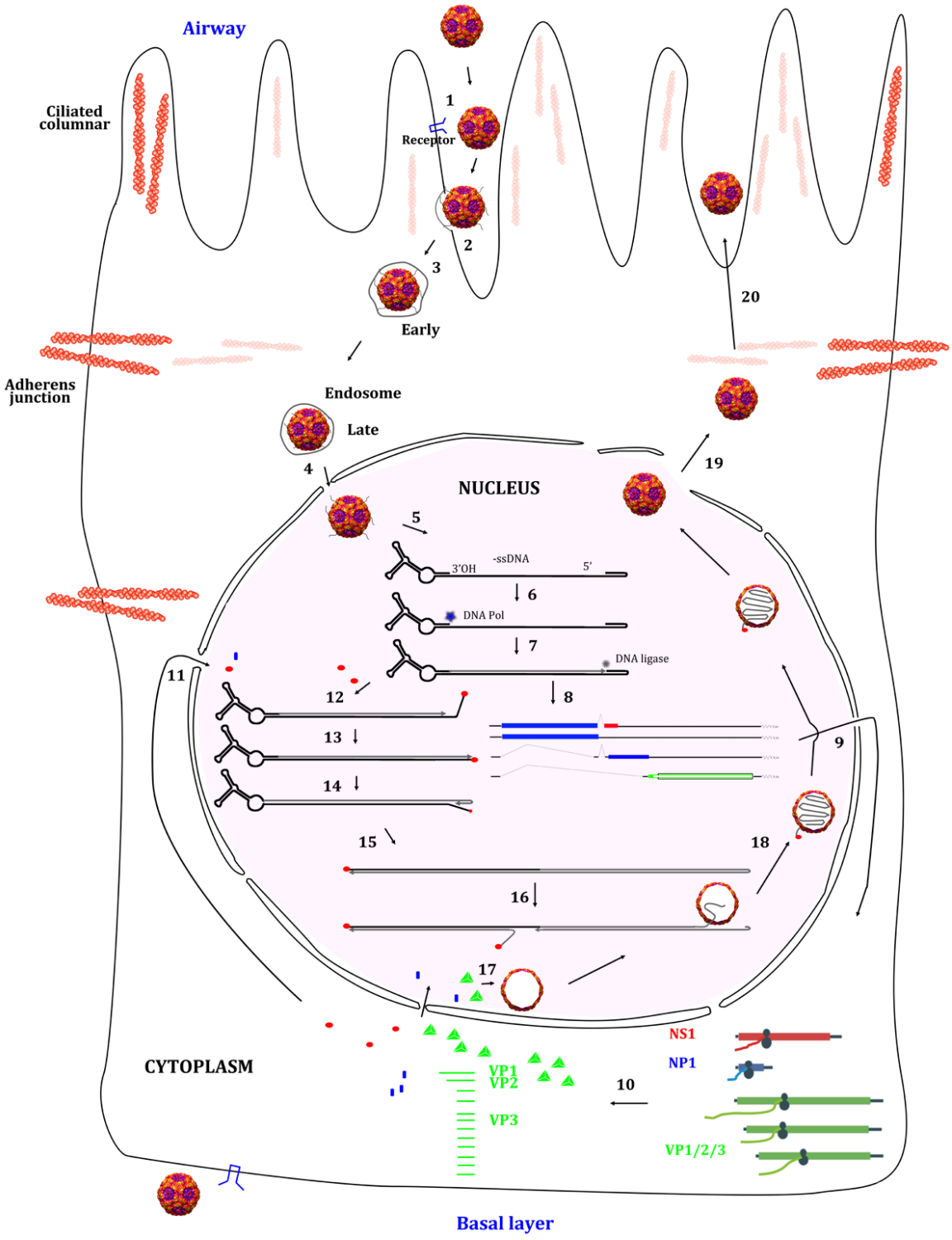
Airway
Ciliated columnar
Receptor
1
2
3
Early
20
Adherens junction
Endosome
Late
4
19
NUCLEUS
5
3'OH
-ssDNA
5'
6
DNA Pol
7
DNA ligase
8
9
11
12
13
14
15
16
17
18
CYTOPLASM
VP1
VP2
VP3
10
NS1
NP1
VP1/2/3
Basal layer

DNA replication (steps 8-10, 12-16) are further discussed below. Capsid proteins produced in the cytoplasm are assembled into oligomers before translocating into the nucleus (step 11) (95), Capsid is assembled in the nucleus, which captures viral ssDNA that is generated in a mechanism that is still not clear (steps 17-18) (68,167). Finally, the mature virions are released from the nucleus into the cytoplasm and then outside of the infected cells (steps 19-20).

Transcriptional expression profiles of bocaparvoviruses

The transcription profiles of BPV, MVC, and HBoV1 were studied during virus infection (**Fig. 1-3**) (17,45,133). The HBoV1 transcription profile was studied in detail by transfection of a non-replicated HBoV1 clone, in which both termini were not included (16). All three bocaparvoviruses shared similarities in their transcriptional expression profiles but with features different from other parvoviruses. Bocaparvoviruses have only one promoter and two polyadenylation sites, proximal and distal polyadenylation site [(pA)p and (pA)d] respectively. Therefore, bocaparvovirus transcribes one single pre-mRNA from its promoter. This pre-mRNA undergoes alternative splicing and alternative polyadenylation. The left half of the viral genome encodes NS proteins, and the right half encodes structural proteins (16,119,143,145). One unique feature of bocaparvovirus is the expression of NP1 protein, whose ORF is located in the middle of the genome (69,119,145). Due to the small genome capacity, NP1 ORF largely overlaps with the NS1 ORF at the 3' end.

At least 7 mRNA transcripts of HBoV1 were identified, and the splicing of HBoV1 precursor mRNA (pre-mRNA) appears more complex than those of MVC and BPV (**Fig. 1-3**). Similar to MVC and BPV, HBoV1 utilizes one promoter and two polyadenylation sites located in the middle and right end of the genome, respectively. NS1-encoded mRNA is spliced at D2-A2 sites (intron 2), which results in a shift of the NS1 ORF at the C-terminus. Without splicing of intron 2, the unspliced N1-encoding mRNA expresses NS1-70 protein which is terminated early

Figure 1-3. Transcription maps of HBoV1, BPV and MVC.

The approximately 5.6 kb genomes of the three bocaparvoviruses shown is based on previous publications (16,119,145). The major transcription landmarks include the terminal repeats (LEH and REH), promoter (P), splice donors (D) and acceptors (A), and (pA)p and (pA)d sites. All identified mRNA transcripts are listed below the map (designated R1 to R6), with their respective sizes shown on the left and the expected MW of the expressed proteins or detected proteins sizes shown to the right. Different ORFs are illustrated in blue, red or green colors.

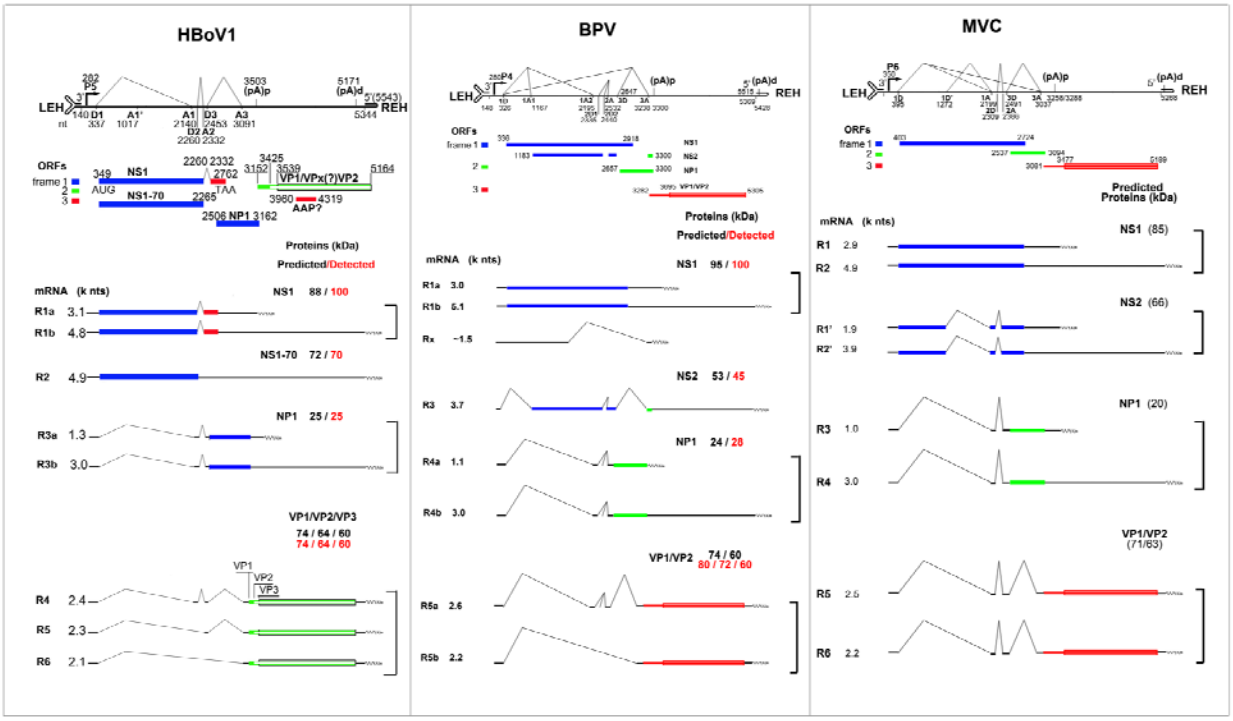
HBoV1
LEH
REH
ORFs
frame 1
2
3
NS1
NS1-70
NP1
VP1/VPx(?)VP2
AUG
AAP?
Proteins (kDa)
Predicted/Detected
mRNA (k nts)
R1a 3.1
R1b 4.8
R2 4.9
R3a 1.3
R3b 3.0
R4 2.4
R5 2.3
R6 2.1
NS1 88 / 100
NS1-70 72 / 70
NP1 25 / 25
VP1/VP2/VP3
74 / 64 / 60
74 / 64 / 60
VP1
VP2
VP3
BPV
LEH
REH
(pA)p
5' (pA)d
ORFs
frame 1
2'
3'
NS1
NS2
NP1
VP1/VP2
Proteins (kDa)
Predicted/Detected
mRNA (k nts)
R1a 3.0
R1b 5.1
Rx ~1.5
R3 3.7
R4a 1.1
R4b 3.0
R5a 2.6
R5b 2.2
NS1 95 / 100
NS2 53 / 45
NP1 24 / 28
VP1/VP2 74 / 60
80 / 72 / 60
MVC
LEH
REH
(pA)p
5' (pA)d
ORFs
frame 1
2
3
Predicted
Proteins (kDa)
mRNA (k nts)
R1 2.9
R2 4.9
R1' 1.9
R2' 3.9
R3 1.0
R4 3.0
R5 2.5
R6 2.2
NS1 (85)
NS2 (66)
NP1 (20)
VP1/VP2
(71/63)

at the NS1 ORF. An additional A1-1 splice site was identified, but its implications for viral NS protein expression was unknown (16). Intriguingly, three major NS proteins were detected by using an anti-NS1 C-terminus antibody in either HBoV1 DNA-transfected or HBoV1 infected cells (31). The largest NS protein was believed to be the full-length NS1 at a MW of ~100 kDa, however, the nature of the other two small NS bands is unknown (16). R3 and R4 mRNAs that are spliced at both D1-A1 and D2-A2 introns, are responsible for NP1 expression.

R5, R6 and R7 mRNAs are proposed to encode HBoV1 VP proteins, all of which are spliced at the D1 donor site and the A1, A2, and A3 acceptors, respectively (**Fig. 1-3**). Northern blot analysis of the RNA isolated from infectious clone-transfected cells showed that the R5 mRNA was the most abundantly expressed VP-encoding mRNA. However, there is a translation initiation codon downstream of the A1 site and upstream of VP-encoding region, which does not seem to be used during VP translation. This leaking mechanism is commonly used in members of the *Densovirinae* subfamily but is unusual for vertebrate parvoviruses (55,93,153). Moreover, the VP2 protein is translated from a non-canonical start codon (GUG) located between VP1 and VP3 (173). The (pA)d signal localizes immediately upstream of VP stop codon. There is a large genome sequence between the VP-encoding region and the REH with an unknown function.

Functions of the NS proteins of bocaparvovirus

The amino acid conservation between BPV and MVC NS1 protein versus HBoV1 NS1 is 31% and 39%, respectively. NS1 is the key protein for parvovirus DNA replication (29,32). In bocaparvovirus, NP1 is also indispensable for viral DNA replication. Interestingly, BPV and MVC NP1 are exchangeable with each other, and HBoV1 NP1 could also supplement the function of MVC NP1 (145). Though there is a relatively low similarity among the NP1 of different bocaparvoviruses in amino acid sequence, NP1 seems functionally conserved.

Parvovirus NS1, also named replication protein 78/68 (Rep78/68) for AAVs, could be functionally divided into three domains. The N-terminal domain binds the replication origin (Ori)

of viral RF DNA, referred to as the origin-binding domain (OBD), which has both sequence and strand specific endonuclease activity (152). The OBD structures of AAV5 Rep68, MVM NS1 and HBoV1 NS1 have been resolved (54,150,152). Superimposition of the OBDs of these three proteins displayed a conserved beta-sheet core, flanked by several alpha helices on both the left and right sides (152). They share similarities with and belong to the HUH-nuclease superfamily. One loop and an alpha helix protrusion are sequence specific and specifically bind to Ori DNA major and minor grooves. For AAVs, the interaction between Rep78/68 OBD and the Ori has been studied in detail by analyzing the structure of the Rep78/68 and Ori complex (72). Rep78/68 oligomerizes and binds to sequence specific tetra-nucleotides repeats (67,72). In HBoV1, the two DNA binding regions of the HBoV1 OBD are highly positively charged, but their specific interactions with DNA have not been confirmed.

The middle domain of Rep78/68 and NS1 protein contains four conserved walkers motif (boxes A, B, B' and C), which belong to the SF3 helicase family and perform 3'-5' helicase function (35,62,72). The C-terminal domain of bocaparvoviruses are longer than other parvoviruses, and the HBoV1 C-terminal domain is one of the longest. It is predicted to have transactivation capability but its function is largely unknown (88,137). The molecular weight for BPV and MVC NS1 are 95 kDa and 80 kDa, respectively. The C-terminal domains of the three bocaparvoviruses share two conserved domains, of which the function is unknown (16). Intriguingly, HBoV1 NS1 appeared to have an increase of ~12 kDa in size on SDS-PAGE gel. There is evidence to support that this size increase is due to the C-terminal domain (134). We wonder whether this size increase could be a covalently linked post-translational modification at the C-terminus domain.

The function of bocaparvovirus NS2 has not been studied. However, its coding sequence largely overlaps with NS1, and thus they possibly share similar functions as the Rep 78 vs Rep 52 of AAVs. Rep52 shares the helicase domain, and C-terminal domain with Rep78. Rep52 plays an important role in viral genome packaging (83,136).

Conserved among all bocaparvoviruses, NP1 has ~200 aa and is expressed from an ORF that overlaps with the C-terminus of the NS1. NP1 plays a significant role in viral DNA replication. It has a non-canonical nuclear localization signal located at 7-50 aa (92). Transfection with a NP1-knockout mutant of either HBoV1 or MVC barely produced monomeric and dimeric RF DNA of viral replication intermediates (69,143). The function of the three NP1 proteins in viral DNA replication is conserved since they are exchangeable for MVC DNA replication (145). Notably, NP1 could also overcome the deficiency of NS2 of MVM at the early replication stage by localizing at the viral DNA replication centers, but could not compensate for the late steps of MVM infection after virions are produced (106). Moreover, NP1 plays multiple roles during processing viral pre-mRNA (53,143,173). Both MVC and HBoV1 NP1 help transcription read through the (pA)p site to generate full-length VP-encoding transcripts. Moreover, HBoV1 NP1 facilitates viral mRNA splicing at the D3-A3 sites, which helps VP mRNA production and protein expression (173).

Structural proteins of bocaparvoviruses

Bocavirus VP proteins are structural proteins for capsid assembly. Different from BPV and MVC, HBoV1 expresses three VP proteins, and the VP2 uses a non-canonical start codon (173). More interestingly, construction of VP1 cDNA under human cytomegalovirus (CMV) immediate early gene promoter could not initiate VP1 translation. The capsid proteins are expressed in a ratio ~1:1:10 during infection, which is similar to that of AAVs. VP3, the main structure protein, can form virus like particles (VLPs), which contain putative neutralization and receptor binding sites (64). A monoclonal antibody 15C6 has been developed that reacts with all the VLPs formed by HBoV1, 2 or HBoV3 (64). In addition, most *Parvovirinae* members, except Aleutian mink disease virus (AMDV), contain a phospholipase A2 (PLA2) domain within the VP1 unique region (VP1u). Because of the newly identified VP2, HBoV1 has a short VP1u of 90 aa. Conserved with other parvoviruses, the VP1u region exhibits a PLA2 activity within the domain 11-66 aa (78,171). The PLA2 domain and function of the VP1u was also confirmed in MVC

(145). This activity is proposed to be important for sequential structural changes from receptor mediated endocytosis to endosome escape.

In the absence of VP1 (and VP2 for HBoV1), VLPs can be formed by expression of only VP2 (VP3 for HBoV1) from insect cells infected with VP2-expressed baculovirus. VLP structures of parvoviruses have been resolved by cryo-electrophoresis microscopy, 3-D reconstruction and X-ray crystallization (38,60,64,75,81,161). Conserved with other parvovirus structures, HBoV1 shares the icosahedral 5-fold axis tunnel, 3-fold axis trimeric protrusions and a 2-fold axis depression. BPV is different in a raised surface loop at the two-fold axis. Both of them have a conserved core with one alpha-helix linked with 8 beta sheet structure but different in emanating loop(s) radially under the 5-fold axis tunnel (64,75). These differences produce new surface structures for both viruses and may be important for vaccine development.

DNA replication of autonomous parvovirus

The proposed model of parvovirus DNA replication is different between dependoparvovirus and autonomous parvoviruses (6,7,10,30,35,128,164). Autonomous parvovirus DNA replication could be summarized as a hairpin transfer model (**Figure 1-4),** which is derived from MVM studies (35,116,146,147). MVM has a 'Y' shaped LEH with two mismatches within the stem sequence (**Figure 1-4**). The REH is linear in structure, with one mismatch in the stem and another mismatch at the tip. Upon entering the nucleus, the viral genome is recognized by cellular DNA replication polymerase that synthesizes the complementary strand, primed by the 3'-OH at the LEH (**Figure 1-4**, Step 1). Upon reaching the 5' end of the genome, the DNA polymerase is stopped by the duplex structure, and a "nick" is left in the genome. After the ligation of the "gap" by a cellular DNA ligase, a covalently closed double-stranded DNA (cc RF DNA) with mismatches on both ends is formed. Acting as a transcription template, this molecule produces viral NS proteins, which are translocated into the

Figure 1-4. The replication model of MVM.

A negative sense MVM genome is diagrammed with the ‘Y’ shaped LEH and “U” shaped REH at the ends. The complementary strand of the viral ssDNA is synthesized by cellular DNA polymerase through priming of the 3’-OH at LEH (Step 1). The newly synthesized strand is ligated with the 5’ end of the REH, followed with specific nicking performed with NS1 (Step 2). NS1 is then covalently linked at the newly nicked 5’ end (Step 3). Oligomerized NS1 and the cellular replication machinery open and copy the REH (Steps 3-4). The 3’ REH is refolded into a hairpin structure and uses itself as a template to replace the lower strand DNA (Steps 5-6). Further extension of 3’ end leads to the formation of dRF DNA (Step 7). The extended 3’ REH refolds again and progresses further for DNA synthesis, resulting in tetrameric RF DNA (Steps 8-9). The tetrameric RF DNA is resolved into ssDNA genomes, which are packaged into empty virions.

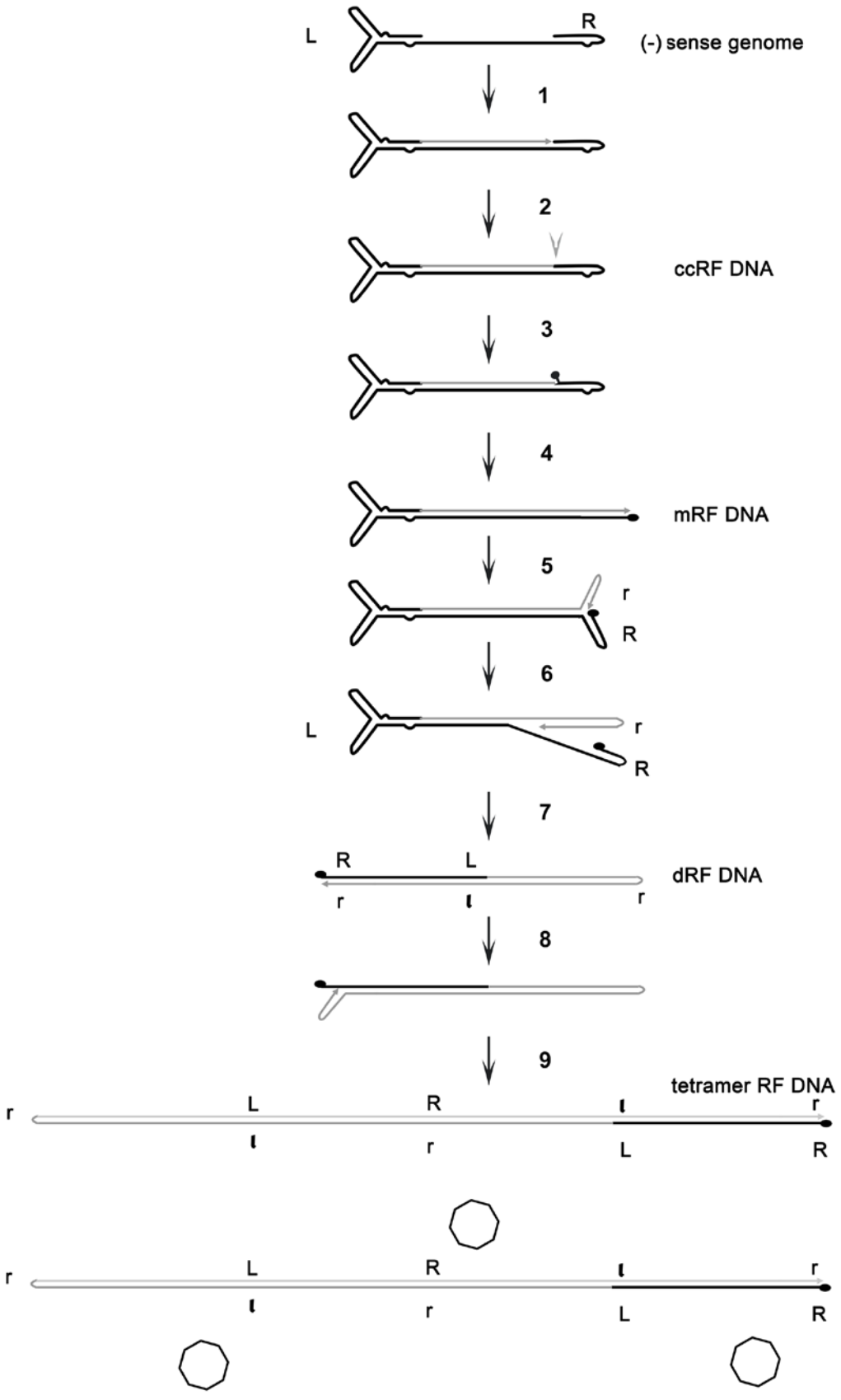
L
R
(-) sense genome
1
2
ccRF DNA
3
4
mRF DNA
5
r
R
6
L
r
R
7
R
L
dRF DNA
r
r
8
9
tetramer RF DNA
r
L
R
r
L
R
r
L
R
r
L
R

nucleus and specifically recognizes the NS1-binding site on the REH. NS1 has endonuclease activity, and nicks the REH at a NS1-specific nicking site upstream of the NS1-binidng site. Meanwhile, the helicase activity of NS1 facilitates unfolding (extending) the REH. Then, cellular DNA polymerase copies the extended REH into the upper strand (primed by the 3'-OH released from the NS1 specific nicking). This step is called hairpin transfer (**Figure 1-4**, Steps 3-4). This intermediate is named monomer replication form (mRF) DNA. Interestingly, NS1 protein covalently links to the 5' end of the replication intermediate. With the help of NS1, both strands of the extended REH are refolded into hairpin structures, while the one with 3'─OH is further synthesized by using itself as a template (**Figure 1-4**, steps 5-6). The lower strand is thus replaced by the newly synthesized DNA. This step is called strand-displacement.

The product of the strand-displacement is dimeric RF DNA intermediate (dRF) (**Figure 1-4**, Step 7). As the tetrameric size of RF DNA was frequently detected during MVM DNA replication (on Southern blotting of 2-dimentional gel to resolve DNA structures) (155), it is believed that the dRF DNA goes through the hairpin refolding and strand-displacement steps again (**Figure 1-4**, steps 8-9). The tetrameric RF DNA is resolved on both the LEH and the REH, which produces ssDNA genomes that are packaged by empty virions.

For HBoV1 replication, NS1 and NP1 are both required. They localize within the nucleus but their interaction has not been examined (16). During MVM replication, it has been reported that cellular factors binds LEH or REH. These DNA binding sites have been shown to be necessary for the MVM DNA replication (25,26,34). For the HBoV1 replication of HBoV, such cellular factors have not been identified yet.

In members of the *Parvovirinae* subfamily, the NS1/Rep78/68 binding sequences harbor tetra-nucleotides repeats (29,97,142,151,166). MVM has cognate or degenerated NS1 binding sites throughout its genome (24). However, Densoviruses *Galleria mellonella densovirus* (GmDNV) and *Junonia coenia densovirus* (JcDNV) contain an NS1 binding site of trimer

nucleotides repeated four times (46,153). The binding and nicking properties of bocaparvovirus NS1 with their respective genomes have not yet been explored.

It is well acknowledged that the full-length hairpin sequences of parvoviruses are required for their replication in the so called rolling hairpin DNA replication model as described above. However, B19 could replicate with truncated termini, which could not form hairpin structures (63). This phenomenon is repeated during HBoV1 DNA replication in the HBoV1-transfected HEK293 cell system (16). The mechanism underlying hairpin structure-independent parvovirus DNA replication warrants further investigation.

Chapter II:
Identification and Functional Analysis of Novel Non-structural Proteins of Human Bocavirus 1

Abstract

Human bocavirus 1 (HBoV1) is a single-stranded DNA parvovirus that causes lower respiratory tract infections in young children worldwide. In this study, we identified novel splice acceptor and donor sites, namely A1' and D1', in the large non-structural protein (NS1)-encoding region of the HBoV1 precursor mRNA. The novel small NS proteins (NS2, NS3, and NS4) were confirmed to be expressed following transfection of an HBoV1 infectious proviral plasmid and viral infection of polarized human airway epithelium cultured at an air-liquid interface (HAE-ALI). We constructed mutant pIHBoV1 infectious plasmids which harbor silent mutations smA1' and smD1' at the A1' and D1' splice sites, respectively. The mutant infectious plasmids maintained production of HBoV1 progeny virions at a level less than five times lower than that of the wild-type plasmid. Importantly, the smA1' mutant virus that does not express NS3 and NS4 replicated in HAE-ALI as effectively as the wild-type virus, however, the smD1' mutant virus that does not express NS2 and NS4 underwent an abortive infection in HAE-ALI. Thus, our study identified three novel NS proteins, NS2, NS3, and NS4, and suggests an important function of the NS2 in HBoV1 replication in HAE-ALI.

Introduction

Human bocavirus 1 (HBoV1) belongs to genus *Bocaparvovirus* of the *Parvoviridae* family (3). HBoV1 causes lower respiratory tract infections, especially in infants less than two years old (2,23,104,105,111). Severe and deadly cases associated with high viral load, anti-HBoV1 IgM antibody detection, or increased IgG antibody production, have been documented

(23,85,158). In vitro, HBoV1 infects polarized primary human airway epithelium cultured at an air-liquid interface (HAE-ALI) (45), and causes damage of the airway epithelium (40,42,69). Currently, no specific treatments for HBoV1 infection are available for hospitalized infants.

The RNA transcription profiles of three species in the genus *Bocaparvovirus*, i.e., canine minute virus (CnMV/MVC) (133), bovine parvovirus type 1 (BPV1) (17), and HBoV1 (45), have been studied during virus infection. These species share similarities in their gene expression with distinguishing features among various parvovirus clades. They use one promoter to transcribe a single precursor mRNA transcript (pre-mRNA), which is both alternatively spliced and polyadenylated, to generate matured mRNA transcripts for encoding viral non-structural (NS) and structural (VP) proteins (16,119,144,145). Members of *Bocaparvovirus* express one large NS protein (NS1) from the left viral genome, VP proteins from the right side of the viral genome, and at least one small NS protein (NP1) that is encoded by an open reading frame (ORF) located in the middle of the viral genome (69,119,145). During MVC infection, we have detected another small NS protein (NS1~66kd), which contains the N-terminus of the NS1 (144).

The *Bocaparvovirus* NS1, like the NS1 or Rep78/68 of other parvoviruses, is a multifunctional protein that has site-specific origin DNA binding domain (OBD) endonuclease activity at its N-terminus (152), ATPase and helicase activities in the middle (35,62), and a transactivation domain at its C-terminus (88,137). NS1 is essential to viral DNA replication, while NP1 is required for efficient viral DNA replication (69,145). MVC NP1 protein plays a role in facilitating VP-encoding mRNAs to read through the proximal polyadenylation site that lies in the middle of the viral genome (144). Nothing is known about the functions of the newly identified MVC NS1~66kd protein. The protein expression profile of HBoV1 has been characterized using an incomplete HBoV1 genome lacking both the left and right inverted termini by transfection (16). Expression of the NS1, NP1 and VP from their respective encoding

transcripts were identified, however, the identities of the NS proteins with approximately (~) molecular weight (MW) of 66 kDa and 34 kDa, which were detected by an anti-NS1 C-terminus antibody, are unknown (16).

In this study, we explored the expression profile of HBoV1 NS proteins in transfection of either non-replicating plasmids or replicating infectious plasmids in HEK293 cells, or during HBoV1 infection of HAE-ALI cultures. We identified three novel HBoV1 NS proteins, NS2, NS3, and NS4, in both the HBoV1 genome replicating 293 cell system and the HBoV1 infection of HAE-ALI system. The functions of these proteins were further explored in these two systems.

Materials and Methods

Cell culture

Cell line: Human embryonic kidney 293 (HEK293) cells (CRL-1573) were obtained from American Type Culture Collection (ATCC, Manassas, VA), and were cultured in HyClone™ Dulbecco's Modified Eagle Medium (DMEM, GE Healthcare Bio-Sciences, Piscataway, NJ) with 10% fetal calf serum (FCS, #F0926, Sigma-Aldrich, St Louis, MO).

Primary human airway epithelium cultures: Polarized human airway epithelium cultures at an air-liquid interface (ALI), termed HAE-ALI, were generated by growing isolated human bronchial airway epithelial cells on collagen-coated, semipermeable membrane inserts (0.33 cm^2, Transwell®, Corning, Corning, NY). They then were allowed to differentiate at an air-liquid interface (ALI) either in an Ultraser G-containing medium as described previously (69) or in PneumaCult™-ALI medium (StemCell, Vancouver, BC, Canada), in 5% CO_2 at 37°C. After 3-5 weeks, the polarity of the HAE-ALI cultures was determined based on the transepithelial electrical resistance (TEER), the cultures that had a TEER of over 1,000 $\Omega.cm^2$ were used for HBoV1 infection.

DNA constructs

pHBoV1NSCap-based constructs: The parent pHBoV1NSCap that harbors HBoV1 *NS* and *Cap* genes but lacks the left and right termini (GenBank accession no.: DQ000496) (16) was used to construct pHBoV1NS^{1HA}Cap, in which an HA tag sequence was inserted after the ATG of the NS1 coding sequence. pHBoV1NS^{1HA65*}Cap and pHBoV1NS^{1HA303*}Cap were constructed by inserting a stop codon in the NS1 coding sequence after amino acid residue (aa) 65 and 303, respectively, in the pHBoV1NS^{1HA}Cap. pHBoV1NS^{1HA296Strep}Cap was constructed by further introducing a Strep tag after aa 296 of the NS1 coding sequence. pHBoV1NS^{1HA65*}Cap(smA1') and pHBoV1NS^{1HA303*}Cap(smD1') were constructed by moving the smA1 and smD1' mutations, as described below, into pHBoV1NS^{1HA65*}Cap and pHBoV1NS^{1HA303*}Cap, respectively.

pIHBoV1-based constructs: pIHBoV1, the infectious plasmid clone of HBoV1, which contains the HBoV1 full-length genome (GenBank accession no.:JQ923422), has been described previously (69). pIHBoV1(smA1') and pIHBoV1(smD1') were constructed by mutating the A1' acceptor site "AG/C" at nt 1015 to "TC/G" and the D1' donor site "G/GTAGGA" at nt 1212 to "A/GTTGGC", respectively, in pIHBoV1.

pGEX-4T-3-based constructs: The NS1-encoding sequences, nt 349-708 and nt 349-1284 were inserted into pGEX-4T-3 vector (GE Healthcare) to generate pGEX-4T-NS1N and pGEX-4T-NS1NL, respectively.

pGEM-4Z-based construct: Plasmid p4Z-PA1'D1' was constructed by inserting HBoV1 DNA nt 916-1263 into pGEM-4Z (Promega, Madison, WI) through BamHI and HindIII sites.

All nucleotide (nt) numbers of the HBoV1 genome refer to the HBoV1 full-length genome (GenBank accession no.:JQ923422), unless specified. Constructs were verified for HBoV1 sequence by Sanger sequencing at MCLAB (South San Francisco, CA)

Antibody production and antibodies used

pGEX-4T-3-based plasmids were used to express GST-fused HBoV1 NS proteins, GST-NS1aa1-120 and GST-NS1aa1-313. These proteins were used for the production of anti-NS1 N-terminus short (anti-NS1N) and anti-NS1 N-terminus long (anti-NS1NL), respectively. Purified GST-fused proteins were used to immunize rats following the antiserum production protocol that was described in our previous publication (145). All animal procedures were approved by the Institutional Animal Care and Use Committee of the University of Kansas Medical Center. Anti-NS1 C-terminus aa 640-781 antibody (anti-NS1C), anti-HBoV1 NP1 antibody (anti-NP1), and anti-HBoV1 VP antibody (anti-VP) have been described previously (16,69). Anti-HA (clone HA-7, Sigma), anti-Flag (clone M2, Sigma), anti-Strep (Clone 5A9F9, Genscript, Piscataway), anti-β-actin (#A5441, Sigma), anti-β-tubulin IV (#T7941Sigma), and anti-ZO-1 (#610966, BD Biosciences) were purchased.

Transfection

HEK293 cells grown in 60-mm dishes were transfected with 3 μg of plasmid as indicated in the figures, LipoD293 transfection reagent (SignaGen, Rockville, MD) was used following manufacturer's instructions. pBluescript SK plasmid was used as control (Ctrl).

RNA isolation and RNA analyses

RNA isolation. At 48 hours (hrs) post-transfection, transfected HEK293 cells from two 60-mm dishes were used to extract total RNA using TRIzol® reagent (Life Technologies). At 14 days post-infection (p.i.), at least 2 infected HAE-ALI cultures were used for total RNA extraction using TRIzol® reagent following manufacturer's instructions.

RT-PCR. For identification of A1' and D1' splice sites, viral cDNA was synthesized by using M-MLV kit (Life Technologies) and HBoV1-specific primer (HBoV1 nt 2560-2536). PCR reactions were performed using forward (F) and reverse (R) primers as indicated in **Fig. 1A**. PCR fragments were sequenced at MCLAB. Oligos were synthesized at IDT (Coralville, IA).

RNase protection assay (RPA). Probe PA1'D1' was generated by in vitro transcription of the EcoRI-linearized p4Z-PA1'D1' plasmid using T7 RNA polymerase. Ten µg of the total RNA was used for RPAs, following the methods described previously (122). Gels were imaged using a GE Typhoon FLA 9000 and processed with ImageQuant TL 8.1 (GE Healthcare) software for quantification.

DNA isolation and Southern blotting

Low-molecular-weight (Hirt) DNA was extracted and digested with or without DpnI essentially as previously described (63). DNA samples were run on a 1% agarose gel, and Southern blotting was performed as described previously (118). The blot was hybridized with an HBoV1 *NSCap* probe (16), and was then processed using a GE Typhoon FLA 9000 and ImageQuant TL 8.1 (GE Healthcare) for quantification.

Immunoprecipitation, SDS-polyacrylamide gel electrophoresis (PAGE) and Western blotting

Pierce™ Crosslink IP Kit (#26147, Life Technologies) was used for immunoprecipitation. At 48 hrs post-transfection, HEK293 cells from a 60-mm dish were collected and lysed for immunoprecipitation with an anti-HA or anti-Strep antibody following the manufacturer's instructions.

Immunoprecipitated proteins, or cell lysates taken 2 days post-transfection or 14 days p.i., were separated by SDS-10%PAGE, except the blots shown in panels of **Fig. 4C&E**, and **Fig. 7C&D**, which were separated by SDS-8%PAGE. Proteins were then electrotransferred onto a nitrocellulose membrane. The membrane was first blocked in 5% nonfat milk in 20mM Tris-HCl, pH7.6, 150 mM NaCl buffer with 0.1% Tween 20 (TBST), then incubated with a monoclonal antibody against Flag, HA, or Strep tag, or with anti-sera raised against various regions of the HBoV1 NS1 (anti-NS1N, anti-NS1NL, or anti-NS1C), or with anti-NP1, anti-VP, and anti-β-actin. Thoroughly washed with TBST after each step of incubation, the membrane was incubated with an HRP-conjugated secondary antibody (Jackson ImmunoResearch Inc., West Grove, PA), and subsequently with SuperSignal West Pico Chemiluminescent Substrate (Life Technologies) for signal development under the imager FUJIFILM LAS 4000 *(*FUJIFILM Life Sciences*).* Images were processed with Multi Gauge V2.3 software (FUJIFILM Life Sciences).

Virus production and infection

Virus production: HEK293 cells cultured on five 145-mm plates in DMEM-10%FCS were transfected with 30 μg of pIHBoV1 or its mutant per dish using PEI (1 mg/ml, #23966,

Polysciences, Warrington, PA) at a ratio of DNA:PEI=1:2. At two days post-transfection, cells were lysed for virus purification as previously described (69).

Virus infection of HAE-ALI: Polarized HAE-ALI cultures were apically infected with purified virus at a multiplicity of infection (MOI) of 10 DNaseI-resistant particles (DRP) per cell in 50 µl of phosphate buffered saline, pH7.4 (PBS). After incubation for 2 hrs, apical medium was aspirated, and the insert was washed 3 times with PBS. Following infection, released virus was collected daily by incubating the apical side of the insert with 100 µl of PBS.

Both purified virus preparations and the viruses released from the apical side were quantified for virus particles as DRP using quantitative PCR (qPCR) as previously described (69).

Immunofluorescence analysis.

At 14 days p.i., HAE-ALI membranes were fixed with 3.7% paraformaldehyde in PBS at room temperature for 15 min. The fixed membranes were cut into small pieces. We then performed immunofluorescence assay with anti-NS1C and anti-β-tubulin IV or with anti-NS1C and anti-ZO-1, as described previously (69).

Results

Novel splice sites, A1' acceptor and D1' donor, are used in processing of HBoV1 pre-mRNA.

We have identified a novel splice donor site, 1D', that lies in the first intron of the pre-mRNA of *Bocaparvovirus* MVC (144). We suspected the presence of a similar donor site in

HBoV1 pre-mRNA (**Fig. 2-1A**, D1'). In addition, we previously identified an A1-1 acceptor site in the first intron of HBoV1 pre-mRNA (**Fig. 2-1A**, A1') (16). To confirm the alternative use of these two splice sites in the processing HBoV1 pre-mRNA, we designed two primer pairs to detect viral mRNA transcripts spliced at D1', A1' or both sites in total RNA isolated from pHBoV1NSCap-transfected 293 cells. The primer pair of F287 and R1210 amplified a DNA fragment of ~250 bp (**Fig. 2-1B**, RT-PCR 1). Sequencing confirmed that the A1' acceptor site is used at nt 1017 (**Fig. 2-1C**, RT-PCR 1). Another primer pair, F1021 and R2250, amplified a band of ~300 bp (**Fig. 2-1B**, RT-PCR 2). Sequencing showed that the D1' site is used at nt 1212 (**Fig. 2-1C**, RT-PCR 2).

Next, using RPAs, we employed an anti-sense RNA probe spanning nt 916-1263 to determine the relative abundance of the HBoV1 mRNAs which were alternatively spliced at the A1' and D1' splice sites (**Fig. 1A**, PA1'D1'). In the RNA samples isolated from transfected cells, we detected 4 protected bands indicated in **Fig. 2-1D**, as predicted (**Fig. 2-1A**), confirming the involvement of the A1' and D1' splice sites in processing HBoV1 pre-mRNA. By quantifying these bands, we found that ~5% of the protected viral RNAs were spliced at either the A1' or D1' splice site in pre-mRNAs generated from either the non-replicating pHBoV1NSCap or the replicating pIHBoV1 plasmid (**Fig. 2-1D**, D1' and A1' Spl). However, the replicating pIHBoV1 generated less RNAs spliced at both splice sites than did the non-replicating pHBoV1NSCap in transfected cells (**Fig. 2-1D**, All Spl). The involvement of the A1' and D1' splice sites was further validated in the processing of viral pre-mRNA during HBoV1 infection of HAE-ALI (**Fig. 2-1E**, lane 3). Notably, virus infection produced much less viral RNA spliced at both the A1' and D1' sites than did the pIHBoV1 in transfection (**Fig. 2-1E**, lane 3 vs. **Fig. 1D**, lane 4, All Spl).

Since the HBoV1 pre-mRNA is significantly spliced at the A1' and D1' splice sites, we searched for potentially encoded small NS proteins spanning the NS1 coding sequence from these alternatively spliced mRNAs. As shown in **Fig. 2-2**, $R2_{S/L}$ mRNA, in which the D1'-A1

Figure 2-1. HBoV1 pre-mRNA is processed at novel A1' acceptor and D1' donor sites.

(A) Primers and probe used to detect viral mRNAs spliced at the A1' and D1' splice sites. The genome of HBoV1 is shown to scale with transcription landmarks, including the P5 promoter, splice donor (D1, D1', D2 and D3) and acceptor (A1, A1', A2 and A3) sites, the internal proximal polyadenylation site [(pA)p], and the distal polyadenylation site [(pA)d]. The RPA probe PA1'D1' (nt 916 to 1263) is shown, along with the designated bands that are expected to protect and their predicted sizes (nts). Primers used for RT-PCR are also shown. **(B&C) RT-PCR analyses of HBoV1 RNAs.** Total RNA was isolated from HEK293 cells transfected with pHBoV1NSCap. cDNA was synthesized and amplified with two pairs of HBoV1-specific primers as shown. **(B)** Amplified DNA fragments were electrophoresed on 1.6% agarose gel and visualized using ethidium bromide staining. **(C)** The amplified DNA fragments were excised from the agarose gel and purified. The purified DNA was subjected to sequencing by Sanger method. The histograms of the sequences at the exon junctions of D1/A1' and D1'/A1 splice sites, with alignment of the sequences with the HBoV1 genome sequence (at the bottom), are shown. **(D&E) Determination of the usage of the D1' and A1' splice sites by RPA.** Ten μg of total RNA isolated at 2 days post-transfection from *pBluescript* SK (Ctrl), pHBoV1NSCap- and pIHBoV1-transfected 293 cells **(D)** or at 14 days p.i. from mock- and HBoV1-infected HAE cells **(E)**, was protected by the P1A1'D1' probe as indicated. Lane 1 (M), ^{32}P-labeled RNA markers (121), with sizes indicated to the left. The origins of the protected bands in the lanes are indicated to the right. Spl, spliced RNAs, Unspl, unspliced RNAs.

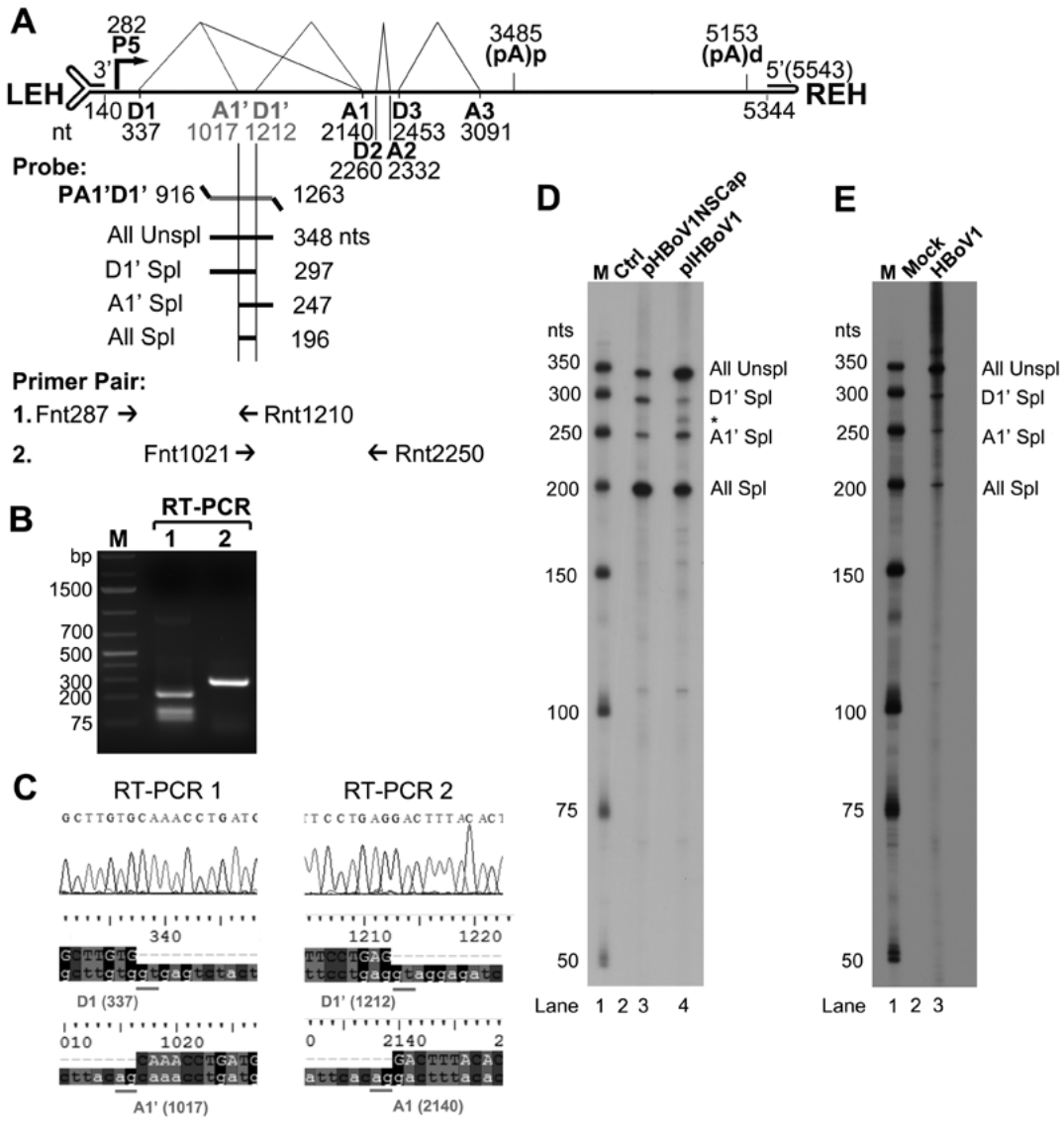
A
282
P5
3'
LEH
140 D1
nt
337
A1' D1'
1017 1212
A1
2140
D2 A2
2260 2332
D3
2453
A3
3091
3485
(pA)p
5153
(pA)d
5'(5543)
5344
REH
Probe:
PA1'D1' 916
1263
All Unspl
348 nts
D1' Spl
297
A1' Spl
247
All Spl
196
Primer Pair:
1. Fnt287 →
← Rnt1210
2. Fnt1021 →
← Rnt2250
B
RT-PCR
M
1
2
bp
1500
700
500
300
200
75
C
RT-PCR 1
RT-PCR 2
340
1210
1220
D1 (337)
D1' (1212)
010
1020
0
2140
A1' (1017)
A1 (2140)
D
M Ctrl
pHBoV1NSCap
pIHBoV1
nts
350
300
250
200
150
100
75
50
All Unspl
D1' Spl
*
A1' Spl
All Spl
Lane 1 2 3 4
E
M Mock
HBoV1
nts
350
300
250
200
150
100
75
50
All Unspl
D1' Spl
A1' Spl
All Spl
Lane 1 2 3

Figure 2-2. Putative expression of HBoV1 NS proteins from alternatively processed mRNAs.

A putative expression profile of HBoV1 NS proteins is shown with transcription landmarks and putative NS proteins. Major species of HBoV1 mRNA transcripts that are alternatively processed at the A1' and D1' splice sites and their putatively encoding NS proteins are shown with their relative sizes (minus a poly A tail of ~150 nts). Putative protein sizes and the actually detected sizes in the next experiments are shown side by side at the right. Antibodies raised against various portions of the NS1 protein are diagramed at the bottom.

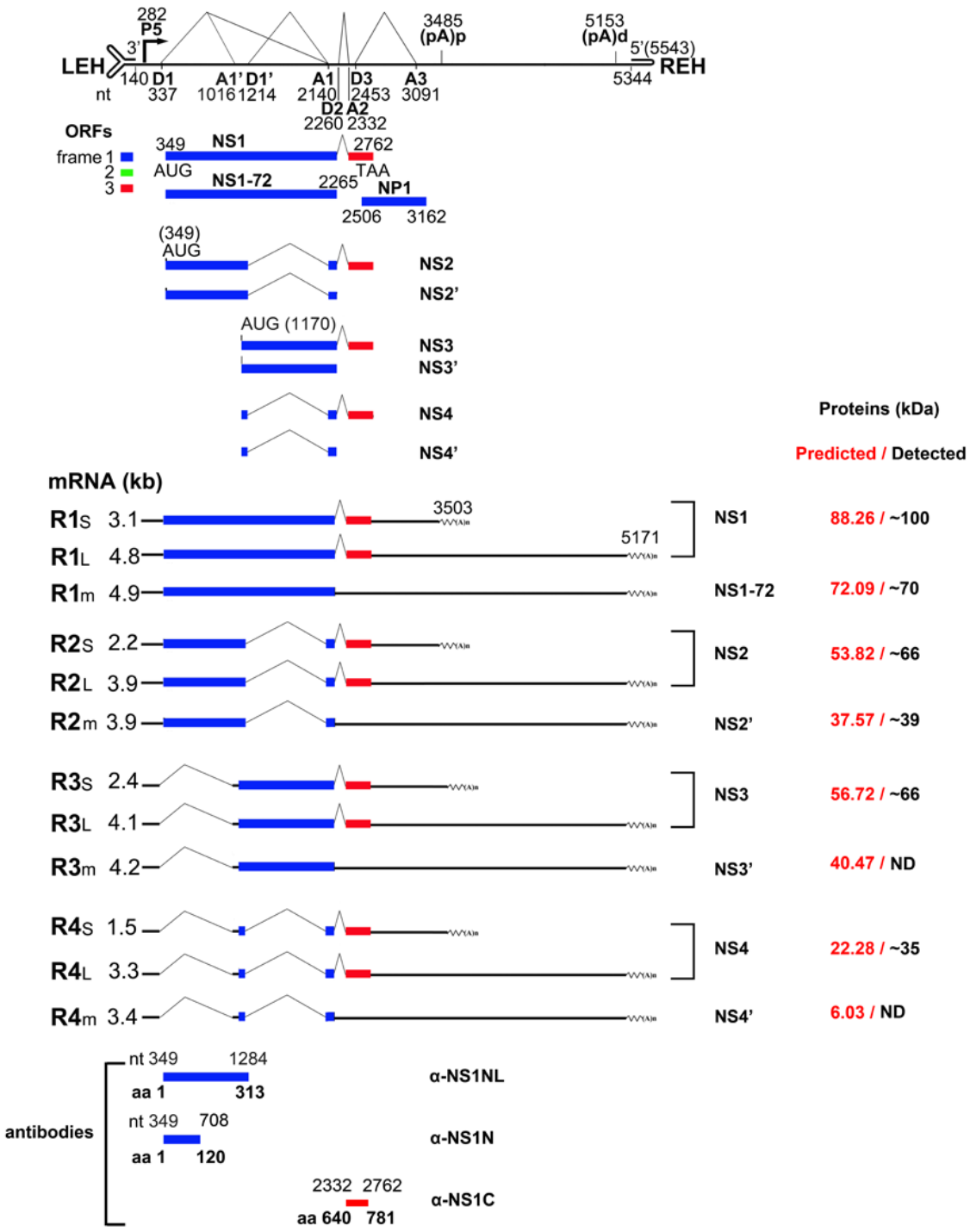
282
P5
3'
LEH
140
nt
D1
337
A1'
1016
D1'
1214
A1
2140
D3
2453
A3
3091
D2
2260
A2
2332
3485
(pA)p
5153
(pA)d
5'(5543)
5344
REH
ORFs
frame 1
2
3
349
NS1
2762
AUG
TAA
NS1-72
2265
NP1
2506
3162
(349)
AUG
NS2
NS2'
AUG (1170)
NS3
NS3'
NS4
NS4'
Proteins (kDa)
Predicted / Detected
mRNA (kb)
R1S 3.1
3503
R1L 4.8
5171
R1m 4.9
NS1
88.26 / ~100
NS1-72
72.09 / ~70
R2S 2.2
R2L 3.9
R2m 3.9
NS2
53.82 / ~66
NS2'
37.57 / ~39
R3S 2.4
R3L 4.1
R3m 4.2
NS3
56.72 / ~66
NS3'
40.47 / ND
R4S 1.5
R4L 3.3
R4m 3.4
NS4
22.28 / ~35
NS4'
6.03 / ND
antibodies
nt 349
1284
aa 1
313
α-NS1NL
nt 349
708
aa 1
120
α-NS1N
2332
2762
aa 640
781
α-NS1C

intron is excised, can express NS2 protein, $R3_{S/L}$ mRNA, in which the D1-A1' intron is excised, can translate NS3 protein, and $R4_{S/L}$ mRNA, in which both the D1-A1' and D1'-A1 introns are excised, is expected to have the capability to translate the NS4 protein.

The predicted sizes of the NS2, NS3, and NS4 proteins are 53.8, 56.7, and 22.2 kDa, respectively. However, in both HBoV1 plasmid-transfected and virus-infected cells, we previously detected two NS protein bands at ~66 kDa and ~34 kDa, in addition to the NS1 band at ~100 kDa, using an anti-NS1C antibody (**Fig. 2-2**, α-NS1C) (16,69). NS1's predicted MW of 88.2 kDa led us to speculate that the C-terminus of the NS1 is highly post-translationally modified, which gives an increment of ~12 kDa in its apparent molecular weight. Since all the predicted NS2, NS3, and NS4 proteins share the C-terminus with the NS1, we further postulate that NS2, NS3, and NS4 experience similar post-translational modification, resulting in detected MW of ~66, ~69 and ~34 kDa, respectively, with an increment of ~12 kDa from the modification (**Fig. 2-2**).

In addition, an in-frame stop codon would terminate NS protein expression in viral mRNAs that retain the D2-A2 intron. NS1-70, NS2', NS3', and NS4' could be expressed from the $R1_m$, $R2_m$, $R3_m$ and $R4_m$ mRNAs (**Fig. 2-2**), which are not abundantly expressed mRNAs, since splicing of the D2-A2 intron is efficient. The ratio of spliced vs. unspliced RNA at the D2 site is over 20:1 (16). NS1-70 has been detected previously in HBoV1 plasmid-transfected cells (16).

Detection of NS2, NS3, and NS4 proteins in HEK293 cells transfected with non-replicating HBoV1 constructs.

In the following sets of experiments, we aimed to validate expression of NS2, NS3 and NS4 in HEK293 cells transfected with pHBoV1NSCap-based plasmids. We first introduced a stop codon to experimentally early terminate the NS1 and NS3 coding sequences in

pHBoV1NS^{1HA}Cap. Transfection of the pHBoV1NS^{1HA303*}Cap produced two major protein bands at ~66 kDa and ~35 kDa, as detected by an anti-HA antibody (**Fig. 2-3B,** lane 3), supporting the notion that the NS1 was truncated to ~35 kDa. The truncated NS3 should be ~3 kDa and was undetectable on the blot. We believe that the ~66 kDa band is NS2, which is assumed to be translated from the NS2 mRNAs that excise the D1'-A1 intron (**Fig. 2-3A**, NS2). A weak band at ~37 kDa was also detected by the anti-HA, which fits the size of NS2' (**Fig. 2-3A**, NS2'). Since NS1-70 was detected at a much lower level relative to the abundant NS1 (**Fig. 2-3B**, lane 2), we believe that the NS1-70, NS2', NS3', and NS4' proteins are minimally expressed.

We next introduced a stop codon after aa 65 of the NS1 coding sequence in pHBoV1NS^{1HA}Cap, which early terminates both the NS1 and NS2 proteins, but not the NS3 and NS4 proteins. Using an anti-NS1C antibody, we detected only protein bands at ~66 kDa and ~34 kDa in pHBoV1NS^{1HA65*}Cap-transfected cells (**Fig. 2-3D**, lane 3), which confirms that the NS1 and NS2 proteins are early terminated, and suggests that NS3 and NS4 proteins are expressed. On the other hand, only bands at ~66 kDa and ~34 kDa were detected in pHBoV1NS^{1HA303*}Cap-transfected cells (**Fig. 2-3D**, lane 4), confirming that NS2 and NS4 proteins are expressed. When all the NS1, NS2 and NS3 coding sequences were early terminated in pHBoV1NS^{1HA65*303*}Cap (**Fig. 2-3C**), only NS4 protein was detected in transfected cells (**Fig. 2-3D**, lane 5), validating the expression of NS4 from the mRNAs that excised both the D1-A1' and D1'-A1 introns.

Furthermore, we tagged the NS1 coding sequence with an HA tag after aa 1 and with a Strep tag after aa 296 that lies in the intron of D1'-A1 in pHBoV1NSCap (**Fig. 2-4A**), and used an immunoprecipitation (IP) strategy to confirm the expression of NS2, NS3 and NS4. Anti-HA antibody-conjugated beads were used to pull down HA-tagged NS proteins from the lysate of the HEK293 cells transfected with pHBoV1NS^{1HA296Strep}Cap. In the precipitated proteins, we

Figure 2-3. Detection of HBoV1 NS1, NS2, NS3, and NS4 proteins in HEK293 cells transfected with pHBoV1NSCap-based plasmids.

(A&B) Expression of HBoV1 NS2 protein. (A) Expected HA-tagged NS proteins expressed from pHBoV1NS^{1HA303*}Cap. The NS-encoding viral mRNAs, which have the potential to produce HA-tagged NS proteins and C-terminus-containing NS proteins, are diagramed. The expected NS proteins and their predicted and detected sizes are shown at the right. (B) HEK293 cells were transfected with pHBoV1NS^{1HA}Cap or pHBoV1NS^{1HA303}*Cap as indicated. At two days post-transfection, cells were lysed for Western blotting using an anti-HA antibody. **(C&D) Expression of HBoV1 NS3 and NS4 proteins.** (C) Expected NS1 C-terminus (NS1C)-containing NS proteins expressed from pHBoV1NS^{1HA65*}Cap and pHBoV1NS^{1HA65*303*}Cap. The NS-encoding viral mRNAs, which have the potential to produce NS1C-containing NS proteins, are diagramed. The expected NS proteins and their predicted and detected sizes are shown at the right. (D) HEK293 cells were transfected with pHBoV1NSCap-based plasmids as indicated. At two days post-transfection, cells were lysed for Western blotting using the anti-NS1C antibody.

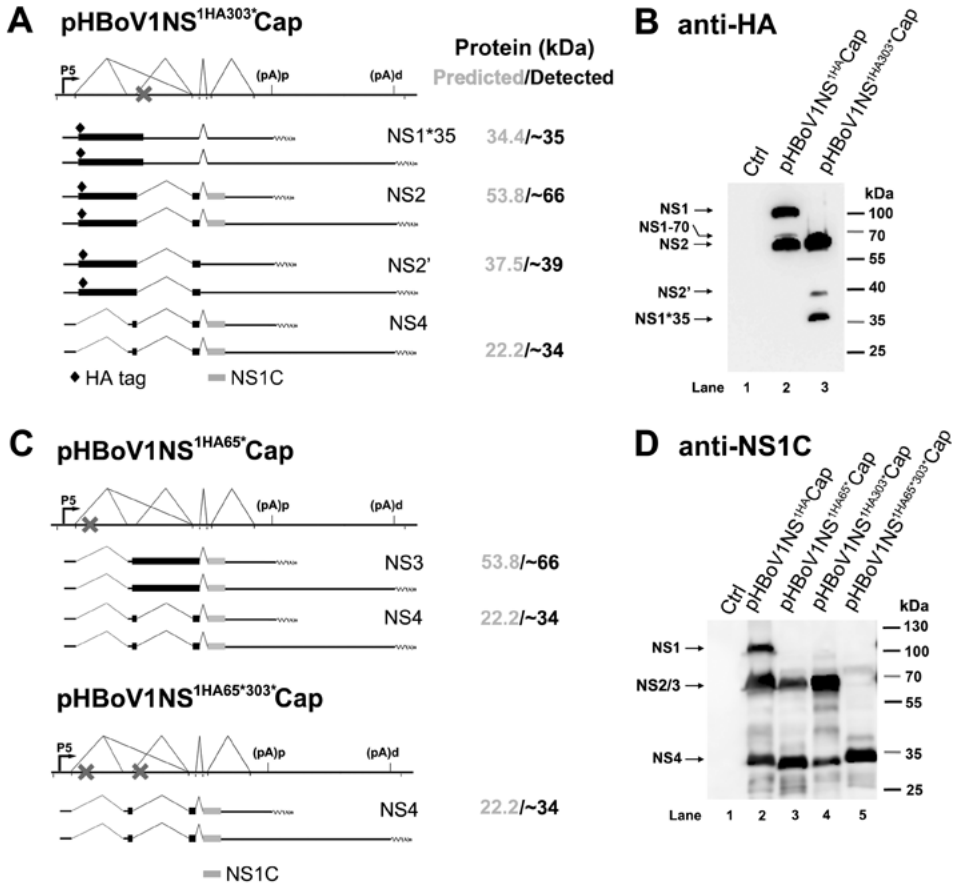
A
pHBoV1NS1HA303*Cap
Protein (kDa)
Predicted/Detected
P5
(pA)p
(pA)d
NS1*35
34.4/~35
NS2
53.8/~66
NS2'
37.5/~39
NS4
22.2/~34
HA tag
NS1C
B
anti-HA
Ctrl
pHBoV1NS1HACap
pHBoV1NS1HA303*Cap
kDa
NS1
NS1-70
NS2
NS2'
NS1*35
100
70
55
40
35
25
Lane 1 2 3
C
pHBoV1NS1HA65*Cap
NS3
53.8/~66
NS4
22.2/~34
pHBoV1NS1HA65*303*Cap
NS4
22.2/~34
NS1C
D
anti-NS1C
Ctrl
pHBoV1NS1HACap
pHBoV1NS1HA65*Cap
pHBoV1NS1HA303*Cap
pHBoV1NS1HA65*303*Cap
kDa
NS1
NS2/3
NS4
130
100
70
55
35
25
Lane 1 2 3 4 5

Figure 2-4. Detection of HBoV1 NS1, NS2, NS3, and NS4 proteins in transfected HEK293 cells using immunoprecipitation assays.

(A) Putative NS expression from transfection of the pHBoV1NS^{1HA296Strep}Cap plasmid. A putative expression profile of HBoV1 NS proteins is schematically diagramed with only HA, Strep, or NS1 C-terminus-containing NS-encoding mRNAs. Sizes of the putative NS proteins and the actually detected sizes are shown side by side at the right. **(B-D) Western blot (WB) analysis of the NS proteins immunoprecipitated (IP) by an anti-HA antibody.** HEK293 cells were transfected with pHBoV1NS^{1HA296Strep}Cap. At two days post-transfection, cells were lysed for immunoprecipitation using the anti-HA antibody or mouse IgG (as a control). Precipitated proteins, together with 10% of the input cell lysate, were analyzed by Western blot using anti-HA (B), anti-Strep (C), and anti-NS1C (D) antibodies, respectively. **(E-G) Western blot analysis of the NS proteins immunoprecipitated by an anti-Strep antibody.** HEK293 cells were transfected with pHBoV1NS^{1HA296Strep}Cap. At two days post-transfection, cells were lysed for immunoprecipitation using the anti-Strep antibody or mouse IgG (as a control). Precipitated proteins, together with 10% of the input cell lysate, were analyzed by Western blot using anti-HA (E), anti-Strep (F), and anti-NS1C (G) antibodies, respectively. The identities of detected protein bands are shown with lines to the left of the blot. The asterisk indicates bands that likely originated from degraded, unmodified or cleaved proteins.

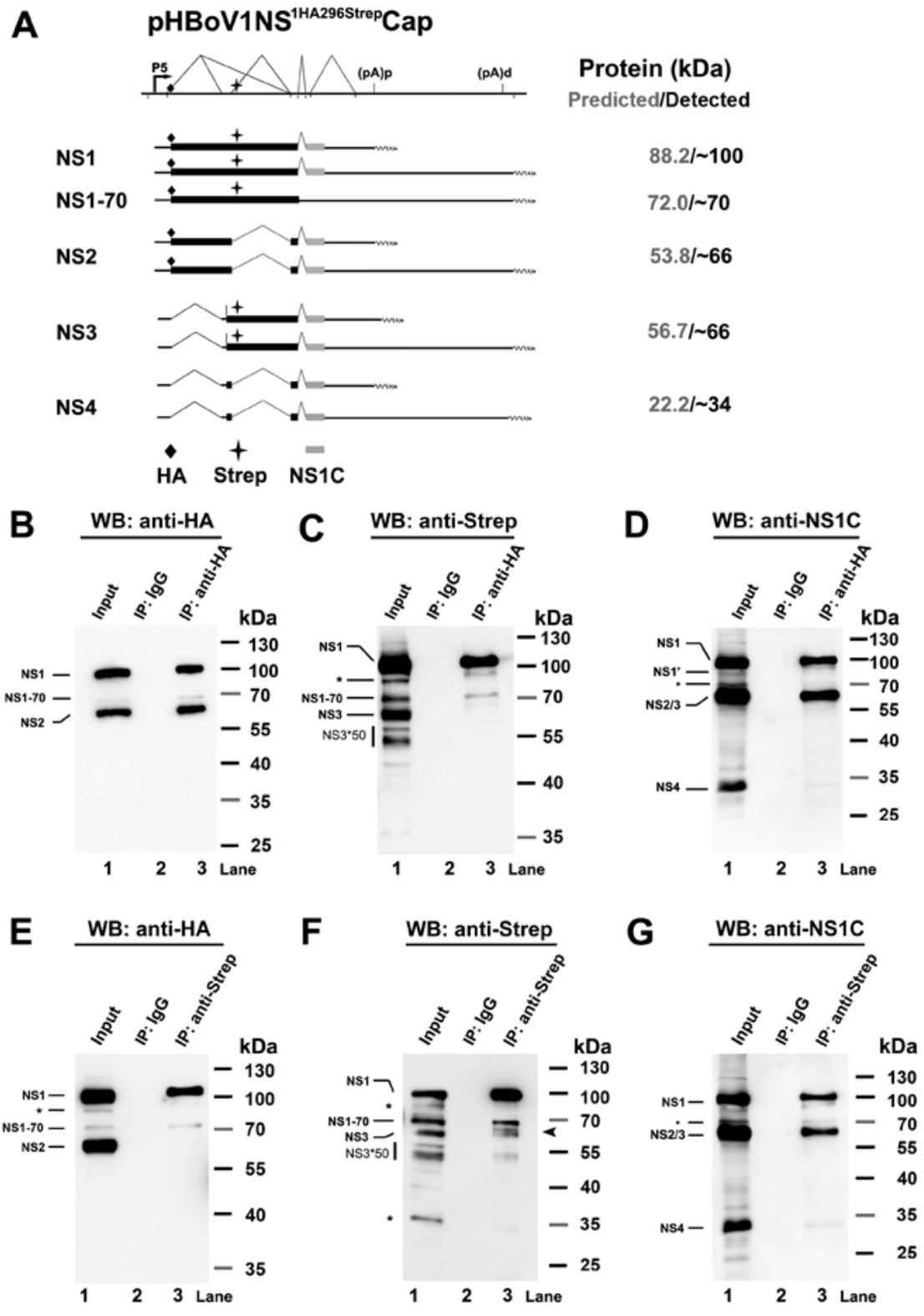
A
pHBoV1NS1HA296StrepCap
P5
(pA)p
(pA)d
Protein (kDa)
Predicted/Detected
NS1
NS1-70
NS2
NS3
NS4
88.2/~100
72.0/~70
53.8/~66
56.7/~66
22.2/~34
HA
Strep
NS1C
B
WB: anti-HA
C
WB: anti-Strep
D
WB: anti-NS1C
Input
IP: IgG
IP: anti-HA
kDa
130
100
70
55
40
35
25
NS1
NS1-70
NS2
NS3
NS3*50
NS1'
NS2/3
NS4
1
2
3
Lane
E
WB: anti-HA
F
WB: anti-Strep
G
WB: anti-NS1C
IP: anti-Strep

detected NS1 at ~100 kDa using anti-HA, anti-Strep, or anti-NS1C antibodies (**Fig. 2-4B-D**, lane 3). However, an NS protein at ~66 kDa was only detected with an anti-HA or anti-NS1C antibody (**Fig. 2-4B&D**, lane 3). These results confirmed that the ~66 kDa protein, pulled down with anti-HA, is an NS2 protein that initiates at the HA tag, skips the D1'-A1 intron-encoding region tagged with a Strep tag after aa 295, and ends at the C-terminus of the NS1 protein (**Fig. 2-4A**, NS2).

Next, a reverse IP using anti-Strep-conjugated beads was performed with the same lysate of the cells transfected with pHBoV1NS^{1HA296Strep}Cap. In the precipitated proteins, the NS1 was always detected at ~100 kDa by all three antibodies (**Fig. 2-4E-G**, NS1), and an NS protein at ~66 kDa was detected with the anti-Strep and anti-NS1C antibodies (**Fig. 2-4F&G**, lane 3), but not with the anti-HA antibody (**Fig. 2-4E**, lane 3), confirming that the ~66 kDa protein, pulled down by the anti-Strep, is NS3 protein that spans the D1'-A1 intron-encoding region, tagged with a Strep tag and the C-terminus of the NS1 protein, but is not initiated from the HA tag at the N-terminus (**Fig. 2-4A**, NS3). Protein bands clustered at ~50 kDa were also detected by the anti-Strep (**Fig. 2-4F**, lanes 1&3 and **Fig. 2-4C**, lane 1, NS3*50). Whether these proteins are cleaved or degraded bands of the NS3 or encoded from a new coding sequence remains unclear.

To further understand the NS4 protein expression strategy, we constructed pHBoV1NS^{275Flag}Cap, in which a Flag tag is inserted after aa 275 of the NS1 protein, immediately after a putative AUG at nt 1,171, before the D1' donor site, and pIHBoV1NS^{622Flag}Cap, in which a Flag tag is inserted after aa 622 that lies in the A1-D2 small exon. We detected an NS protein at ~34 kDa with an anti-Flag antibody in cells transfected with either of the plasmids, in addition to the protein bands at ~100 kDa and ~66 kDa (**Fig. 2-5**, lanes 2&3). Together with evidence of the detection of the ~34 kDa protein with the anti-NS1C as shown in **Fig. 2-3&2-4**, our results confirm that the ~34 kDa protein is an NS4 protein that

Figure 2-5. Detection of the HBoV1 NS4 protein in HEK293 cells transfected with plasmid pHBoV1NS^{275Flag}Cap or pHBoV1NS^{622Fag}Cap.

293 cells were transfected with pHBoV1NS^{275Flag}Cap or pHBoV1NS^{622Fag}Cap as indicated. At two days post-transfection, cells were lysed for Western blotting using an anti-Flag antibody. The identities of detected proteins are shown with arrows at the right of the blot.

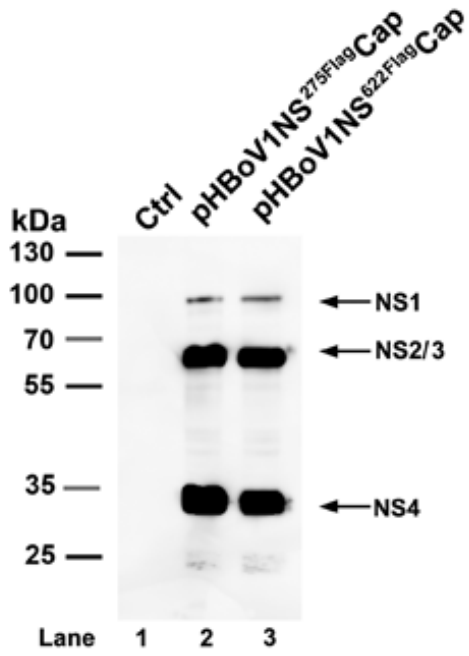
Ctrl
pHBoV1NS275FlagCap
pHBoV1NS622FlagCap
kDa
130
100
70
55
35
25
NS1
NS2/3
NS4
Lane 1 2 3

initiates at the AUG at aa 275 of the NS1 protein, skips the D1'-A1 intron-encoding region, reads through the A1-D2 exon, and extends to the C-terminus of the NS1 (**Fig. 2-5**, NS4).

Detection of NS2, NS3, and NS4 during HBoV1 replication in HEK293 cells and HBoV1 infection of HAE-ALI cultures.

We next sought to detect the NS2, NS3, and NS4 proteins in the HBoV1 reverse genetics system and following HBoV1 infection of HAE-ALI cultures. Using an anti-NS1C antibody, we detected NS1 at ~100 kDa, a mixed band of NS2 and NS3 at ~66 kDa, and NS4 at ~34 kDa in HEK293 cells transfected with the replicating pIHBoV1(**Fig. 2-6A**, lane 3), as well as in cells of the HAE-ALI cultures infected with HBoV1 (**Fig. 2-6A**, lane 5). Using an anti-NS1NL antibody, which was raised against aa 1-313 of the NS1, we detected NS1, mixed NS2 and NS3, and NS4 proteins at their expected sizes, as indicated, both in transfected and infected cells (**Fig. 2-6B**, lanes 2, 3, and 5). Additionally, a band at ~50 kDa was detected by the anti-NS1NL (**Fig. 2-6B**, NS3*50), which is similar to the ~50 kDa protein band detected in the lysate of the cells transfected with the pHBoV1NS^{1HA296Strep}Cap with the anti-Strep (**Fig. 2-4C&F**, lane 1, NS3*50). However, this protein was not detected with an anti-NS1N antibody, which was raised against aa 1-120 of the NS1 (**Fig. 2-6C**, lanes 2, 3&5), suggesting that the ~50 kDa protein is likely a derivative of the NS3, named NS3*50.

Notably, two significant bands grouped at ~35-40 kDa were detected by both the anti-NS1NL and anti-NS1N antibodies in infected cells but not in transfected cells (**Fig. 2-6B&C**, NS1/2*35-40), suggesting that the NS1/2*35-40 proteins are likely cleaved or degraded proteins of the NS1 and NS2 proteins or, perhaps, that they are NS2' proteins that are highly expressed in infected cells. As expected, an anti-NS1N antibody detected both ~100 kDa NS1 and ~66 kDa NS2 proteins in either transfected or infected cells (**Fig. 2-6C**, lanes 2, 3 and 5). As noted,

Figure 2-6. Detection of HBoV1 NS2, NS3, and NS4 proteins in pIHBoV1-transfected HEK293 cells and HBoV1-infected HAE cells.

HEK293 cells were transfected with pHBoV1NSCap or pIHBoV1. At two days post-transfection, cells were lysed. HAE-ALI cultures were infected with HBoV1 at an MOI of 10 (DRP/cell). At 14 days p.i., infected cells in the ALI cultures were lysed. The lysates of both transfection and infection, as indicated, were then analyzed by Western-blot using anti-NS1C (**A**), anti-NS1NL (**B**), and anti-NS1N (**C**) antibodies, respectively. The identities of detected proteins are shown with arrows at the right of the blot. Blots were reprobed for β-actin as a loading control.

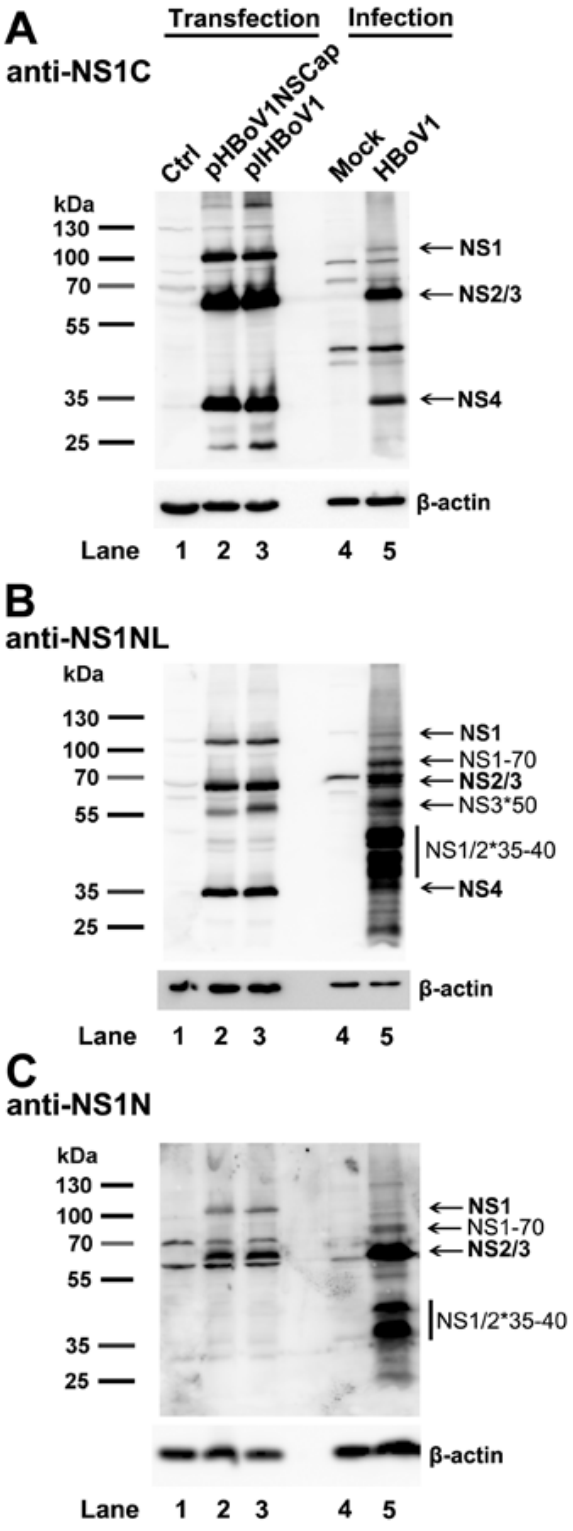
A
anti-NS1C
Transfection
Infection
Ctrl
pHBoV1NSCap
pIHBoV1
Mock
HBoV1
kDa
130
100
70
55
35
25
NS1
NS2/3
NS4
β-actin
Lane 1 2 3 4 5
B
anti-NS1NL
kDa
130
100
70
55
35
25
NS1
NS1-70
NS2/3
NS3*50
NS1/2*35-40
NS4
β-actin
Lane 1 2 3 4 5
C
anti-NS1N
kDa
130
100
70
55
35
25
NS1
NS1-70
NS2/3
NS1/2*35-40
β-actin
Lane 1 2 3 4 5

NS1-70 was detected at a higher level in infected cells than in transfected cells (**Fig. 2-6B&C**, lane 5 vs. lanes 2&3). This result may suggest a potential function of the NS1-70 during infection. NS4 was clearly detected at ~34 kDa by the anti-NS1C and anti-NS1NL antibodies (**Fig. 2-6A&B**, lane 2, 3&5), but not by the anti-NS1N (**Fig. 2-6C**, lane 2, 3&5), in both transfected and infected cells.

Taken together, these results confirm the expression of the novel NS2, NS3 and NS4 proteins in HEK293 cells transfected with the infectious clone and, more importantly, in HAE-ALI cells infected with HBoV1. However, only HBoV1 infection demonstrated relatively abundant expression of these short version NS proteins (NS1-70, NS1/2*35-40, and NS3*50).

NS2, NS3, and NS4 proteins are dispensable for efficient viral DNA replication and virion production in the HBoV1 reverse genetics system.

To investigate the function of the NS2, NS3, and NS4 in HBoV1 replication, we constructed pIHBoV1(smA1') and pIHBoV1(smD1'), knocking out the A1' and D1' splice sites, respectively, in the context of the infectious clone pIHBoV1 (**Fig. 2-7A**). Both mutants maintained the encoded NS protein sequences. Analyses of total RNA extracted from HEK293 cells transfected with pIHBoV1(smA1') or pIHBoV1(smD1') using RPAs with a homologous PA1'D1' probe confirmed that splicing at the A1' or D1' splice site was abolished (data not shown). In order to examine the knockout efficiency of the NS3 and NS2, we constructed smA1' and smD1' mutations in non-replicating plasmids pHBoV1NS^{1HA65*}Cap and pHBoV1NS^{1HA303*}Cap, respectively. The smA1' mutation knocked down NS3 expression nearly to the background of the blot and NS4 expression by ~10-fold (**Fig. 2-7B**, compare lanes 4 to 3). The smD1' mutation knocked out both NS2 and NS4 expression (**Fig. 2-7B**, compare lanes 6 to 5). Furthermore, protein analysis of the mutant infectious clones confirmed that pIHBoV1(smD1')

Figure 2-7. Analyses of virus production from transfection of mutant HBoV1 infectious clones in HEK293 cells.

(A) Diagrams of pIHBoV1 and its mutants. pIHBoV1(ΔIHBo that has a stop codon after the NS1 aa 65 (69), and pIHBoV1(smA1') and pIHBoV1(smD1') that knock out the A1' and D1' splice sites, respectively, are diagramed with transcription, splicing, and polyadenylation units. **(B) NS Knockdown efficiency from smA1' and smD1' mutations.** HEK293 cells were transfected with plasmids with smA1' and smD1' mutations in the context of pHBoV1NSCap, as indicated. At two days post-transfection, cells were lysed for Western-blotting using anti-NS1C antibody. **(C-E) Western blot analysis of proteins from infectious clones.** HEK293 cells were transfected with plasmids as indicated. Cells were harvested and lysed at two days post-transfection. The lysates were analyzed by Western-blot using anti-NS1C antibody (C) and reprobed with anti-NS1NL and anti-β-actin antibodies (D), and using anti-VP antibody (E). The identities of detected proteins are shown with arrows at the right of the blot. The asterisk indicates a band that likely a cleaved VP or an unknown VP. **(F&G) Southern blot analysis of viral DNA replication.** (F) HEK293 cells were transfected with plasmids as indicated. At 2 days post-transfection, cells were harvested for Hirt DNA preparations. The Hirt DNA samples were digested with DpnI and analyzed by Southern blot with an HBoV1*NSCap* probe (16). The identities of detected bands are shown. dRF/mRF, double/monomer replicative form, ssDNA, single-stranded DNA. (G) Quantification of the RF bands, which were normalized by the DpnI-digested DNA, from three independent experiments is shown with means and standard deviations. **(H) Quantification of virus production.** HEK293 cells were transfected with plasmids as indicated. At 2 days post-transfection, cells were harvested for virus preparation. The final virus preparations (2 ml for each) were quantified for DNaseI-resistant particles (DRP) using qPCR, and are shown as DRP/μl in a log scale (Y-axis). Means and standard deviations

are calculated from three independent experiments. P values are calculated using a student “*t*” test.

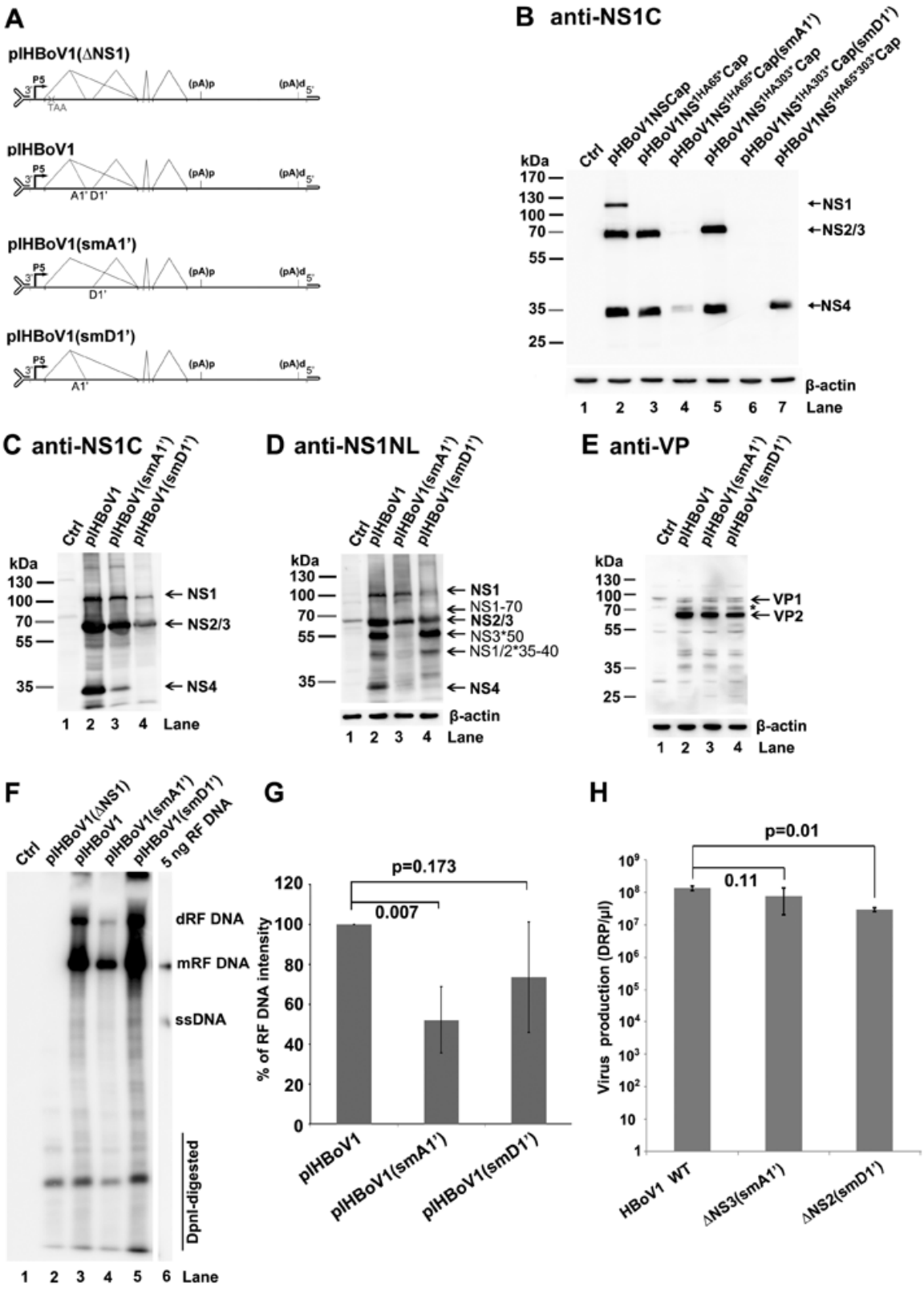
A
pIHBoV1(ΔNS1)
P5
(pA)p
(pA)d
TAA
pIHBoV1
A1' D1'
pIHBoV1(smA1')
D1'
pIHBoV1(smD1')
A1'
B anti-NS1C
Ctrl
pHBoV1NSCap
pHBoV1NS1HA65*Cap
pHBoV1NS1HA65*Cap(smA1')
pHBoV1NS1HA303*Cap
pHBoV1NS1HA303*Cap(smD1')
pHBoV1NS1HA65*303*Cap
kDa
170
130
100
70
55
35
25
←NS1
←NS2/3
←NS4
β-actin
1 2 3 4 5 6 7 Lane
C anti-NS1C
Ctrl
pIHBoV1
pIHBoV1(smA1')
pIHBoV1(smD1')
kDa
130
100
70
55
35
← NS1
← NS2/3
← NS4
1 2 3 4 Lane
D anti-NS1NL
Ctrl
pIHBoV1
pIHBoV1(smA1')
pIHBoV1(smD1')
kDa
130
100
70
55
35
← NS1
← NS1-70
← NS2/3
← NS3*50
← NS1/2*35-40
← NS4
β-actin
1 2 3 4 Lane
E anti-VP
Ctrl
pIHBoV1
pIHBoV1(smA1')
pIHBoV1(smD1')
kDa
130
100
70
55
35
25
← VP1
* ← VP2
β-actin
1 2 3 4 Lane
F
Ctrl
pIHBoV1(ΔNS1)
pIHBoV1
pIHBoV1(smA1')
pIHBoV1(smD1')
5 ng RF DNA
dRF DNA
mRF DNA
ssDNA
DpnI-digested
1 2 3 4 5 6 Lane
G
p=0.173
0.007
% of RF DNA intensity
120
100
80
60
40
20
0
pIHBoV1
pIHBoV1(smA1')
pIHBoV1(smD1')
H
p=0.01
0.11
Virus production (DRP/μl)
10⁹
10⁸
10⁷
10⁶
10⁵
10⁴
10³
10²
10
1
HBoV1 WT
ΔNS3(smA1')
ΔNS2(smD1')

did not produce NS4 (**Fig. 2-7C&D**, lane 4), and that pIHBoV1(smA1') decreased NS3*50 expression nearly to the background level of the blot (**Fig. 2-7D**, lane 3) and decreased NS4 by over 10-fold (**Fig. 2-7C**, lane 3). All these mutants produced capsid proteins VP1 and VP2 at a level similar to that of the wild-type (WT) (**Fig. 2-7E**), as well as NP1 (data not shown).

Next, we tested the replication capability of the mutants in HEK293 cells. pIHBoV1(smA1') had an ~2-fold decrease in the production of replicative form (RF) DNA, while pIHBoV1(smD1') replicated as effectively as the WT (**Fig. 2-7F&G**). We then produced mutant viruses ΔNS2(smD1') and ΔNS3(smA1') by transfecting HEK293 cells with pIHBoV1(smD1') and pIHBoV1(smA1'), respectively, and compared viral production against WT. As shown in **Fig. 2-7H**, the WT virus was produced at a total yield of 2×10^{11} DRP (2 ml of 1×10^{8} DRP/μl) from five 145-mm plates of transfected HEK293 cells, and the mutant ΔNS3 and ΔNS2 viruses were also produced efficiently, with only a moderate decrease of 1.7- and 4.5-fold, respectively.

Collectively, these results indicate that NS2, NS3 and NS4 are dispensable for viral DNA replication and for virus production in the 293 cell reverse genetics system.

The HBoV1 NS2, but not the NS3 and NS4, plays an essential role in HBoV1 replication of HAE-ALI.

We finally infected HAE-ALI cultures with the WT, ΔNS2, or ΔNS3 virus. We collected progeny virions produced from the apical side of the ALI cultures for a period of 14 days, and quantified their titers. At 2 days p.i., we observed an ~10-fold increase in virion release from the ALI cultures infected with either WT or mutant viruses (**Fig. 2-8A**, 2 dpi), confirming that both the WT and mutant viruses infected HAE-ALI. ΔNS2 virus lunched an initial infection at 2 days p.i., as shown by an 1-log increase of apical virus release (**Fig. 2-8A**). However, at 2 days p.i, ΔNS2 virus-infected cultures showed a gradual decrease in apical virus release, which

Figure 2-8. Analyses of virus infection of HAE-ALI cultures.

HAE-ALI cultures were prepared in Transwell inserts, and infected with HBoV1 WT or its mutants, respectively, from the apical surface at an MOI of 10 (DRP/cell). **(A) Apical virus release.** At the indicated days p.i., the apical surface was washed with 100 µl of PBS to collect released virus. Virion particles (DRP) were quantified by qPCR (y-axis) and plotted to the days p.i. as shown. Means and standard deviations are shown. **(B-D) Western blot analysis of HBoV1-infected HAE cultures.** At 14 days p.i., the cells of the infected ALI culture were lysed for Western blotting with anti-NS1C (B), anti-NS1NL (C), or anti-VP antibody (D). Blots were reprobed for β-actin, and the blot in panel C was further reprobed with an anti-NP1 antibody. The identities of detected proteins are shown with arrows at the right of the blot. In panel D, the band indicated by an asterisk is likely a cleaved band of VP1 or a new VP. **(E) Southern blot analysis of viral DNA replication**. At 14 days p.i., the cells of the infected HAE-ALI cultures were lysed for Hirt DNA preparation. The Hirt DNA samples were analyzed by Southern blot with an HBoV1 *NSCap* probe, and a mitochondrial (mito) DNA-specific probe (141), respectively. Detected mitochondrial DNA was used for normalization of viral DNA quantification. The identities of detected bands are shown to the right.

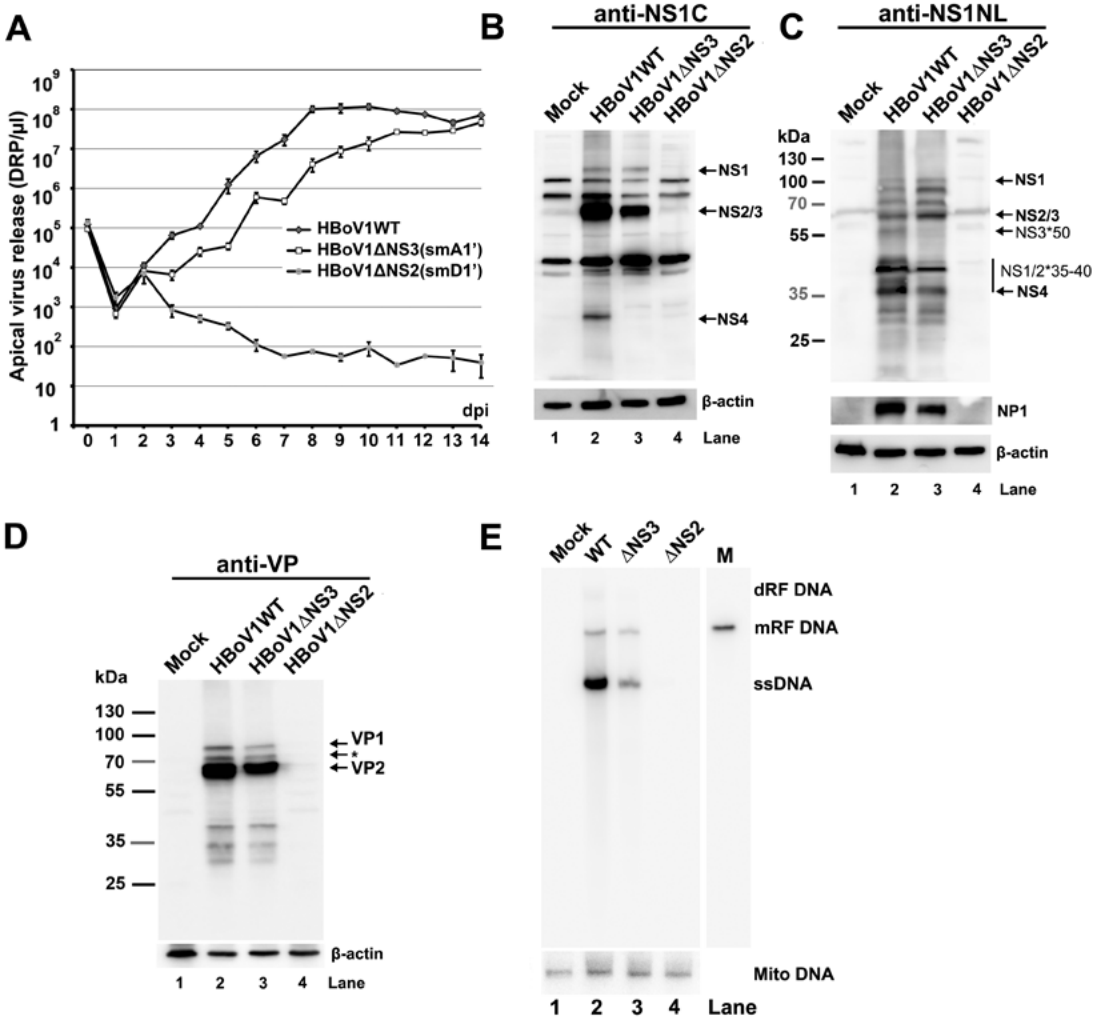
A
Apical virus release (DRP/μl)
dpi
HBoV1WT
HBoV1ΔNS3(smA1')
HBoV1ΔNS2(smD1')
B
anti-NS1C
Mock
HBoV1WT
HBoV1ΔNS3
HBoV1ΔNS2
NS1
NS2/3
NS4
β-actin
Lane
C
anti-NS1NL
kDa
NS1
NS2/3
NS3*50
NS1/2*35-40
NS4
NP1
β-actin
Lane
D
anti-VP
VP1
*
VP2
β-actin
Lane
E
Mock
WT
ΔNS3
ΔNS2
M
dRF DNA
mRF DNA
ssDNA
Mito DNA
Lane

remained at a level less than 100 DRP/µl after 6 days p.i. (**Fig. 2-8A**, ΔNS2). On the other hand, though ΔNS3 virus-infected cultures produced virions at a level ~10 times lower than that of the WT-infected cultures from 3-9 days p.i., they eventually reached a similar level in apical virus release (less than 2 times difference) at days 13 and 14 p.i. (**Fig. 2-8A**, compare ΔNS3 with WT).

At 14 days p.i., we analyzed NS expression of the infected HAE cells. No NS and capsid (VP) proteins were detectable in ΔNS2 virus-infected cells (**Fig. 2-8B-D**, lane 4). ΔNS3 virus-infected cells expressed NS1, NS2 (**Fig. 2-8B&C**, lane 3), NS1/2*35-40 (**Fig. 2-8C**, lane 3), and VP (**Fig. 2-8D**, lane 3), at levels similar to those of the WT counterpart (**Fig. 2-8B-D**, lane 2), but not NS4 (**Fig. 2-8B**, lane 3) and NS3*50 (**Fig. 8C**, lane 3). This result echoes NS expression of the ΔNS3 parent infectious clone pIHBoV1(smA1') (**Fig. 2-7C&D**). Southern blot analysis showed that the ΔNS3 virus infection had a decrease in the level of ssDNA but not the mRF DNA (**Fig. 2-8E**, compare lanes 3 to 2), suggesting that the ΔNS3 virus replicates at a level similar to the WT in HAE-ALI. We confirmed that there was no obvious viral DNA detected in ΔNS2 virus-infected cells at 14 days p.i. (**Fig. 2-8E**, lane 4). Since both the ΔNS2 and ΔNS3 mutants did not express NS4 (**Fig. 2-8B**, lanes 3&4), these results suggest that NS2 is essential, but NS3 and NS4 are dispensable, to HBoV1 replication in HAE-ALI.

Further analyses of the infected HAE by immunofluorescence assays showed that ΔNS3 virus infection caused loss of cilia on the airway epithelium, as shown by staining of β-tubulin (**Fig. 2-9A**, ΔNS3), and redistribution of the tight junction, as shown by staining of ZO-1 (**Fig. 2-9B**, ΔNS3), but to a lesser extent than that of the WT virus (**Fig. 2-9**, WT). This could be due to less expressed NS proteins as detected by the anti-NS1C during infection. On the other hand, the abortive infection of ΔNS2 virus did not cause any disruption of the tight junction and loss of the cilia, as shown by the ZO-1 and β-tubulin staining, respectively (**Fig. 2-9**, ΔNS2), which is consistent with the abortive infection of the ΔNS2 mutant virus.

Figure 2-9. Immunofluorescence analysis of the tight junction protein ZO-1 and the cilia marker β-tubulin IV of infected HAE-ALI.

At 14 days p.i., mock-, WT-, ΔNS2-, and ΔNS3-infected HAE-ALI cultures were co-stained with anti-NS1C and anti-β-tubulin IV **(A)**, or co-stained with anti-NS1C and anti-ZO-1 **(B)**. Confocal images were taken at a magnification of × 40. Nuclei were stained with DAPI (blue).

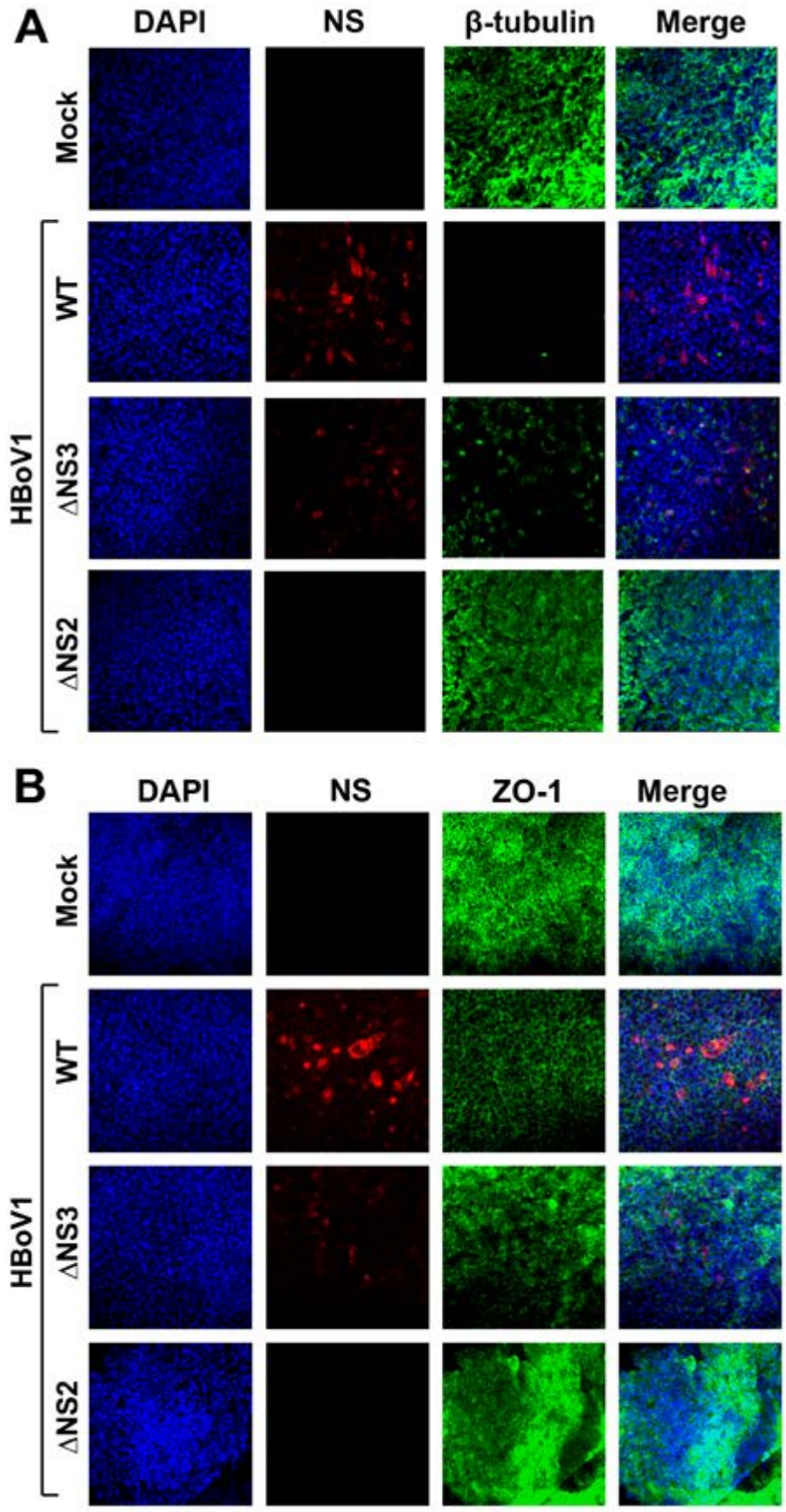
A
DAPI
NS
β-tubulin
Merge
Mock
HBoV1
WT
ΔNS3
ΔNS2
B
DAPI
NS
ZO-1
Merge
Mock
HBoV1
WT
ΔNS3
ΔNS2

Discussion

In this study, we confirmed that two novel splice sites are used to process HBoV1 pre-mRNA, which generate mRNA transcripts that are able to translate small NS proteins, NS2, NS3, and NS4. We detected NS2, NS3, and NS4 proteins expressed during HBoV1 DNA replication in HEK293 cells and HBoV1 infection of HAE-ALI cultures. Although NS2, NS3, and NS4 proteins are dispensable for viral DNA replication and virus production in HEK293 cells, NS2 plays a critical role in HBoV1 replication in HAE-ALI cultures. Interestingly, NS2, NS3, and NS4 proteins contain the predicted domains of origin binding/endonuclease and transactivation, helicase and transactivation, and transactivation, respectively, of the NS1 (**Fig. 2-10**). Importantly, different expression patterns of the NS2, NS3, and NS1-70 were found during HBoV1 infection of HAE-ALI compared to those in HBoV1 replication in HEK293 cells, highlighting the importance of these small NS proteins during HBoV1 infection of human airway epithelia.

Expression strategy of *Bocaparvovirus* NS proteins.

NS1, or Rep78/68 in adeno-associated virus (AAV), is a multifunctional protein that has site-specific origin DNA binding, endonuclease, ATPase, and helicase activities (**Fig. 2-10**, NS1) (35,62). It is expressed from viral mRNAs transcribed from the promoter near the left end of the genome, which are either unspliced, or spliced at the small intron that lies in the middle of the genome (123). HBoV1 uses a strategy similar to that of the AAV2 Rep78/68 proteins (123) to express NS1 and NS1-70 from spliced and unspliced mRNAs, respectively, of the pre-mRNA transcribed from the P5 promoter. However, BPV and MVC, also members of the genus *Bocaparvovirus*, express NS1 at sizes of 100 kDa (119) and 84 kDa (144), respectively.

Parvoviruses also express a number of small NS proteins that are often important for

Figure 2-10. Putative functional domains of HBoV1 NS1, NS2, NS3, NS4 and NS1-70.

A schematic diagram of the HBoV1 NS1 protein is shown. The HBoV1 NS1 protein sequence (GenBank: AFR53039) is aligned with the AAV5 Rep78 (GenBank: AAD13755). N-terminal origin DNA binding domain (OBD, in red) and helicase domain (in purple) are predicted based on structured regions of the AAV5 Rep78 OBD (66) and AAV2 Rep40 helicase domain (72). Unaligned regions positioned between the OBD and helicase domains (shown in green) are predicted by analogy with AAV and MVM to contain NS oligomerization signals. The C-terminal region (shown in yellow) is predicted to contain a zinc-binding motif as seen in AAV2 Rep78 (137), while in MVM this region is highly acidic and serves as a potent transcriptional activator (88). The OBD (aa1-271) was initially predicted based on secondary structured and unstructured regions of the NS1. Its structure has now been determined (152). Dashed lines in the OBD indicate residues that are structured as endonuclease core/DNA binding loop (152), and dashed rectangles in the helicase domain indicate Walker boxes (84).

Domains of the NS2, NS3, NS4, and NS1-70 proteins, deduced from those of the NS1, are diagramed in colored blocks with thin lines indicating protein sequence excision due to ligation of the neighboring exons of their mRNAs.

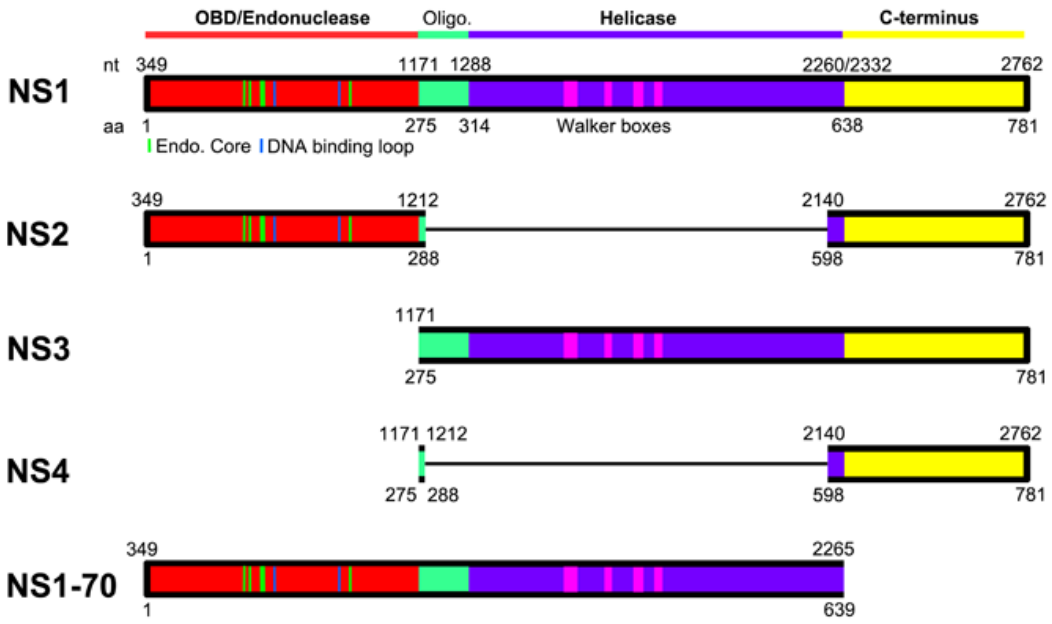
OBD/Endonuclease
Oligo.
Helicase
C-terminus
NS1
nt 349 1171 1288 2260/2332 2762
aa 1 275 314 Walker boxes 638 781
Endo. Core
DNA binding loop
NS2
349 1212 2140 2762
1 288 598 781
NS3
1171
275 781
NS4
1171 1212 2140 2762
275 288 598 781
NS1-70
349 2265
1 639

virus replication, one of which is the *Bocaparvovirus* NP1 (69,145). However, only a few parvoviruses express small NS proteins that share the amino acid sequences at the N-terminus of the NS1. A minute virus of mice (MVM) mRNA excised the large intron, spanned a large portion of the NS1-encoding region, expresses NS2, and, thus, NS2 shares only 85 aa with the NS1 at the N-terminus (37,123). The NS2 and NS3 proteins of Aleutian mink disease virus (AMDV) are expressed by a strategy similar to that of the MVM NS2 (70). They share 60 aa with the AMDV NS1 at the C-terminus. Thus, the HBoV1 NS2 is unique in that it shares aa 1-288 with the NS1, which contains the entire origin DNA binding/endonuclease domain (1-271 aa) of the NS1 (152) (**Fig. 2-10**, NS2). The NS2 also contains the C-terminal aa 598-781 of the NS1. Of note, *Bocaparvovirus* MVC uses the same strategy to express NS1~66kd (144), which is equivalent to the HBoV1 NS2. In BPV, we have previously proposed a viral mRNA that has the potential to express such an NS2 protein (119), but its expression has not been confirmed yet. Altogether, our results suggest that NS2 expression is a common feature among members of the genus *Bocaparvovirus*.

Small NS proteins, like the HBoV1 NS3, that share the helicase activity domain with the NS1 have been identified in viruses of the genus *Dependoparvovirus,* i.e., AAV Rep52/40 (123) and goose parvovirus (GPV) Rep2 (120). But AAV Rep52/40 are expressed from mRNAs that are transcribed from an independent P19 promoter in the middle of the Rep78-encoding region (123,129). GPV Rep2 is expressed from an mRNA that excises the 1D-1A intron lying in the Rep1-encoding region (90,120). Notably, we previously identified a *Bocaparvovirus* BPV R3 mRNA that excises an intron (D1-1A1) encoding N-terminal aa 1-282 of the NS1, and a small NS protein (BPV NS2) is proposed to be expressed from this mRNA at ~45 kDa (119). In fact, multiple NS bands centering at ~45 kDa were detected in BPV-infected cell lysates following immunoprecipitation using convalescent-phase sera from BPV-infected calves (87), these may be candidates of the BPV NS2 protein. Therefore, like the GPV Rep2 and BPV NS2, the HBoV1

NS3 is expressed from the viral mRNA that excises the D1-A1' intron encoding the origin binding domain (aa 1-274) (**Fig. 2-10**). However, such an expression strategy of NS3 has not been identified during MVC infection (144).

HBoV1 NS4 is expressed from a viral mRNA that has never been identified in expression of any parvovirus. The mRNA excises multiple introns (the D1-A1', D1'-A1, and D2-A2). NS4 largely contains the C-terminus (aa 598-781) of the NS1 (**Fig. 2-10**). Currently under investigation is whether, in the genus *Bocaparvovirus*, the NS4 protein expression is conserved in MVC and BPV infections.

Functions of the small NS proteins.

Our results suggest that HBoV1 NS2 is essential to virus replication in HAE-ALI but not to viral DNA replication in 293 cells. The function of the NS2 seems cell-type dependent, like that of the MVM NS2, which is not essential for MVM replication in transformed human cell lines, but is required for MVM infection in murine cells (110,126). The HBoV1 NS2 harbors the whole origin DNA binding domain with endonuclease activity (**Fig. 2-10**, NS2). Considering HBoV1 replicates in differentiated/polarized HAE cells that are out of cell cycle (G0 phase) (45,69), we speculate that the endonuclease feature of the NS2 may be required for HBoV1 DNA replication in non-dividing cells. The function of the MVC counterpart (NS1~66kd) in MVC replication is not yet understood (144).

HBoV1 NS3 is dispensable for virus DNA replication and progeny virus production in 293 cells, as well as in infection of the HAE-ALI. These results suggest that NS3 is not required for viral genome packaging, in contrast to the AAV Rep52/40 that are involved in packaging single-stranded viral genomes into capsid structures (136), which is mediated by their helicase activities (83). Since the ΔNS3 mutant virus expresses little NS4, we believe that the NS4 is also

not essential to virus replication and production in HAE-ALI, however, we cannot rule out functions of the NS3 and NS4 that may modulate host cell innate immune response during infection. Obviously, the function of NS3 and NS4 in the host innate immunity response to HBoV1 infection of HAE-ALI warrants further investigation.

NS1-70 and other small NS proteins that terminate at a stop codon in mRNAs retaining the D2-A2 intron.

NS1-70 was expressed at a higher level during virus infection of HAE-ALI than in pIHBoV1-transfected 293 cells. NS1/2*35-40 were expressed at a relatively higher level than NS1-4 during infection, but the NS1/2*35-40 are not expressed in cells transfected with the infectious or non-replicating plasmids. These differences between transfection and infection are not understood, but may be due to differences in the types of host cells, or to the cell differentiation status between the dividing HEK293 cells and non-dividing HAE cells. The NS1/2*35-40 are unlikely to be NS2' proteins (**Fig. 2-2**, NS2'), since they were still expressed from infection of a mutant virus that bears the intron D2-A2 deletion (data not shown). Similarly, the NS3*50 was expressed in HEK293 cells transfected with a mutant infectious clone that has the D2-A2 intron deleted, indicating that the NS3*50 is not the NS3' protein (**Fig. 2-2**, NS3'). We speculate that NS1/2*35-40 and NS3*50 are specifically cleaved products of the NS1/2 and NS3 proteins. Further studies are required to investigate the nature of the NS1/2*35-40 and NS3*50 proteins.

The NS1-70 contains the origin DNA binding/endonuclease and helicase domains of the NS1 but without the C-terminus (**Fig. 2-10**, NS1-70). A mutant infectious clone that expresses only the NS1-70 still replicates in 293 cells, but to an extent ~10 times less than of the WT (data not shown), suggesting that the C-terminus of the NS1 plays a helper role in HBoV1 DNA

replication. Although NS2' was detectable in transfected cells (**Fig. 2-3A**, lane 3), NS2' and NS3' proteins were not obviously detected in infected cells in our study, suggesting that NS4' is not expressed during infection.

In contrast to the acute infection of most other autonomous parvoviruses, HBoV1 infection is persistent, with the virus replicating in non-dividing airway cells. Taken together, our results support the hypothesis that the NS2-4, NS1-70, NS1/2*35-40 and NS3*50 are required for the virus to balance replication and host cell death during infection of human airway epithelia. The creation of replication defective HBoV1 mutants may have utility in vaccine development for this virus.

Chapter III:
Analysis of the Cis and Trans Requirements for DNA Replication at the Right End Hairpin of the Human Bocavirus 1 Genome

Abstract

Parvoviruses are single-stranded DNA viruses that use the palindromic structures at the ends of the viral genome for their replication. The mechanism of parvovirus replication has been studied mostly in *Dependoparvovirus* adeno-associated virus 2 (AAV2) and *Protoparvovirus* minute virus of mice (MVM). Here, we used human bocavirus 1 (HBoV1) to understand the replication mechanism of *Bocaparvovirus*. HBoV1 is pathogenic to humans, causing acute respiratory tract infections, especially in young children under 2 years old. By using the duplex replicative form of the HBoV1 genome in human embryonic kidney (HEK) 293 cells, we identified the HBoV1 minimal replication origin at the right-end hairpin (OriR). Mutagenesis analyses confirmed the putative NS1 binding and nicking sites within the OriR. Of note, unlike the large non-structural protein (Rep78/68 or NS1) of other parvoviruses, HBoV1 NS1 did not specifically bind OriR in vitro, indicating that other viral and cellular components or NS1 oligomerization are required for the NS1 binding to the OriR. In vivo studies demonstrated that residues responsible for NS1 binding and nicking are within the origin-binding domain. Further analysis identified that the small non-structural protein NP1 is required for HBoV1 DNA replication at OriR. The NP1 and other viral non-structural proteins (NS1-4) colocalized within the viral DNA replication centers in both OriR-transfected cells and virus-infected cells, highlighting a direct involvement of the NP1 in viral DNA replication at OriR. Overall, our study revealed characteristics of HBoV1 DNA replication at OriR, suggesting novel characteristics of autonomous parvovirus DNA replication.

Introduction

Human bocavirus 1 (HBoV1) is a recently identified respiratory virus associated with acute respiratory tract infections in young children (2,13,50,59,61,73,74,104,132). HBoV1 belongs to the *Bocaparvovirus* genus within the *Parvoviridae* (3,28) family. Other species in the *Bocaparvovirus* genus include minute virus of canines (MVC), bovine parvovirus 1 (BPV1), porcine bocavirus, and gorilla bocavirus (18,28,77,119,145).

A unique feature of bocaparvoviruses, differed from other parvoviruses, is that they express the small nuclear phosphoprotein NP1 from an open-reading frame (ORF) located in the middle of the genome (16,119,145). NP1 is a non-structural protein and is indispensable for viral DNA replication (69,145). The role of the NP1 proteins of HBoV1 and BPV1 in viral DNA replication is conserved to that of MVC, and they are exchangeable in supporting MVC DNA replication (145). While the mechanism defining how NP1 facilitates bocaparvovirus DNA replication remains largely unknown, it has been revealed that NP1 plays an important role in processing viral precursor mRNA (pre-mRNA) to matured viral mRNA polyadenylated at the distal polyadenylation site, and therefore is important for capsid protein expression (53,143,173). In addition, HBoV1 holds unique features in the genus *Bocaparvovirus*: it naturally replicates in non-dividing/polarized human airway epithelial cells, and the replication is dependent on the cellular DNA damage and repair machinery (41). Upon transfection, the duplex replicative form genome (RF DNA) of HBoV1 replicates in human embryonic kidney (HEK) 293 cells and produces infectious progeny virions (69). Aside from the NP1, HBoV1 expresses two large non-structural proteins, NS1 and NS1-70 (an isoform of the NS1), and three other small nonstructural proteins, NS2, NS3, and NS4 (134). They share a C-terminus of 144 amino acids (aa). NS2 is indispensable for viral replication during infection of polarized human airway epithelial cells (134), whereas NS2-4 proteins are dispensable for viral DNA replication in HEK293 cells. NS1-70 is expressed at very low level in HEK293 cells transfected with the duplex HBoV1 genome, compared to that during HBoV1 infection of differentiated human airway epithelial cells (134).

Parvovirus replication generates monomer and dimer replicative form DNA (mRF and dRF DNA, respectively) intermediates via a unidirectional strand-displacement mechanism, from which the ends of progeny genomes are excised by viral replication initiator protein Rep78/68 or NS1 (10,35,164). For homotelomeric parvoviruses (e.g., adeno-associated virus [AAV]), in which the two genomic termini are inverted in sequence and identical in structure, the replication process is symmetrical. The tip of the T structure formed on the termini is critical for Rep78/68 to nick the replication origin (128). For heterotelomeric autonomous parvoviruses (e.g., MVM and HBoV1), in which the two genomic termini are dissimilar, the 3' end (left-end) hairpin (LEH) structure of the negative sense single stranded DNA (ssDNA) viral genome that has a replication origin is critical to progress the replication intermediates and to produce the ssDNA genome for progeny virion production, and the 5' end right-end hairpin (REH) structure contains another replication origin that is required to replicate viral RF DNA (35). In MVM, the cruciform structure at REH is required for RF DNA replication (30). As most of the bocaparvovirus genome are negative in sense (145), we also termed the 3' end of the HBoV1 genome as LEH, and the 5' end as REH, similar to those in MVM. The HBoV1 LEH and REH also have disparity sequences and structures.

At either hairpin end of both homotelomeric and heterotelomeric viruses, the replication origin contains Rep78/68 or NS1 binding elements (RBEs/NSBEs) and a nicking site which is recognized and nicked by Rep78/68 or NS1 (30,33,36,128). Replication at the origins of both termini follows so-called "rolling hairpin replication model" and undergoes a serial of replicative intermediates (37,129). Rep78/68 or NS1 binds to RBEs/NSBEs in the origin, executes its endonuclease activity, nicks the 5'-3' single strand, and free up a hydroxyl (OH) group at the 3' end which functions as a primer for viral DNA synthesis by cellular DNA polymerases. The binding and nicking properties characterized by in vivo or in vitro studies suggest that RBE or NSBE is several tetra-nucleotide repeats, which are directly recognized by the origin binding domain (OBD) of the Rep78/68 or NS1. The nicking site is normally 7-17-nt (nucleotide) ahead

of the RBE or NSBE at the 5' end. The genome structure of HBoV1 is unique among these heterotelomeric parvoviruses. The LEH forms a rabbit-ear structure of 140-nt with mismatched nucleotides ("bubbles") inside, and the REH consists of a perfect palindromic sequence of 200-nt in length (69). Of note, the REH of two other bocaparvoviruses, MVC and BPV1, are able to form a cruciform structure (145).

Because of the unique REH structure of the HBoV1 genome, we sought to define the minimal requirements for HBoV1 DNA replication at the REH both in cis and in trans using the duplex HBoV1 genome in HEK293 cells. We identified a 46-nt minimal replication origin at the REH of HBoV1 (OriR), which contains a nicking site and unconventional NSBEs. In addition, we uncovered new properties of nonstructural proteins NS1 and NP1 during viral DNA replication at the OriR.

Materials and Methods:

Cell culture.

HEK293 cells (CRL-1573, ATCC) were cultured in Dulbecco's Modified Eagle Medium (DMEM) with 10% fetal calf serum (FCS). Cells were incubated at 37°C with 5% CO_2. HEK 293F cells (Life Technologies/Thermo Fisher Scientific Inc, Carlsbad, CA) were cultured in suspension in Freestyle™ 293 medium (Life Technologies) at 37°C with 8% CO_2.

Primary human airway epithelium cultured at an air-liquid interface (HAE-ALI) was generated and cultured as previously described (41,69). HAE-ALI cultures that had a transepithelial electrical resistance (TEER) of >1000 $\Omega \cdot cm^2$ were selected to use in this study.

Plasmid DNA construction.

(i) pIHBoV1-based constructs: The parent HBoV1 infectious clone (pIHBoV1) has been described previously (69). The LEH-deleted plasmid pIHBoV1(LEH-) was constructed by

deleting the HBoV1 genome sequence of nt 1-140 in pIHBoV1. pIHBoV1(NS1-) and pIHBoV1(NP1-), which have the NS1 and NP1 ORFs, respectively, early terminated, and pIHBoV1(VP1/3-) that has both the capsid proteins VP1 and VP3 ORFs early terminated, were previously described (69). pIHBoV1(REH-), the REH-deleted plasmid, was constructed by deleting the HBoV1 sequence of nt 5,303-5,543 in pIHBoV1. pIHBoV1(LEH-VP1/3-) was constructed by deleting LEH and early terminating VP1 and VP3 ORFs. Based on the pIHBoV1(LEH-VP1/3-), an Xba I was inserted at nt 5,344 to construct REH-truncated mutants p∆REH1-24, which are diagrammed in **Fig. 3-2**. pIHBoV1(3'NCR-), the 3' noncoding region (3' NCR)-deleted plasmid, was constructed by deleting the HBoV1 sequence of nt 5,221-5,291 in pIHBoV1. pIHBoV1(VP-) was constructed by deleting the HBoV1 sequence of nt 3,380-5,119 in pIHBoV1.

(ii) pHBoV1Ori and pHBoV1Ori-based constructs: p∆REH21 was renamed pHBoV1Ori that has the minimal replication origin at the REH (OriR) of nt 5,357-5,402.

pHBoV1λ200Ori, pHBoV1λ400Ori, and pHBoV1λ1000Ori were constructed by inserting Lambda (λ) DNA sequences of 200 bp (nt 10,030-10,230), 400 bp (nt 10,030-10,430), and 1,000 bp (nt 10,030-11,030), respectively, in front of the OriR in pHBoV1Ori.

pHBoV1(NS1-)Ori and pHBoV1(NP1-)Ori were constructed by early terminating the NS1 and NP1 ORFs, respectively, in pHBoV1Ori using strategies described previously (69).

pNS1m^{13}QOri (Mut Q), pNS1m^{54}PHP^{56}Ori (Mut P), pNS1m^{123}EGL^{125}Ori (Mut E), pNS1m^{115}HCH^{117}Ori (Mut Endo), pNS1m^{127}KR^{128}Ori (Mut K), and pNS1m^{193}RR^{194}Ori (Mut R) were constructed by mutating the amino acids as indicated by the positions to alanine(s) in the context of pHBoV1Ori. They are diagrammed in **Fig. 3-9**.

pNSBEm1-8 and pTRSm1-7 plasmids were constructed by introducing various mutations in the putative NSBEs and nicking site of the OriR, respectively, in pHBoV1Ori. These plasmids are diagrammed in **Fig. 3-7A** and **Fig. 3-8A**, respectively, with mutations shown.

(iii) HBoV1 NS1 and parvovirus B19 (B19V) NS1-expressing plasmids: HBoV1 and B19V NS1 coding sequences were optimized for mammalian cell expression at Integrated DNA Technologies, Inc. (IDT, Coralville, IA), tagged with a Flag tag at the C-terminus, and were cloned in pCI expression vector (Promega, Madison, WI), resulting in pOptHBoV1NS1 and pOptB19VNS1.

All nucleotide numbers of HBoV1 and Lambda (λ) DNA are referred to as Genbank accession no. JQ923422 and NC_001416, respectively, unless otherwise specified.

In vivo DNA replication analysis.

HEK293 cells were seeded in 6 well plates or 60mm dishes one day before transfection. At a confluence of 70%, cells were transfected with LipoD293 reagent (SignaGen, Gaithersburg, MD) or Lipofactamine and Plus reagent (Life Technologies) following the manufacturers' instructions.

Low-molecular weight DNA (Hirt DNA) was extracted and digested with Dpn I, followed by Southern blotting. These steps were performed exactly as previously described (63). After hybridization, the membrane was exposed to a phosphor screen. The screen was then scanned on a phosphor imager (GE Typhoon FLA 9000, Fuji). The developed image was processed and analyzed using ImageQuant TL8.1 software (GE Healthcare, Marlborough, MA).

BrdU incorporation, immunofluorescence (IF) assay, and proximity ligation assay (PLA).

For virus-infected differentiated airway epithelial cells, we treated the infected HAE-ALI treated with 5 mM EDTA for 5 mins and then trypsinized the infected cells off the insert. We resuspended ~1 × 10^5 cells in 1 ml of the ALI medium with BrdU (Sigma, St Louis, MO) at 30 μM for 20 min. For transfected HEK293 cells, at two days post-transfection, the cells were incubated with BrdU for 30 min, followed a previously published method (99). Then, the labeled cells were cytospun onto slides for IF analysis.

IF analysis was performed following a method described previously (99,100), with antibodies against proteins or BrdU as indicated in **Fig. 3-5**. Confocal images were taken with an Eclipse C1 Plus confocal microscope (Nikon) controlled by Nikon EZ-C1 software. DAPI (4',6-diamidino-2-phenylindole) was used to stain the nucleus.

The Duolink PLA Kit (Sigma) was used to perform PLA according to the manufacturer's instructions as previously described (41).

Antibody production and antibodies used.

HBoV1 anti-NS1C antibody was produced as previously described (16), which reacts with all four NS proteins (NS1-4) (134). All animal procedures were approved by the Institutional Animal Care and Use Committee of the University of Kansas Medical Center. Rabbit anti-HBoV1 NP1 antibody (106) was a kind gift from Dr. Peter Tattersall at Yale University. Rabbit anti-BrdU (cat no.: 600-401-C29, Rockland, Limerick, PA), mouse anti-Flag monoclonal antibody (Sigma, St. Louis, MO), and secondary antibodies for IF assay (Jackson ImmunoResearch Inc., West Grove, PA) were purchased.

Rapid amplification of the 3' end of the nicked DNA.

DNA tailing reaction was performed using terminal transferase (NEB, Ipswich, MA). Basically, the reaction was composed of 5.0 μl of 2.5 mM $CoCl_2$, 1 μl of 10-50 times diluted Hirt DNA (from ~500 cells), 0.5 μl of 10 mM dATP, 0.5 μl of Terminal Transferase (20 units/μl), and deionized H_2O in a final volume of 50 μl. The reaction was incubated at 37°C for 30 min. Two μl of the product was used as template for PCR amplification using forward primer (5'-CTG TCT AGA ATG ATC AAT GTA TGC CAG-3', nt 5,121 to nt 5,138) and reverse primer (5'- is CAC GGA TCC TTT TTT TTT TTT TTT T-3'). Amplified fragments were cloned into pcDNA3 (Life Technologies) through Xba I and BamH I sites. Twenty positive clones were sequenced.

Protein expression and purification.

One 500 ml suspension culture of 293F cells (10^6 cells/ml) was transfected with pOpti-HBoV1NS1 or pOptiB19VNS1, using TransIT-PRO® following the manufacturer's instructions. At 3 days post-transfection, cells were lysed in L buffer (50 mM Tris pH 7.4, 150 mM NaCl, 1 mM EDTA, 1% Triton-X100, 1mM dithiothreitol (DTT), 5mM ATP, and 5 mM $MgCl_2$) supplemented with protease inhibitors (Cat. No: S8820, Sigma). Crude lysate was sonicated for 3 mins at a frequency of 15 sec/25 sec on/off, pulse 70% by the VCX130 sonicator (Sonics & Materials Inc., Newtown, CT). The lysate was then centrifuged at 10,000 rpm for 15 mins and filtrated through a 0.2 μm filter. The filtered lysate was incubated with 1 ml of PBS (phosphate buffered saline, pH7.4)-prewashed anti-Flag G1 affinity resin (Genscript, Piscataway, NJ) at 4°C for at least 1 hr. Then, the beads were washed with washing buffer (50 mM Tris, pH7.4, 500 mM NaCl, 0.05% Triton-X100, and protease inhibitors) 5 times of resin volume, and were eluted with 3 × Flag peptide (APExBIO, Houston, TX) at a concentration of 200 μg/ml. Finally, the eluted protein was dialyzed against PBS twice and against binding buffer (B buffer: 20 mM Tris-HCl, pH 8.0, 125 mM NaCl, 10% glycerol, 1% NP-40, 5 mM DTT, and protease inhibitors) once, and was concentrated 10 times using polyethylene glycol 6000 (PEG). The concentrated protein was quantified, aliquoted, and stored at -80°C.

Gel shift assay.

Gel shift assay was performed essentially following a published method (24). Duplex DNA probe was generated by annealing complementary oligos, at a concentration of 45 μM, in an annealing buffer (10 mM Tris, pH 7.5, 50 mM NaCl, 1 mM EDTA) after boiling for 5 mins. The dsDNA probe was cleaned using a G-50 column (GE Healthcare). Duplex DNA probes are HBoV1 OriR (**Fig. 3-2F**), HBoV1 OriR-mut (5'-CGC GAA ACT CTA TAT CTT TTA ATG GCA GAA TTC AGC ACA TGC GCC A-3'), B19V Ori (5'-GCC GCC GGT CGC CGC CGG TAG GCG

GGA CTT CCG GTA CA-3') (151), and B19V Ori-mut (5'-AGC TAT TGG TCG CTA TTG GTA GGC GGG ACT-3' (151).

One µl of the duplex DNA probe was labeled with γ-p32-ATP using T4 polynucleotide (NEB) following the manufacturer's instructions. The binding reaction consisted of 8 µl of 2.5 × B buffer (see above), 2 µl of diluted duplex DNA probe (at 1:10,000), with/without 2 µl of purified protein (300 ng/µl), 2 µl of unlabeled (cold) probe at a concentration (ratio) specified in **Fig. 3-10**, and dH_2O to a total volume of 20 µl. In some reactions, poly[d(I-C)] was added at a final concentration of 2 µg/ml. The reactions were incubated on ice for 20 mins, loaded directly into a pre-run 5% non-denaturing polyacrylamide gel, and electrophoresed for 45 mins at 100 volts. Finally, the acrylamide gel was dried by vacuum at 70°C and exposed to a phosphor screen.

Nuclear extract (NE) preparation.

Nuclear extraction was performed following a method described previously (44). HEK293 cells of one dish of 100 mm were transfected with pOptiHBoV1NS1 or pOptiB19VNS1. At 2 days post-transfection, cells were collected, washed with ice-cold PBS, and pelleted. The cell pellet was lysed in five volumes of L buffer (10 mM HEPES, pH7.5, 10mM KCl, 0.1 mM EDTA, 1 mM DTT, 0.5% NP-40, and protease inhibitors). The lysate was vortexed and centrifuged at 500 g for 5 mins at 4°C. The pelleted nuclei were washed 3 times with 1 ml W buffer (10 mM HEPES, pH 7.5, 10mM KCl, 0.1 mM EDTA, 1 mM DTT, and protease inhibitors). Nuclei were resuspended in 0.25 ml of NE buffer (20 mM HEPES, pH 7.5, 420 mM NaCl, 1 mM EDTA, 1 mM DTT, 25% glycerol (v/v), and protease inhibitors), and were incubated on ice for 30 mins. Finally, nuclear extract was obtained as the supernatant by centrifuging the lysed nuclei at 12,000 g for 10 mins at 4°C, and was adjusted the NaCl concentration to 100 mM using B1 buffer (=buffer NE without NaCl).

Pull-down assay.

Biotin-labeled probe was generated by annealing two complementary oligos, in which one oligo was biotinylated, at a concentration of 5 μM. Annealed dsDNA probe was desalted using a G-50 column. Streptavidin-conjugated beads (Gold Biotechnology, St. Louis, MO) were prewashed following the manufacturer's instructions. Binding reaction consisted of 200 μl of 2.5 × B buffer with poly[d(I-C)], 100 μl of nuclear extract (~5 μg/ml), 1 μl of biotinylated probe, with/without unlabeled probe, and dH_2O in a total volume of 0.5 ml. The reactions were rotated at 4ºC overnight, and were pelleted by centrifugation at 1,000 g for 3 mins. The pellet was then washed 3 times with cold PBS before adding loading buffer. The samples were boiled for 5 mins and analyzed by SDS-polyacrylamide gel electrophoresis, followed by Western blotting.

Immunoprecipitation (IP) assay.

HEK293 cells cultured in one 60mm dish were mock-transfected or transfected with plasmids. At 2 days post-transfection, the cells were washed and lysed with 300 μl radioimmunoprecipitation assay (RIPA) buffer (50 mM Tris-HCl, pH 8.0, 150 mM NaCl, 1% NP-40, 0.5% sodium deoxycholate, 0.1% SDS, and protease inhibitors) with constant agitation for 30 mins at 4ºC. The cell lysates were centrifuged at 14,000 g for 3 mins at 4ºC, and the supernatant was collected. The rest supernatant (~220 μl) was pre-incubated with 40 μl of normal rat serum, 30 μl of prewashed protein A/G bead (ThermoFisher), and 2 μl of benzonase (ThermoFisher) for 3 hr at 4ºC with rotation. After preclearing, the supernatant was equally divided for incubation with either 2 μl of normal rat IgG (0.4 mg/ml, Santa Cruz, Dallas, TX) or 20 μl of rat antisera, 30 μl of protein A/G beads, and 300 μl of RIPA buffer at 4ºC overnight. Finally, the protein A/G beads were pelleted down and washed 3 times with ice cold PBS before mixing with loading dye for Western blotting.

Results

Identification of viral elements required in cis or in trans for HBoV1 replication.

To understand the DNA replication mechanism of HBoV1, we first delineated viral DNA signals and viral proteins that are required for viral DNA replication. As diagrammed in **Fig. 3-1A**, the HBoV1 genome contains four noncoding sequences (LEH, P5 promoter region, 3' NCR, REH) and three ORFs that encode NS1-4, NP1, and VP1-3 proteins, respectively (134,173). The 3' non-coding region (3' NCR) contains a sequence of ~200 nts between the polyadenylation signal of VP mRNA and the REH. To dissect the minimal requirements for viral DNA replication, we carried out sequential deletions of the noncoding regions and early termination of the ORFs in the context of pIHBoV1. Southern blotting results showed a representative pattern of HBoV1 DNA replication including the Dpn I-digestion resistant bands: viral single-strand DNA (ssDNA, genome size), viral RF DNA and double RF (dRF) DNA, and plasmid-replicated DNA (**Fig. 3-1B**, lane 1). The results suggested that, without the LEH sequence, pIHBoV1(LEH-) still replicated but failed to excise the HBoV1 RF DNA out of the plasmid (**Fig. 3-1B**, lane 2). VP1/3-knockout plasmid pIHBoV1(VP1/3-) replicated better than the parent pIHBoV1 (**Fig. 3-1B**, lanes 5 *vs* 1). As noted, ssDNA was only produced from the transfections of pIHBoV1 and pIHBoV1(VP1/3-). However, pIHBoV1(NS1-), pIHBoV1(3'NCR-), and pIHBoV1(REH-) did not replicate (**Fig. 3-1B**, lanes 3, 6 and 7, respectively), and pIHBoV1(NP1-) replicated very poorly (**Fig. 3-1B**, lane 4), suggesting that the sequence at the 3' end, including REH and 3' NCR, and expression of NS1 and NP1 proteins were apparently critical to HBoV1 DNA replication. pIHBoV1(VP-), in which the VP encoding ORFs were largely deleted, replicated as well as the pIHBoV1 (**Fig. 3-1C**, lane 2).

Taken together, our results suggest that REH and 3' NCR are largely responsible for HBoV1 DNA replication as cis-acting elements, while NS1 and NP1 serve trans-acting functions (134). In the following experiments, we used both LEH deletion and the VP1/3 knockout

Figure 3-1. Identification of the cis-acting sequences and trans-acting proteins required for HBoV1 replication.

(A) Diagram of HBoV1 genome and mutants. HBoV1 genome is shown as a negative sense ssDNA. Sequentially from left to right, the functional elements are left-end hairpin (LEH, 3' end), P5 promoter, NS-coding region, NP1-coding region, VP-coding region, 3' noncoding region (3' NCR), and the right-end hairpin (REH, 5' end). The wild-type infectious clone is shown as duplex form DNA (dsDNA). Non-coding sequences LEH, 3' NCR, and REH were deleted as described in Materials and Methods. The ORF of NS, NP1, or VP was terminated as described in Materials and Methods. Dotted lines indicate sequence deletion, vertical bars indicate nucleotide mutations. **(B&C) Southern blot analysis.** The wild-type infectious clone (pIHBoV1) or the indicated mutants were transfected into HEK293 cells. At 2 days post transfection, low molecular weight (Hirt) DNA was extracted and applied for Southern blotting after Dpn I digestion. One hundred and twenty ng of pIHBoV1 digested with Dpn I at the same condition as Hirt DNA samples was used as Dpn I digestion control (Dpn I-Dig. Ctrl). RF, replicative form DNA intermediate, dRF, double RF DNA intermediate, ssDNA, single-stranded DNA. An arrow in panel A and an asterisks panel B indicate replicated DNA from the entire HBoV1 DNA-contained plasmid. M: a size marker.

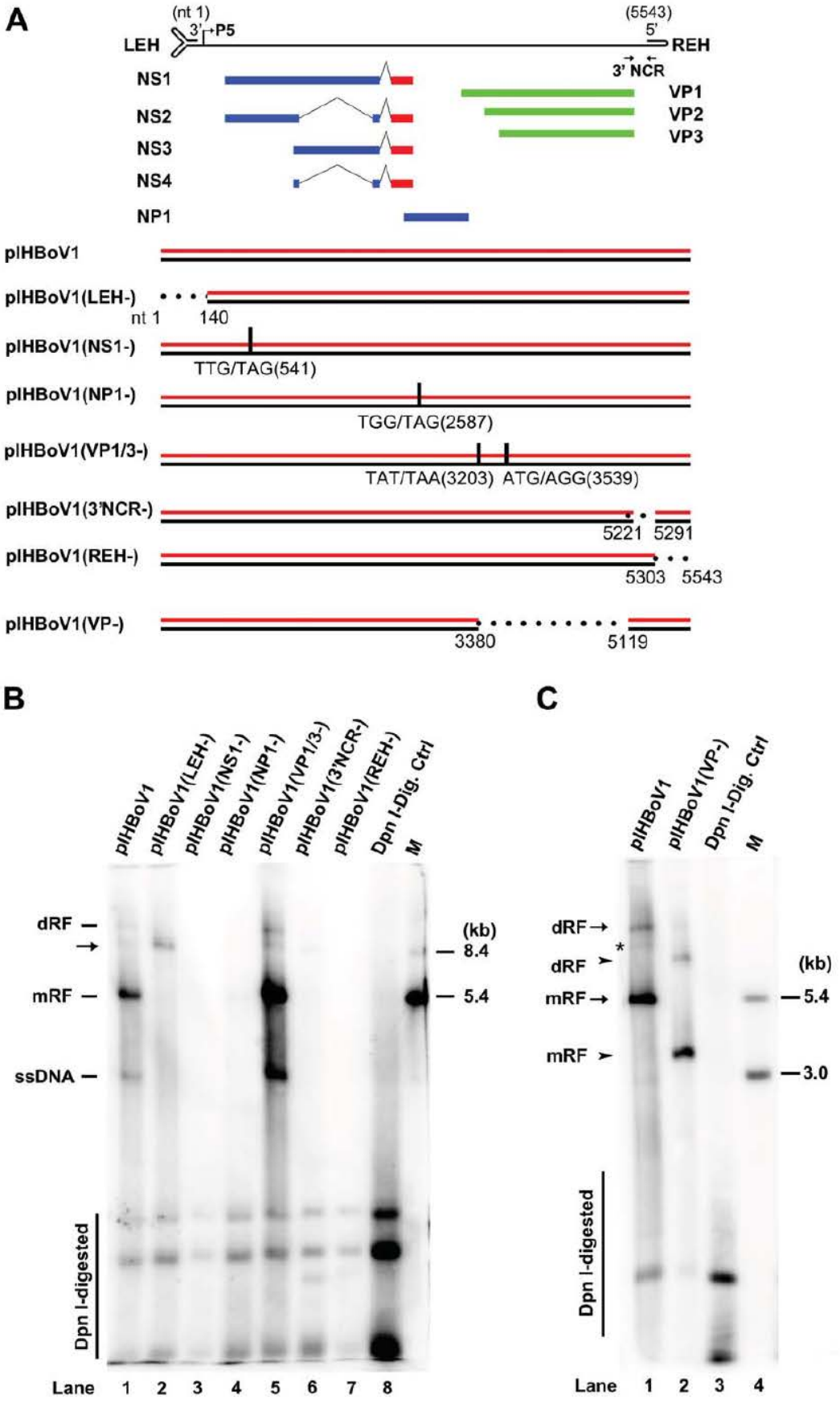
A
(nt 1)
3'
P5
LEH
(5543)
5'
REH
3' NCR
NS1
NS2
NS3
NS4
NP1
VP1
VP2
VP3
pIHBoV1
pIHBoV1(LEH-)
nt 1
140
pIHBoV1(NS1-)
TTG/TAG(541)
pIHBoV1(NP1-)
TGG/TAG(2587)
pIHBoV1(VP1/3-)
TAT/TAA(3203)
ATG/AGG(3539)
pIHBoV1(3'NCR-)
5221
5291
pIHBoV1(REH-)
5303
5543
pIHBoV1(VP-)
3380
5119
B
pIHBoV1
pIHBoV1(LEH-)
pIHBoV1(NS1-)
pIHBoV1(NP1-)
pIHBoV1(VP1/3-)
pIHBoV1(3'NCR-)
pIHBoV1(REH-)
Dpn I-Dig. Ctrl
M
dRF
mRF
ssDNA
(kb)
8.4
5.4
Dpn I-digested
Lane 1 2 3 4 5 6 7 8
C
pIHBoV1
pIHBoV1(VP-)
Dpn I-Dig. Ctrl
M
dRF
*
dRF
mRF
mRF
(kb)
5.4
3.0
Dpn I-digested
Lane 1 2 3 4

HBoV1 plasmid, pIHBoV1(LEH-VP1/3-), for further characterization of HBoV1 DNA replication at REH.

Identification of an HBoV1 right-end minimal replication origin (OriR).

For DNA replication of either dependoparvovirus or autonomous parvovirus, RBEs or NSBEs and a nicking site are requisite at the end palindromic hairpinned sequence (30,33,36,128). These two cis-signals are necessary for Rep78/68 or NS1 to recognize the replication origin and perform strand-specific nicking, and to initiate DNA replication. To identify the minimal replication-requisite sequence on REH, we constructed a serial of truncation mutants of the REH on the base of plHBoV1(LEH-VP1/3-) (**Fig. 3-2A**). We used linearized HBoV1 DNA for in vivo DNA replication analysis, in order to avoid circular plasmid DNA replication as that seen from pIHBoV1(LEH-) (**Fig. 3-1B**, lane 2). The first group of truncations contained a progressive deletion from the 3' end of the REH (**Fig. 3-2A**, Group I). The results showed that the level of viral DNA replication decreased as 3' end nucleotides of the REH were removed (**Fig. 3-2B**). As there was a clear decrease of viral DNA replication resulting from ΔREH2 to ΔREH3 HBoV1 DNA (**Fig. 3-2B**, lanes 3 vs 4), we fixed the right end at nt 5,430 of the ΔREH2 HBoV1 DNA, and started progressive truncations from the 5' end (nt 5,344) (**Fig. 3-2A**, Group II). Results of viral DNA replication analysis showed a large decrease in RF DNA from ΔREH10 to ΔREH11 (**Fig. 3-2C**, lanes 3 vs 4). Thus, we determined the 5' end of the OriR to be at nt 5,357, the 5' end of ΔREH10.

To define the 3' end of the OriR more carefully, we performed progressive deletions from the 3' end of ΔREH10 (nt 5,357). DNA replication analysis of the mutants from ΔREH17 and ΔREH19-24 showed that further deletions of the 3' end after nt 5,402 (**Fig. 3-2D**, ΔREH21/lane 6) significantly decreased the level of RF DNA (**Fig. 3-2E**). This result defined the 3' end of the OriR at nt 5,402. In addition, we created ΔREH18, in which three nucleotides were

Figure 3-2. Identification of the minimal replication origin at the REH (OriR).

(A) Diagram of REH deletion mutants. All REH deletion mutants were constructed based on the LEH-deleted and VP1/3-knockout plasmid pIHBoV1(LEH-VP1/3-). Group I mutants had deletions at the 3' end from nt 5,543 to 5,383. Group II mutants shared the 3' end deletion to nt 5,430 and were further deleted at the 5' end from nt 5,354nt to 5,384. Group III mutants shared the 5' end deletion to nt 5,357 except for ΔREH18, which had a 5' end at nt 5,360. The deletion at the 3' end started from nt 5,410nt to 5,390. **(B-D) Southern blot analyses.** HEK293 cells were transfected with linearized mutant HBoV1 DNAs, and Hirt DNA samples were extracted at two days post transfection. DpnI digested Hirt DNA samples were applied for Southern blotting. **(E) Quantification.** Three experiments were repeated for panel D, and the RF DNA was quantified in each lane. The level of RF DNA from the wild-type HBoV1 was set up as 100% (Lane 1) after normalization with the main Dpn I-digested bands. N.S., not significant, *, $P<0.05$, **, $P<0.01$. **(F) Minimal replication origin (OriR).** The sequence of the identified OriR is shown in duplex DNA.

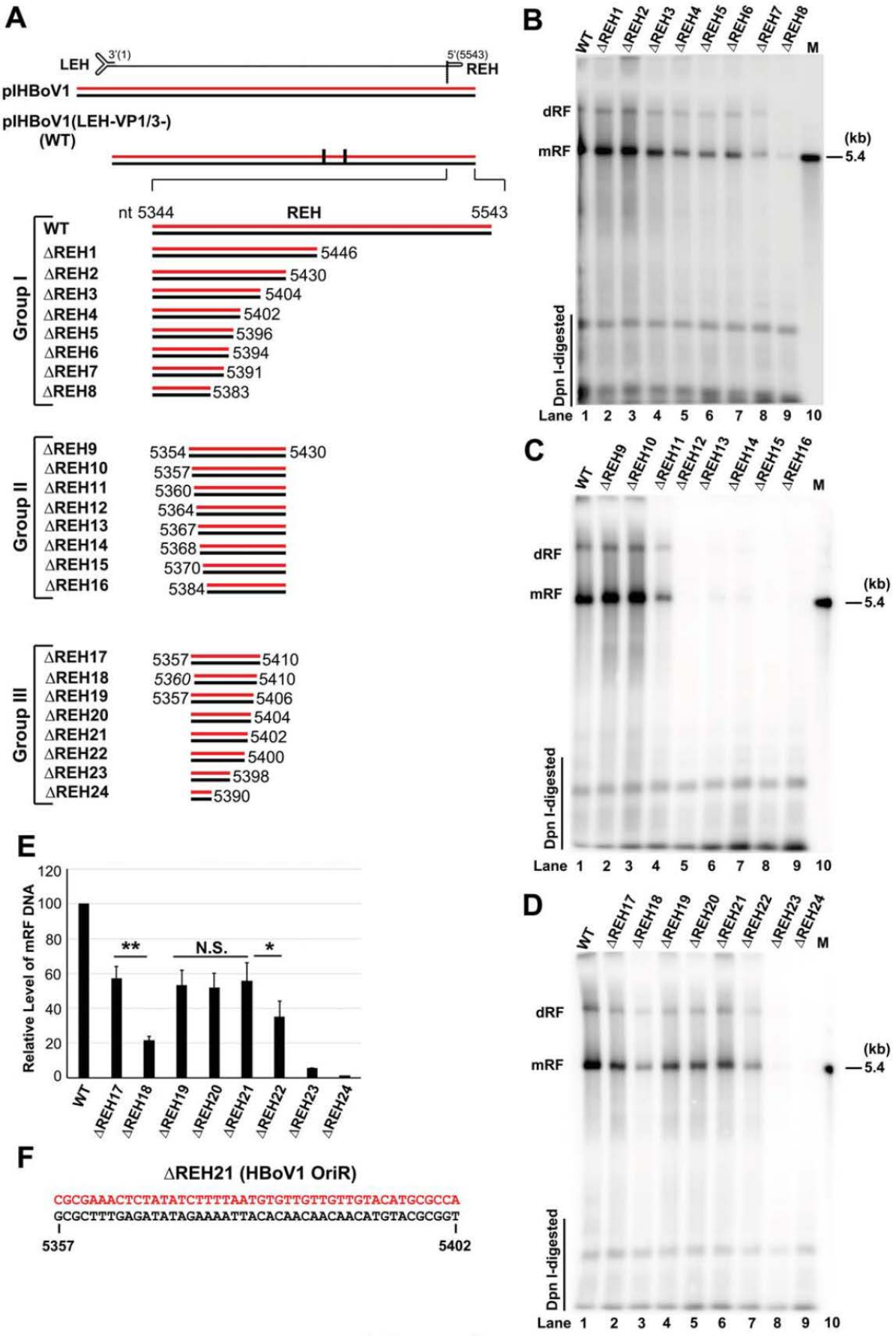
A
LEH
3'(1)
5'(5543)
REH
pIHBoV1
pIHBoV1(LEH-VP1/3-)
(WT)
nt 5344
REH
5543
WT
ΔREH1
ΔREH2
ΔREH3
ΔREH4
ΔREH5
ΔREH6
ΔREH7
ΔREH8
Group I
5446
5430
5404
5402
5396
5394
5391
5383
ΔREH9
ΔREH10
ΔREH11
ΔREH12
ΔREH13
ΔREH14
ΔREH15
ΔREH16
Group II
5354
5430
5357
5360
5364
5367
5368
5370
5384
ΔREH17
ΔREH18
ΔREH19
ΔREH20
ΔREH21
ΔREH22
ΔREH23
ΔREH24
Group III
5357
5410
5360
5410
5357
5406
5404
5402
5400
5398
5390
B
WT
ΔREH1
ΔREH2
ΔREH3
ΔREH4
ΔREH5
ΔREH6
ΔREH7
ΔREH8
M
dRF
mRF
(kb)
5.4
Dpn I-digested
Lane 1 2 3 4 5 6 7 8 9 10
C
WT
ΔREH9
ΔREH10
ΔREH11
ΔREH12
ΔREH13
ΔREH14
ΔREH15
ΔREH16
M
dRF
mRF
(kb)
5.4
Dpn I-digested
Lane 1 2 3 4 5 6 7 8 9 10
D
WT
ΔREH17
ΔREH18
ΔREH19
ΔREH20
ΔREH21
ΔREH22
ΔREH23
ΔREH24
M
dRF
mRF
(kb)
5.4
Dpn I-digested
Lane 1 2 3 4 5 6 7 8 9 10
E
Relative Level of mRF DNA
120
100
80
60
40
20
0
**
N.S.
*
WT
ΔREH17
ΔREH18
ΔREH19
ΔREH20
ΔREH21
ΔREH22
ΔREH23
ΔREH24
F
ΔREH21 (HBoV1 OriR)
CGCGAAACTCTATATCTTTTAATGTGTTGTTGTTGTACATGCGCCA
GCGCTTTGAGATATAGAAAATTACACAACAACAACATGTACGCGGT
5357
5402

deleted at the 5' end in ΔREH17, to confirm the 5' end of the OriR. The result showed that replication from ΔREH17 was significantly decreased by ~3-fold (**Fig. 3-2D**, lane 3).

Collectively, we defined HBoV1 OriR as a 46-nt DNA of nt 5,357-5,402 (**Fig. 3-2F**). Although these deleted sequences which flank the OriR are dispensable for the replication at the OriR, they are required for the maximum DNA replication at the REH. Of note, HBoV1 has a long 3' NCR in front of the OriR. To clarify whether the OriR replicates viral DNA independent of the 3' NCR, we inserted various λ DNA of 0.2, 0.4, and 1.0 kb between the 3' NCR and the OriR in HBoV1Ori DNA (**Fig. 3A**). DNA replication analysis showed that the OriR conferred viral DNA replication regardless of the insertion sizes between the 3' NCR and OriR, supporting that the OriR functions as a template of DNA replication independently of the adjacent 3' NCR (**Fig. 3-3B**).

NP1 colocalized with NS proteins within the viral DNA replication centers, and is required for viral DNA replication at OriR.

We next checked the trans-acting factors that facilitate viral DNA replication at OriR. We constructed NS1 or NP1 knockout plasmids based on pHBoV1Ori, and performed viral DNA replication analysis. We observed that, without NS1/2 or NP1 expression, replication at the OriR was abolished (**Fig. 3-4**, lanes 2&3), reflecting that NS1 and NP1 are required for HBoV1 DNA replication at the OriR, since NS2 is not required for HBoV1 DNA replication in HEK293 cells (134).

Replication of parvovirus MVM and H-1 takes place in discrete subnuclear compartments, where termed autonomous parvovirus-associated replication (APAR) bodies (9,38). APAR bodies are active sites of viral DNA replication and contain cellular DNA replication factors and parvovirus NS1 (9). We located the APAR bodies using BrdU to pulse chase active replicating viral ssDNA (99,100). Similar to other parvoviruses (9,38), the APAR bodies of HBoV1 replication showed various patterns in different cells, from foci-like dots

Figure 3-3. HBoV1 OriR replicated independent of upstream 3' NCR.

(A) Diagram of λ DNA insertion mutants. Based on pHBoV1Ori, 200 bp, 400 bp, or 1000 bp of λ DNA was inserted between 3' NCR and REH. **(B) Southern blot analysis.** HEK293 cells were transfected with linearized mutants. At two days post transfection, Hirt DNA samples were extracted and digested with Dpn I before they were applied for Southern blotting. Sixty ng of IHBoV1 was digested as Dpn I digestion control.

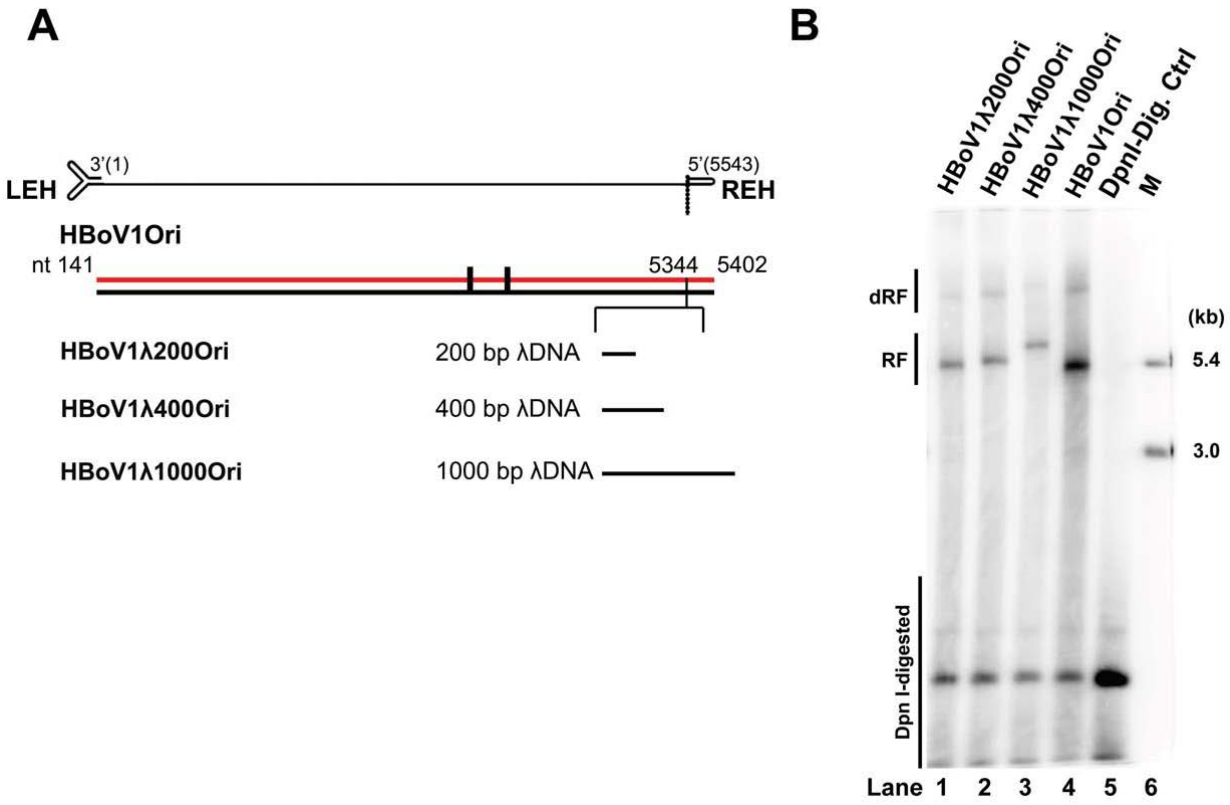
A
LEH
3'(1)
5'(5543)
REH
HBoV1Ori
nt 141
5344
5402
HBoV1λ200Ori
200 bp λDNA
HBoV1λ400Ori
400 bp λDNA
HBoV1λ1000Ori
1000 bp λDNA
B
HBoV1λ200Ori
HBoV1λ400Ori
HBoV1λ1000Ori
HBoV1Ori
DpnI-Dig. Ctrl
M
dRF
RF
(kb)
5.4
3.0
Dpn I-digested
Lane 1 2 3 4 5 6

Figure 3-4. Both NS1 and NP1 are required for DNA replication at OriR.

HEK293 cells were transfected with HBoV1Ori or its mutants HBoV1(NS1-)Ori and HBoV1(NP1-)Ori. Hirt DNA samples were extracted at two days post transfection and were digested with Dpn I for Southern blotting. Sixty ng of IHBoV1 digested by DpnI was used as a digestion control.

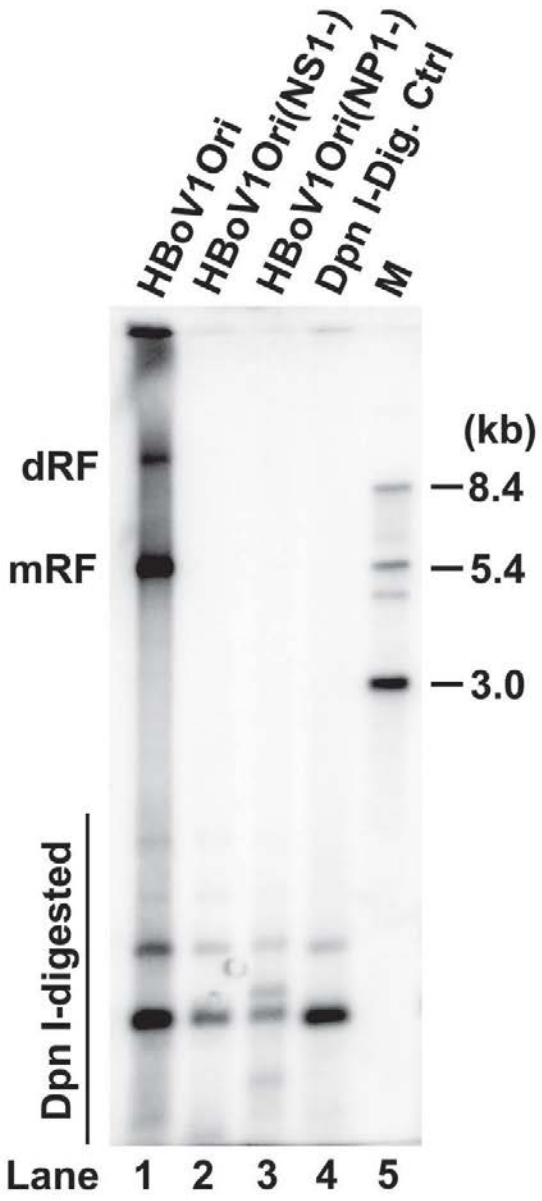
HBoV1Ori
HBoV1Ori(NS1-)
HBoV1Ori(NP1-)
Dpn I-Dig. Ctrl
M
(kb)
dRF
mRF
8.4
5.4
3.0
Dpn I-digested
Lane 1 2 3 4 5

to broad distribution in the nucleus, and colocalized with NS proteins stained with anti-NS1C in HEK 293 cells transfected with pHBoV1Ori or pIHBoV1 (**Fig. 3-5A**, NS/BrdU). Notably, co-localization patterns of NP1 and BrdU staining were similarly observed as the NS and BrdU co-staining, suggesting that both NP1 and NS localized within APAR bodies (**Fig. 3-5B**, NP1/BrdU). In support of this hypothesis, NS and NP1 proteins colocalized in the nucleus of pHBoV1Ori or pIHBoV1-transfected cells (**Fig. 3-5C**, NP1/NS). More importantly, in HBoV1-infected HAE cells, NS and NP1 co-localized well within the BrdU-chased APAR bodies (**Fig. 3-5D-F**). To confirm the localization of NP1, we used proximity ligation assay (PLA) to visualize interactions of NP1 with BrdU-labeled viral ssDNA or dsDNA/ssDNA intermediates. We observed clearly positive fluorescent foci in the nucleus of pHBoV1Ori and pIHBoV1-transfected, or HBoV1-infected cells stained with anti-NP1 and anti-BrdU antibodies (**Fig. 3-5G**). PLA shows bright signals only if the two molecules localize proximately at a distance of ~20 nm (138).

To explore a direct interaction between NS1 and NP1, we performed immunoprecipitation assays. Cells transfected with pHBoV1Ori were lysed and pre-cleared with normal rat sera. Pre-clear lysates were immunoprecipitated with control rat IgG or anti-NP1 serum in the presence of nuclease treatment, and were then evaluated for NS1 by Western blotting. Neither NS1, NS2, NS3 nor NS4 were co-immunoprecipitated with NP1 (**Fig. 3-6A**, lanes 6 vs 4). As a control, using an anti-NS1C antibody, all NS proteins could be immunoprecipitated (**Fig. 3-6B**, lanes 3 vs 1). These results suggest that NS1-4 and NP1 proteins do not directly interact.

Taken together, these results suggest that either by transfection of pIHBoV1/pHBoV1Ori or during viral infection, HBoV1 NS1-4 and NP1 proteins function synergistically in the viral DNA replication centers (APAR bodies) but without a direct interaction. More importantly, these results confirm a direct involvement of the HBoV1 NP1 during viral DNA replication at OriR.

Figure 5. NS and NP1 co-localized with the BrdU-chased viral DNA replication centers.

(A-C) Localization of NS, NP1, and BrdU-incorporated HBoV1 DNA in transfected cells. HEK 293 cells were transfected with pBB (vector backbone), pIHBoV1, or pHBoV1Ori. At two days post transfection, the cells were incorporated with BrdU before being harvested and then applied for immunofluorescence staining. Anti-NS1C with anti-BrdU (A), anti-NP1 with anti-BrdU (B), and anti-NS1C with anti-NP1 were co-stained. **(D-F) Localization of NS1, NP1, and BrdU incorporated HBoV1 DNA during infection.** HAE-ALI cultures were infected by HBoV1 at an MOI of 10. At 7 days post infection, cells were incorporated with BrdU and applied for immunofluorescence analysis. NS, NP1, or BrdU were co-stained in different combinations. **(G)** Interaction of NP1 with BrdU-chased viral DNA. Transfected cells, as indicated, were pulse chased with BrdU, and were analyzed by PLA with anti-NP1 and anti-BrdU antibody. DAPI was used to stain the nucleus. Confocal images were taken at 100 × under a Nikon confocal microscope.

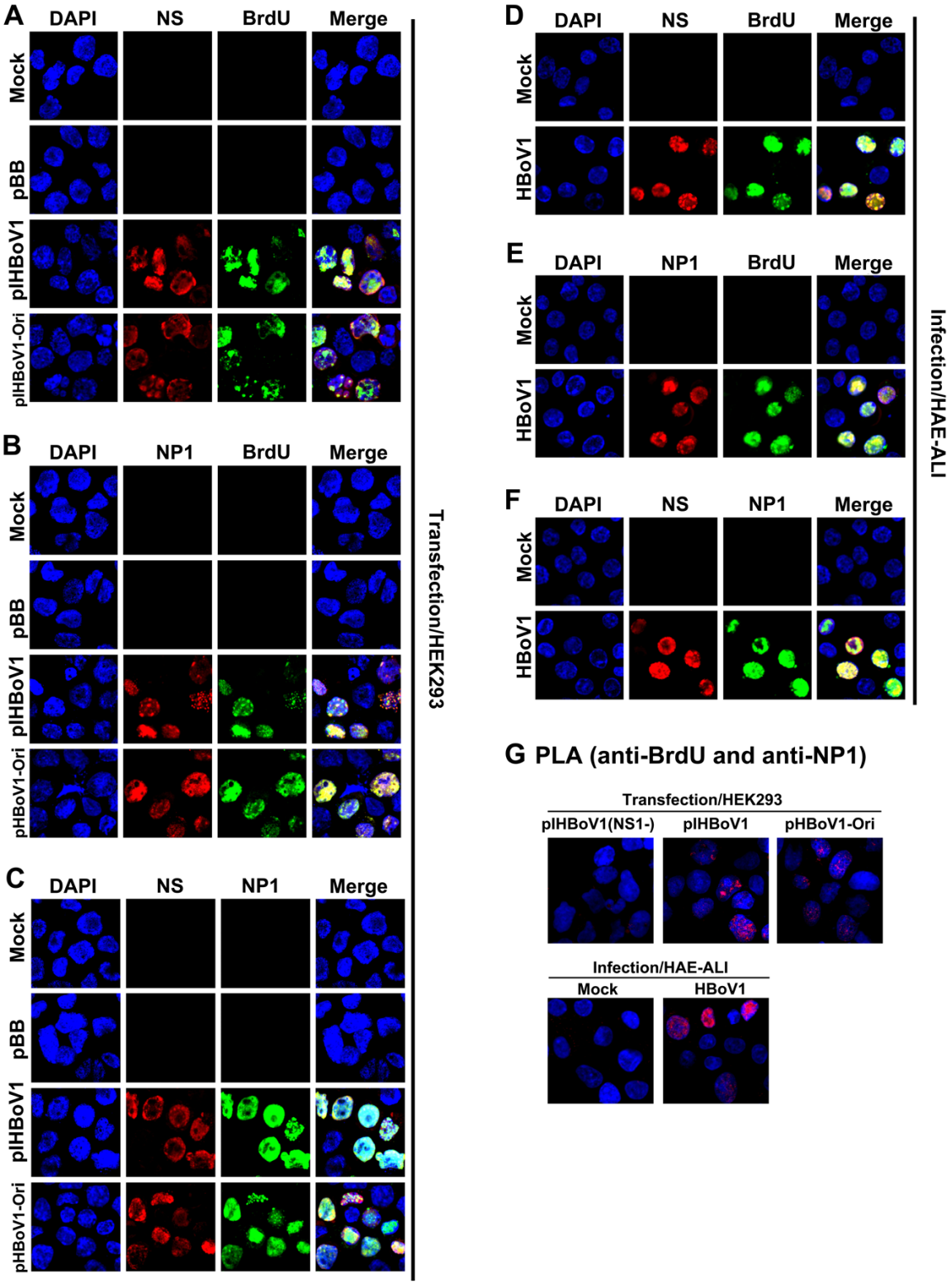
A
DAPI
NS
BrdU
Merge
Mock
pBB
plHBoV1
plHBoV1-Ori
B
DAPI
NP1
BrdU
Merge
Mock
pBB
plHBoV1
pHBoV1-Ori
C
DAPI
NS
NP1
Merge
Mock
pBB
plHBoV1
pHBoV1-Ori
Transfection/HEK293
D
DAPI
NS
BrdU
Merge
Mock
HBoV1
E
DAPI
NP1
BrdU
Merge
Mock
HBoV1
F
DAPI
NS
NP1
Merge
Mock
HBoV1
Infection/HAE-ALI
G PLA (anti-BrdU and anti-NP1)
Transfection/HEK293
plHBoV1(NS1-)
plHBoV1
pHBoV1-Ori
Infection/HAE-ALI
Mock
HBoV1

Figure 3- 6. NS and NP1 did not interact directly.

HEK 293 cells were transfected with pHBoV1Ori or mock transfected. At two days post-transfection, cells were washed, lysed and pre-cleared with normal rat serum as described in the Material and Methods. Pre-cleared lysates were immunoprecipitated with either rat IgG and rat anti-NP1 rat serum, respectively (**A**), or rat IgG and rat anti-NS1C serum, respectively (**B**). Immunoprecipitated proteins were analyzed by Western blotting using an anti-NS1C antibody. Ten µl of the pre-cleared lysates were loaded as input controls.

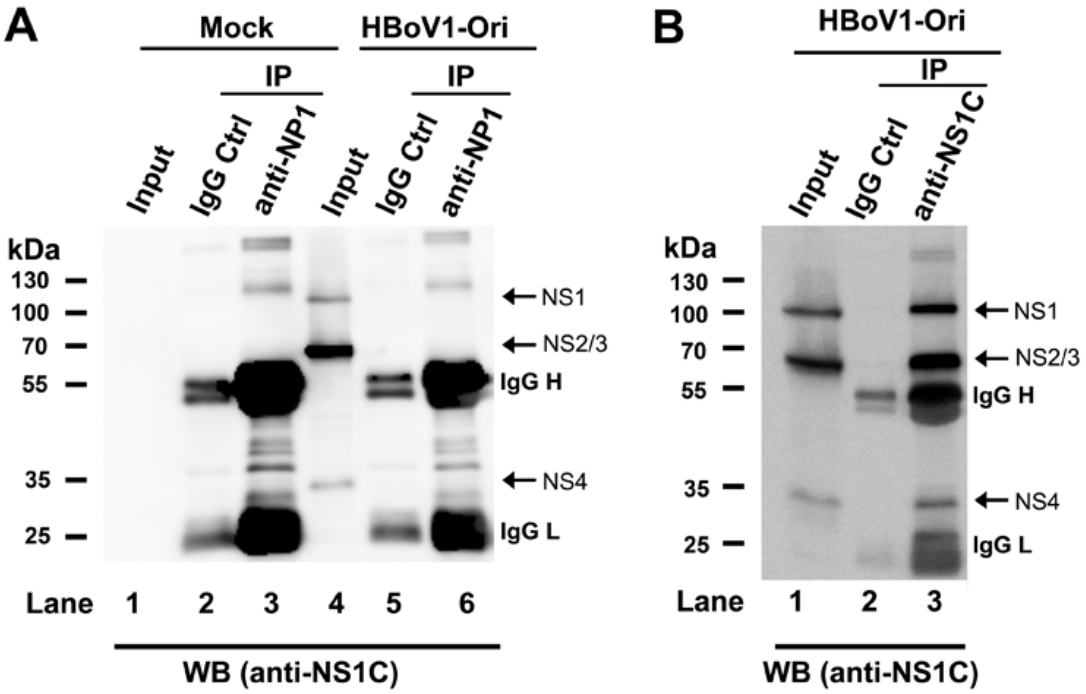
A
Mock
HBoV1-Ori
IP
IP
Input
IgG Ctrl
anti-NP1
Input
IgG Ctrl
anti-NP1
kDa
130
100
70
55
35
25
NS1
NS2/3
IgG H
NS4
IgG L
Lane 1 2 3 4 5 6
WB (anti-NS1C)
B
HBoV1-Ori
IP
Input
IgG Ctrl
anti-NS1C
kDa
130
100
70
55
35
25
NS1
NS2/3
IgG H
NS4
IgG L
Lane 1 2 3
WB (anti-NS1C)

Identification of the NS1 binding elements (NSBES) and nicking site within OriR.

The replication origins of parvoviruses harbor multiple binding elements of Rep78/68 or NS1 and a specific nicking site (30,33,36,128). Therefore, we next aimed to define the NSBE and nicking site by means of mutagenesis. The NSBEs characterized in AAV and MVM by both in vivo and in vitro studies are several tetra-nucleotides repeats, which are directly recognized by the origin binding domain (OBD) of the AAV Rep68/78 or MVM NS1. Notably, there are no identical NSBEs for HBoV1 NS1 binding that can be located in both REH and LEH (69). In contrast, we found that similar to the 4 repeats of tri-nucleotides in *Galleria mellonella densovirus* (GmDNV), there are 4 repeats of "TGT" tri-nucleotides "5'-TGT TGT TGT TGT-3'" in OriR (**Fig. 3-7A**) (153).

We therefore made serial mutations in the "TGT" repeated region in OriR, and performed in vivo DNA replication analysis. The results showed that all these mutations of the "TGT" tri-nucleotides significantly decreased DNA replication to various levels under 40% of the activity of the wild-type (**Fig. 3-7B&C**), moreover, the mutation of multiple "TGT" progressively disable DNA replication to a greater extent. For example, mutating two "TGT" remained DNA replication better than mutating three "TGT" (**Fig. 3-7B&C**, lanes 1&2 vs lanes 4-7). Mutating all four "TGT" decreased DNA replication the most, at level of only 5% of the wild-type (**Fig. 3-7B&C**, lane 3). Thus, our results suggest that this "TGT" repeating sequence is likely the HBoV1 NSBEs.

The nicking sites of parvoviruses are not conserved (36). In principle, after nicking, the Ori reveals transient nicked intermediate (ssDNA breaks) before the free 3'–OH extends by DNA polymerase (35). We employed a strategy of rapid amplification of the nicked 3' end to characterize the intermediates of the resolved OriR after NS1 nicking. Using Hirt DNA extracted from pIHBoV1- or pHBoV1Ori-transfected cells, we added adenosines to extend the 3' end with polyA residues. With subsequent PCR amplification and cloning, we mapped a few transient ending sites in the OriR (**Fig. 3-8A**). To identify the nicking among these ending sites, we

Figure 7. Characterization of the putative NS1 binding element in vivo.

(A) Diagram of NSBE mutants. The wild-type OriR and mutated sequences of the putative NSBE are shown. The putative NSBE include $(TGT)_4$, and the mutants were constructed based on various mutations of the “TGT” repeats. Dotted sites represent identical nucleotides. **(B) Southern blot analysis.** HEK293 cells were transfected with linearized wild-type Ori and NSBE mutants as indicated. Hirt DNA samples were extracted and applied for Southern blotting after Dpn I digestion. **(C) Quantification.** After normalization with Dpn I-digested bands, the RF DNA bands on blots were quantified. Relative levels to the RF DNA from HBoV1Ori (lane 9) are shown with averages and standard deviations from three independent experiments.

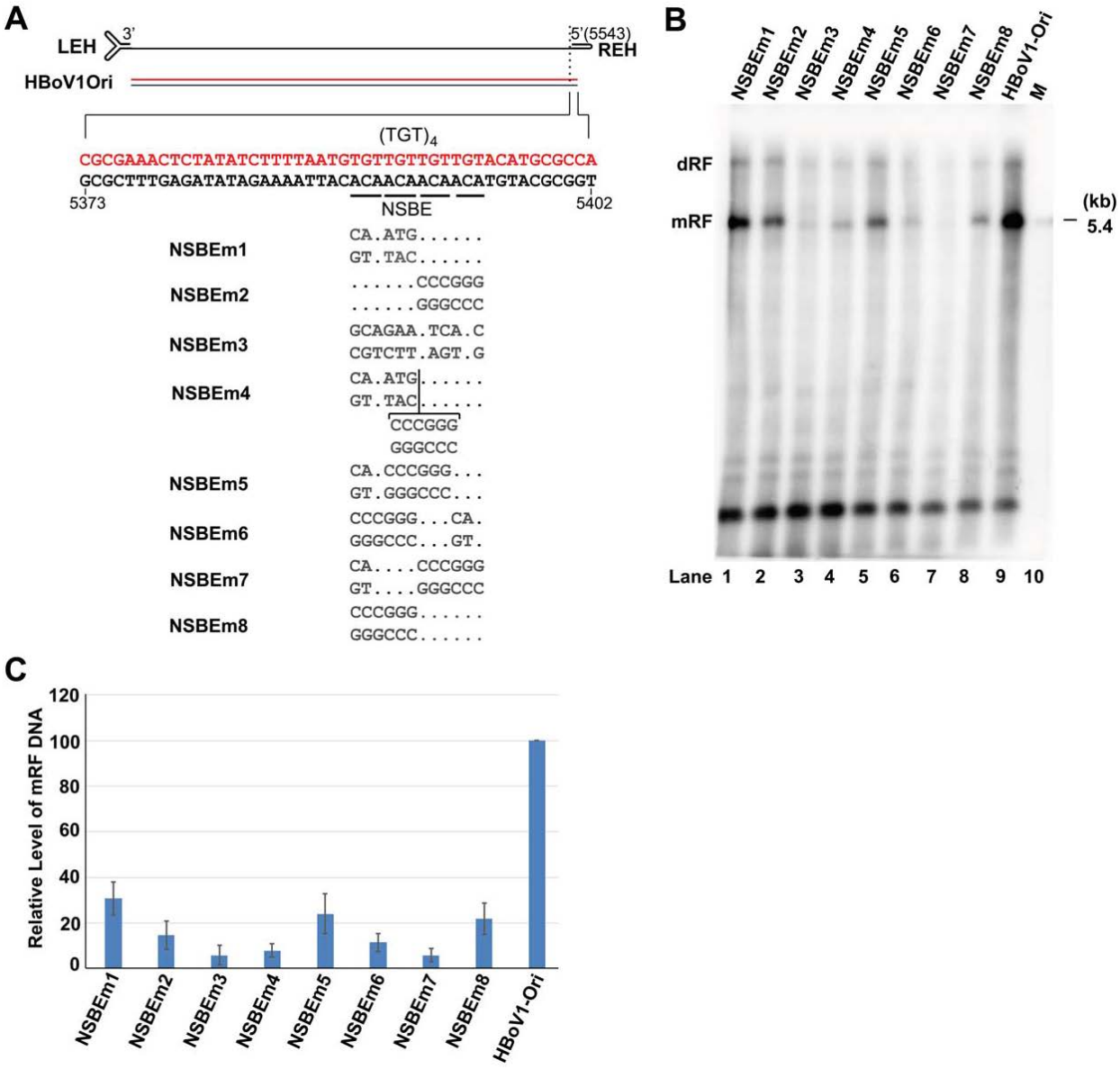
A
LEH
3'
5'(5543)
REH
HBoV1Ori
(TGT)4
CGCGAAACTCTATATCTTTTAATGTGTTGTTGTTGTACATGCGCCA
GCGCTTTGAGATATAGAAAATTACACAACAACAACATGTACGCGGT
5373
NSBE
5402
NSBEm1
CA.ATG.....
GT.TAC.....
NSBEm2
.....CCCGGG
.....GGGCCC
NSBEm3
GCAGAA.TCA.C
CGTCTT.AGT.G
NSBEm4
CA.ATG.....
GT.TAC.....
CCCGGG
GGGCCC
NSBEm5
CA.CCCGGG...
GT.GGGCCC...
NSBEm6
CCCGGG...CA.
GGGCCC...GT.
NSBEm7
CA....CCCGGG
GT....GGGCCC
NSBEm8
CCCGGG.....
GGGCCC.....
B
NSBEm1
NSBEm2
NSBEm3
NSBEm4
NSBEm5
NSBEm6
NSBEm7
NSBEm8
HBoV1-Ori
M
dRF
mRF
(kb)
5.4
Lane 1 2 3 4 5 6 7 8 9 10
C
Relative Level of mRF DNA
120
100
80
60
40
20
0
NSBEm1
NSBEm2
NSBEm3
NSBEm4
NSBEm5
NSBEm6
NSBEm7
NSBEm8
HBoV1-Ori

Figure 3-8. Identification of the nicking site within OriR in vivo.

(A) Diagram of the nicking site mutants. The dynamic nicking site identified by rapid amplification of the 3' end of nicked DNA are indicated by arrows. The sequenced results of poly-adenosine starting sites derived from transfection of the HBoV1 full-length genome (IHBoV1) and HBoV1Ori are shown with green and black arrowheads, respectively. Mutations at seven of these polyA starting sites, as shown, were performed. **(B) Southern blot analysis.** Linearized HBoV1 DNAs were transfected into HEK293 cells. At two days post-transfection, Hirt DNA samples were extracted, Dpn I digested, and analyzed by Southern blotting. Sixty ng of HBoV1Ori was digested by Dpn I as a control.

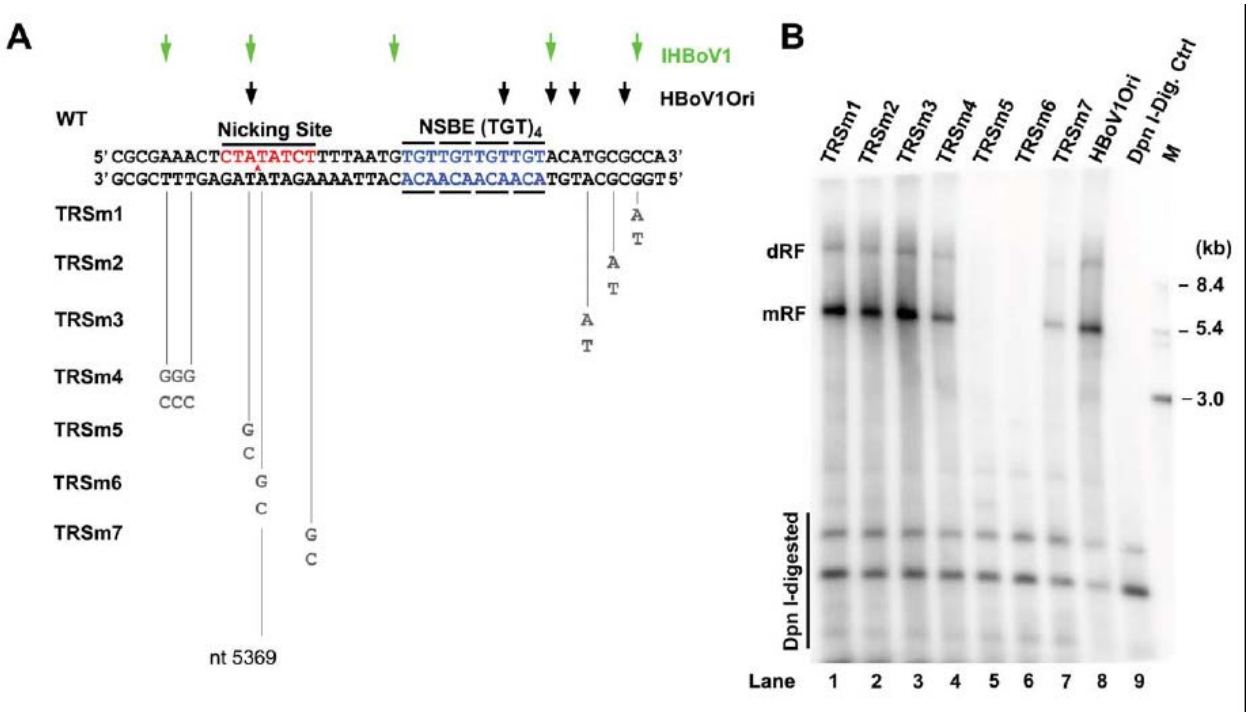
A
IHBoV1
HBoV1Ori
WT
Nicking Site
NSBE (TGT)4
5' CGCGAAACTCTATATCTTTTAATGTGTTGTTGTTGTACATGCGCCA 3'
3' GCGCTTTGAGATATAGAAAATTACACAACAACAACATGTACGCGGT 5'
TRSm1
TRSm2
TRSm3
TRSm4
TRSm5
TRSm6
TRSm7
GGG
CCC
nt 5369
B
TRSm1
TRSm2
TRSm3
TRSm4
TRSm5
TRSm6
TRSm7
HBoV1Ori
Dpn I-Dig. Ctrl
M
dRF
mRF
Dpn I-digested
(kb)
8.4
5.4
3.0
Lane 1 2 3 4 5 6 7 8 9

mutated each site located outside of the NSBEs (**Fig. 3-8A**). Analysis of in vivo DNA replication showed that mutations at either the A or T nucleotide at nt 5,368 or 5,369, but not the mutations in other locations, completely abolished viral DNA replication, (**Fig. 3-8B**, lanes 5&6 vs lanes 1-4). A mutation at nt 5,373 within the putative nicking motif (5'-CTA TAT CG-3') also reduced the level of RF DNA (**Fig. 3-8A**, TRSm7, and **Fig. 3-8B**, lane 7). This result defined the T at nt 5,369 as the nicking site (5'-CTA/TATCT-3').

Identification of the key OriR-binding residues in the origin-binding domain (OBD) of the HBoV1 NS1.

We have previously resolved the structure of the HBoV1 OBD, and predicted that NS1 utilizes two non-structured positively charged loop regions to bind Ori (152). We thus examined the binding residues of the NS1 using a mutagenesis approach (**Fig. 3-9A**). To this end, we performed mutations of either amino acids at the positively charged loops (loop K: ^{127}KR^{128} and loop R: ^{193}RR^{194}) or predicted endonuclease activity motif of the NS1 (^{115}HCH^{117}), together with three control mutations (Mut Q, P, and E), in the context of HBoV1Ori. Mut Q and Mut P mutated the first and the second loops, respectively, of the HBoV1 NS1 OBD structure as controls. Mut E control mutated the nearby amino acids (^{123}EGL^{125}) of putative loop K (**Fig. 3-9B**). Structures of the mutated NS1 OBD were predicted based on the wild-type NS1 OBD (152). Superimposition forms of mutants with wild-type NS1 OBD showed that the mutagenesis did not significantly change the structure (**Fig. 3-9B**). In vivo DNA replication analysis showed that mutating either the basic charged loop region (Mut K and Mut R) or the endonuclease core (Mut Endo) abolished replication, whereas the three control mutations did not alter DNA replication very much (**Fig. 3-9C**). These data suggest that the two positively charged loops of the OBD, as well as the two histidine residues at the predicted endonuclease motif, are required for HBoV1 DNA replication, and that the two positively charged loops likely play a significant role in the NS1 and OriR binding.

Figure 3-9. Characterization of the Ori binding domain (OBD) of the NS1 in vivo.

(A) Diagram of NS1 mutants. The NS1 OBD is diagrammed to scale with putative Ori binding site and endonuclease activity shown. Based on pHBoV1Ori, OBD mutants that have NS1 amino acid mutations at the indicated positions are shown. **(B) Superimposition of three NS1 OBD mutants with the wild-type NS1 OBD structure.** The NS1 OBD structures of Mut K, Mut R, and Mut Endo mutants were predicted by the web server 'I-TASSER' based on the wild-type structure (172). The predicted structures of the mutants were individually superimposed with wild-type NS1 OBD structure using the web server 'Superpose 1.0' (101). The mutated amino acid residues in the putative DNA binding loops K and R and the endonuclease activity core are labeled with green boxes. **(C) Southern blot analysis.** Linearized HBoV1 DNAs, as indicated, were transfected into HEK293 cells. At two days post-transfection, Hirt DNA samples were extracted, digested with Dpn I, and analyzed for DNA replication using Southern blotting. Dpn I digestion control was 60 ng of HBoV1Ori plasmid digested with Dpn I.

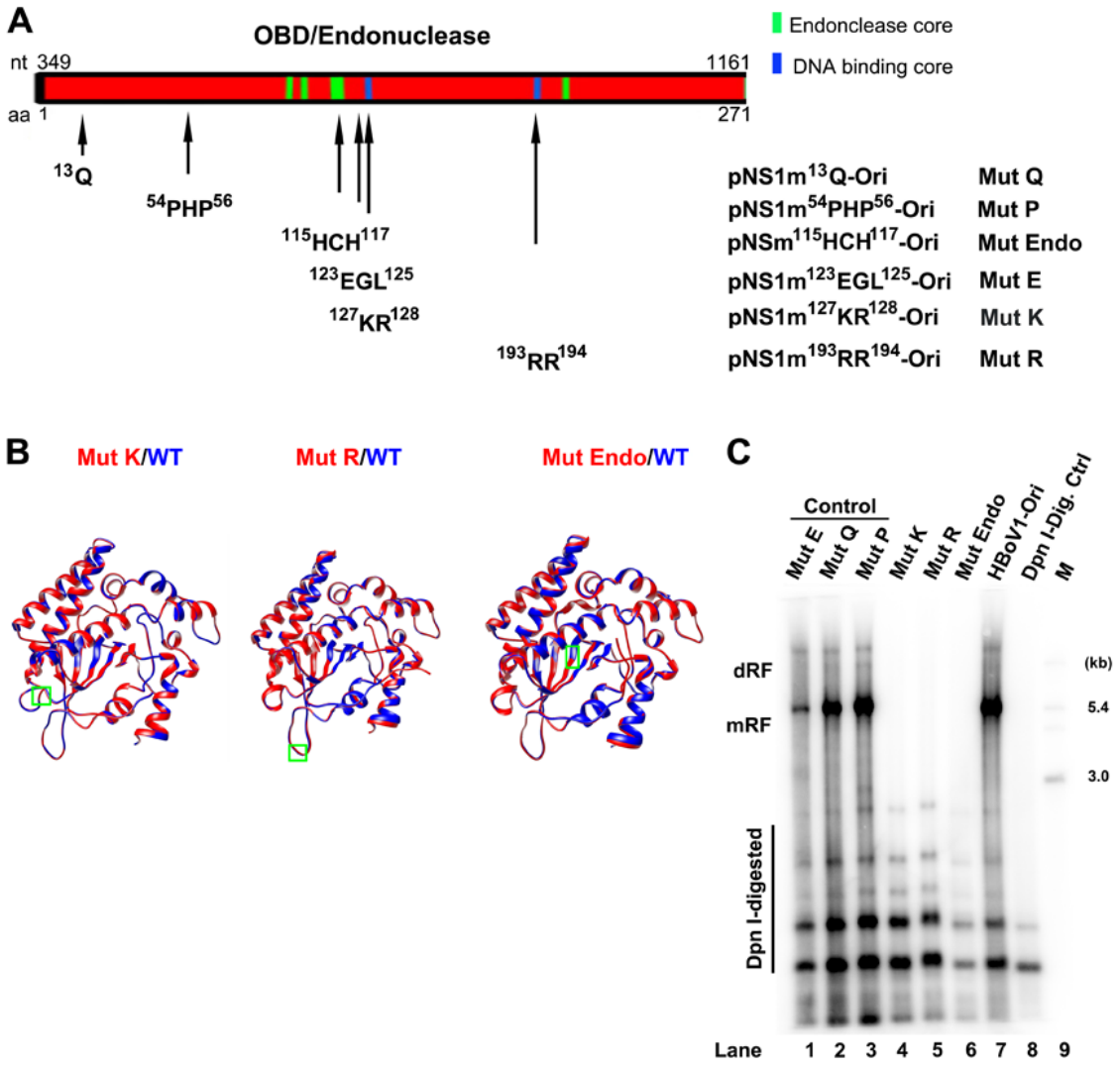
A
OBD/Endonuclease
Endonclease core
DNA binding core
nt 349
1161
aa 1
271
13Q
54PHP56
115HCH117
123EGL125
127KR128
193RR194
pNS1m13Q-Ori Mut Q
pNS1m54PHP56-Ori Mut P
pNSm115HCH117-Ori Mut Endo
pNS1m123EGL125-Ori Mut E
pNS1m127KR128-Ori Mut K
pNS1m193RR194-Ori Mut R
B
Mut K/WT
Mut R/WT
Mut Endo/WT
C
Control
Mut E
Mut Q
Mut P
Mut K
Mut R
Mut Endo
HBoV1-Ori
Dpn I-Dig. Ctrl
M
dRF
mRF
Dpn I-digested
(kb)
5.4
3.0
Lane 1 2 3 4 5 6 7 8 9

HBoV1 NS1 did not specifically bind OriR in vitro.

To understand the interaction between HBoV1 NS1 and OriR (**Fig. 3-2F**), we purified HBoV1 NS1 (**Fig. 3-10A**, lane 2) and studied its binding with the OriR in vitro. As a positive control for NS1 binding to OriR, B19V NS1 was purified (**Fig. 3-10A**, lane 1) and carried along in parallel.

We used B19V NS1 binding to B19V Ori as a positive control because B19V also has a short Ori of 67-nt (63). Electrophoresis gel shift assay showed that B19V NS1 shifted the B19V Ori (**Fig. 3-10B**, lane 2). This binding is specific because it was competed by excess cold B19V Ori but not by excessed cold mutated B19V Ori (Ori-mut) (**Fig. 3-10B**, lanes 4 vs 6). As a negative control, GST protein did not shift the B19V Ori **(Fig. 3-10B**, lane 7), and the B19V Ori-mut was not shifted by B19V NS1 (**Fig. 3-10B**, lanes 8 vs 9). In contrast, however, with the same experimental condition of the electrophoresis gel shift assay, HBoV1 NS1 did not bind its own OriR specifically (**Fig. 3-10C**, lane 2). Adding either cold OriR (**Fig. 3-10C**, lanes 3-5) or cold Ori-mut (**Fig. 3-10C**, lanes 6-8) showed similar negative signals. Of note, we found weak non-specific interaction between HBoV1 NS1 and non-specific DNA in the binding buffer without poly[d(I-C)] (**Fig. 3-10D**, lane 2). This non-specific binding was competed either by excessed cold HBoV1 OriR (**Fig. 3-10D**, lanes 3-5) or cold HBoV1 OriR-mut (**Fig. 3-10D**, lanes 6-8). Thus, the gel shift assays suggest that HBoV1 NS1 alone does not bind HBoV1 OriR specifically in vitro.

To further examine the binding property between HBoV1 NS1 and OriR in the presence of cellular proteins, we designed a biotin pull-down assay. Nuclear extract prepared from NS1-transfected HEK 293 cells was used for pull-down by biotin-labeled OriR (Bio-OriR) and streptavidin-conjugated beads, and then analyzed by Western blotting. In the experiment with B19V Ori, biotinylated B19V Ori (Bio-Ori) pulled down B19V NS1, which was competed by excess B19V Bio-Ori but not by excess mutant Ori (Ori-mut) (**Fig. 3-11A**, lanes 4 vs 5, and **Fig.**

Figure 3-10. HBoV1 NS1 alone did not specifically bind the OriR in an in vitro setting.

(A) NS1 protein purification. Five µl (15 pmol) of purified HBoV1 NS1 (lane 1) and B19V NS1 (lane 2) were analyzed on SDS-PAGE, and stained with Coomassie brilliant blue. Lane 3, 2 µg of bovine serum albumin (BSA), lane 4, a protein ladder. **(B) B19V NS1 specifically binds B19V Ori in vitro.** γ-ATP labeled B19V Ori (lanes 1-7) or Ori-mut (lanes 8 and 9) was incubated with (lanes 2-6 and 9) or without B19V NS1 (lanes 1 and 8) in the binding buffer with 2 µg/ml poly[d(I-C)]. Cold Ori probe at ratios of 20 times (lane 3) and 200 times (lane 4) or cold Ori-mut probe at levels of 20 times (lane 5) and 200 times (lane 6) was added for competition. Free and shifted probes are indicated. GST protein was added as a negative control (lane 7). **(C) HBoV1 NS1 did not bind HBoV1 OriR in vitro.** γ-ATP labeled HBoV1 OriR was incubated with (lane 2-8) or without (lane1) HBoV1 NS1 in the binding buffer with 2 µg/ml poly[d(I-C)]. Cold OriR and OriR-mut probes at 10 times (lanes 3 and 6), 100 times (lanes 4 and 7), and 1,000 times (lanes 5 and 8) were included for competition. Free and shifted probes are indicated. **(D) Non-specific HBoV1 NS1 binding to OriR.** γ-ATP labeled HBoV1 Ori was incubated with (lanes 2-8) or without (lane1) HBoV1 NS1 in the absence of poly[d(I-C)]. Cold OriR/OriR-mut probe at 50 times (lanes 3 and 6), 10 times (lanes 4 and 7), 4 times (lanes 5 and 8) was included for competition. Free and shifted probes are indicated.

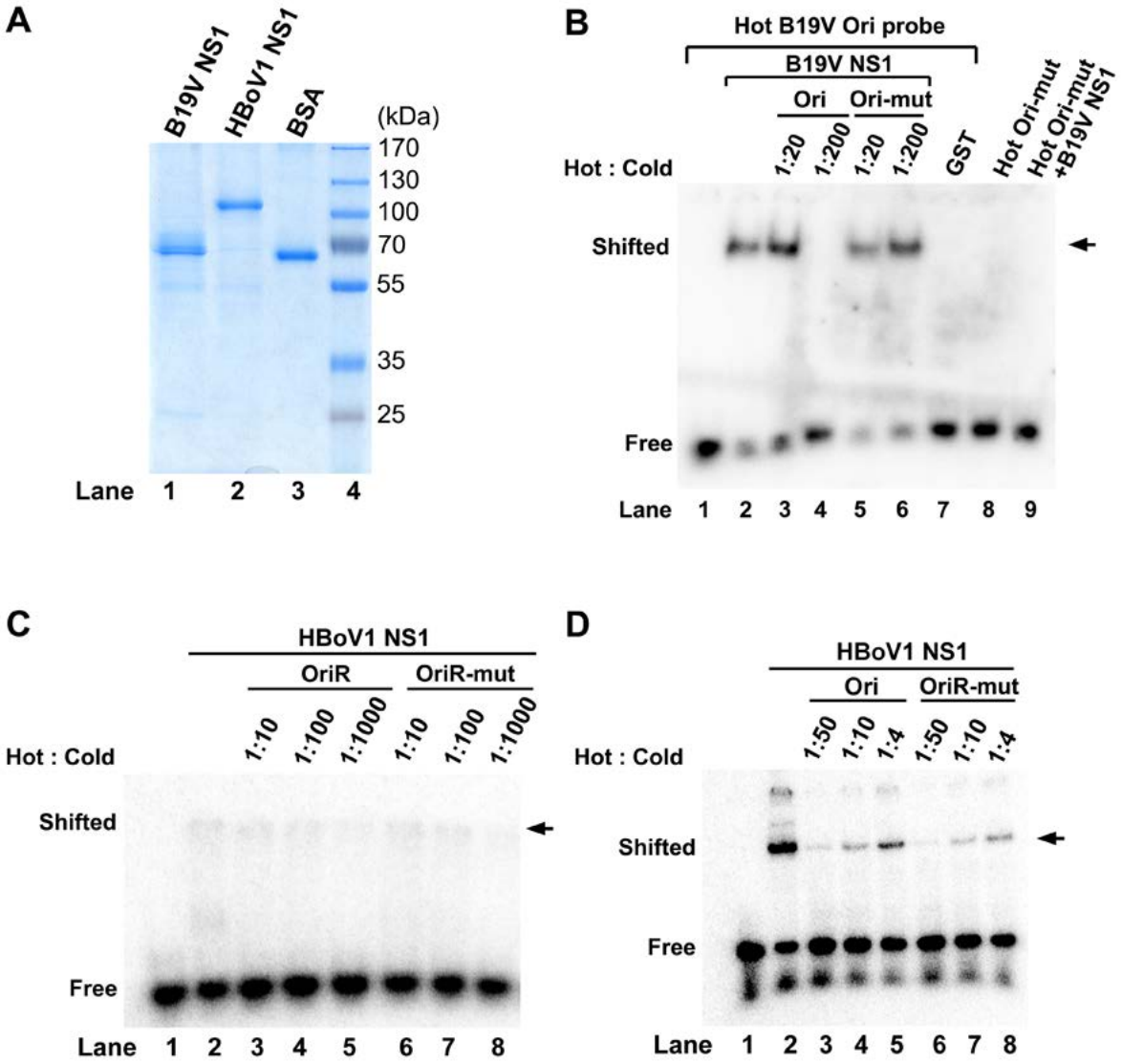
A
B19V NS1
HBoV1 NS1
BSA
(kDa)
170
130
100
70
55
35
25
Lane 1 2 3 4
B
Hot B19V Ori probe
B19V NS1
Ori
Ori-mut
Hot : Cold
1:20
1:200
1:20
1:200
GST
Hot Ori-mut
Hot Ori-mut +B19V NS1
Shifted
Free
Lane 1 2 3 4 5 6 7 8 9
C
HBoV1 NS1
OriR
OriR-mut
Hot : Cold
1:10
1:100
1:1000
1:10
1:100
1:1000
Shifted
Free
Lane 1 2 3 4 5 6 7 8
D
HBoV1 NS1
Ori
OriR-mut
Hot : Cold
1:50
1:10
1:4
1:50
1:10
1:4
Shifted
Free
Lane 1 2 3 4 5 6 7 8

Figure 3-11. HBoV1 NS1 alone or with NP1 did not specifically bind OriR in a pull-down assay.

(A&B) Detection of B19V NS1 and B19V Ori binding. (A) Nuclear extract (NE) prepared from OptiB19VNS1-transfected HEK 293 cells were used to incubate with Biotin-labeled B19V Ori (Bio-Ori, lanes 3-5) and B19V Ori-mut (lane 6), followed with streptavidin-conjugated beads. Additionally, some reactions were additionally incubated with B19V Ori-mut at 30 times (lane 4) and B19V Ori at 30 times (lane 5). NS1 bands pulled down by the Bio-Ori are indicated. (B) The NS1 bands pulled down by Bio-Ori were quantified. Relative levels to the NS1 in lane 4 are shown with averages and standard deviations from three independent experiments. **(C&D) Detection of HBoV1 NS1 and HBoV1 OriR binding.** (C) NE prepared from OptiHBoV1NS1-transfected HEK 293 cells were used to incubate with HBoV1 OriR (lane 2), and HBoV1 OriR-mut (lane 3), followed with streptavidin-conjugated beads. NS1 detected in the input is indicated. (D) NE prepared from OptiHBoV1NS1- and OptiHBoV1NP1-co-transfected HEK293 cells were used to incubate with HBoV1 OriR or OriR-mut, followed with streptavidin-conjugated beads. NS1 and NP1 detected in the input are indicated.

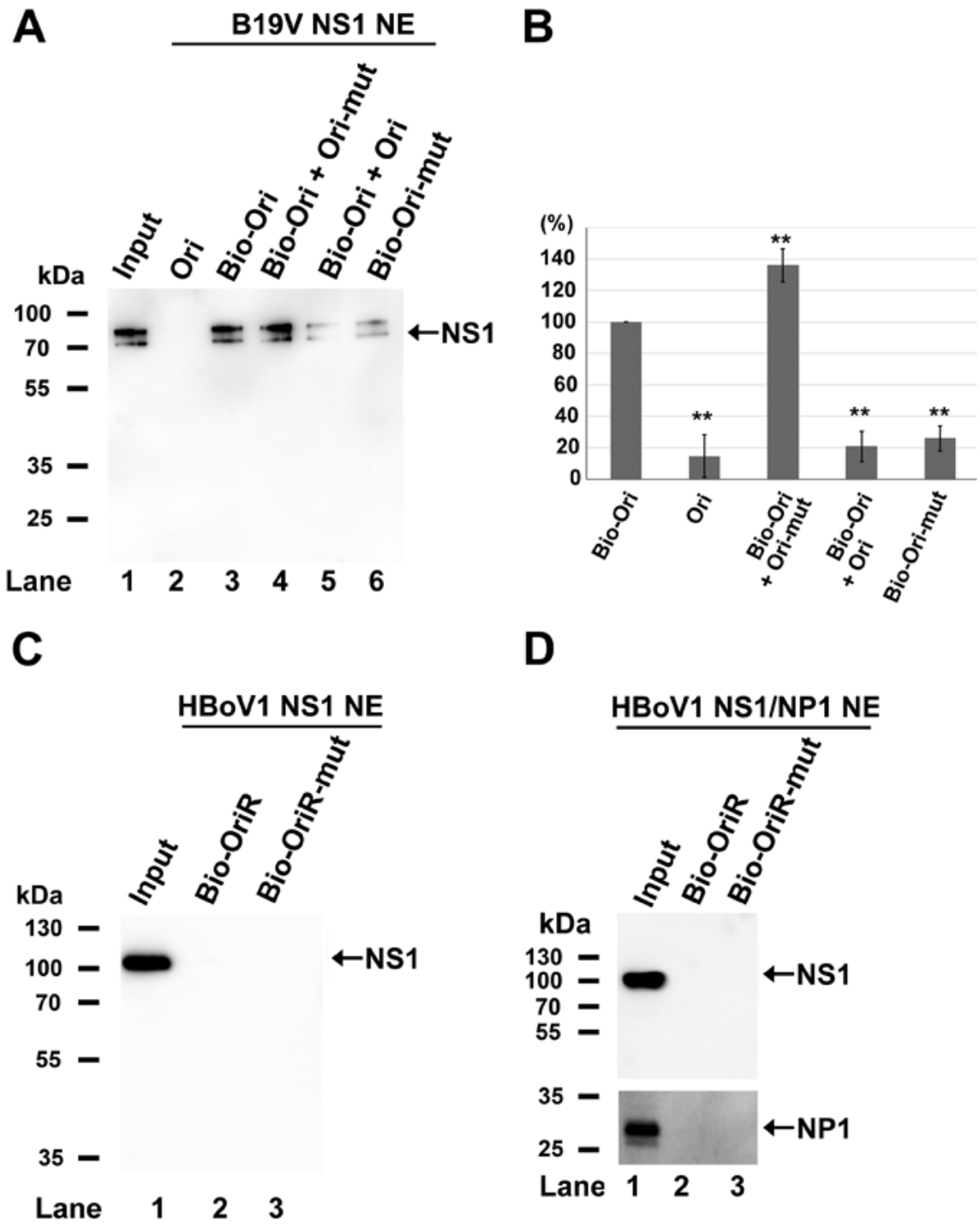
A
B19V NS1 NE
Input
Ori
Bio-Ori
Bio-Ori + Ori-mut
Bio-Ori + Ori
Bio-Ori-mut
kDa
100
70
55
35
25
←NS1
Lane 1 2 3 4 5 6
B
(%)
140
120
100
80
60
40
20
0
**
Bio-Ori
Ori
Bio-Ori + Ori-mut
Bio-Ori + Ori
Bio-Ori-mut
C
HBoV1 NS1 NE
Input
Bio-OriR
Bio-OriR-mut
kDa
130
100
70
55
35
←NS1
Lane 1 2 3
D
HBoV1 NS1/NP1 NE
Input
Bio-OriR
Bio-OriR-mut
kDa
130
100
70
55
35
25
←NS1
←NP1
Lane 1 2 3

3-11B). As a control, non-biotin-labeled B19V Ori did not pull down any B19V NS1 (**Fig. 3-11A**, lane 2, and **Fig. 3-11B**), and Bio-Ori-mut only pulled down a few minor amount of NS1 (**Fig. 3-11A**, lane 6, and **Fig. 3-11B**). By contrast, HBoV1 NS1 was not pulled down by either biotinylated Ori or Ori-mut (**Fig. 3-11C**, lanes 2&3), despite high-level expression of NS1 (**Fig. 3-11C**, lane 1). As NP1 co-localized with BrdU labeled viral replication centers (**Fig. 3-5**), we tested the hypothesis that NP1 is critical for NS1 binding with OriR. We prepared nuclear extracts from cells co-expressing NP1 and NS1, and performed pull-down assays. The results demonstrated that biotinylated HBoV1 OriR did not pull down NS1, even in the presence of NP1 (**Fig. 3-11D**, lane 2). Collectively, the pull-down assays suggest that HBoV1 NS1 does not bind HBoV1 OriR in vitro in the presence of cellular factors and NP1.

Discussion

In this report, we studied the viral components of both in cis and trans that are required for HBoV1 terminal resolution at REH. We defined a 46-nt sequence at nt 5,357-5,402 as the HBoV1 OriR. It contains both the NSBEs and nicking site, and is used as a template for HBoV1 DNA replication at REH. Notably, a cis sequence in the 3' NCR was critical for viral DNA replication at the OriR, while the large NS protein NS1 and the small NP1 played a pivotal role in trans for viral DNA replication at the OriR. These basic findings of HBoV1 DNA replication at the OriR lay a foundation for further understanding the mechanism underlying NS1 binding to and nicking at the OriR, which are the key steps in HBoV1 RF DNA replication. Additionally, in this study, we show, for the first time, the specific binding of the B19V NS1 with B19V Ori in vitro.

Functions of viral proteins in HBoV1 DNA replication at OriR.

NS1 function: The large non-structural protein of parvovirus, Rep78/68 or NS1, is composed of a putative DNA origin binding/endonuclease domain (OBD), helicase activity

domain, and transactivation domain (TAD) at N-terminus, middle, C-terminus, respectively (134). We have previously resolved the crystal structure of the HBoV1 OBD at 2.7-Å resolution, which is similar to the canonical histidine-hydrophobic-histidine superfamily of nucleases. The OBD structure combines two distinct functions: (i) a positively charged region formed by surface β-hairpin (aa190-198) and helix α5 (aa127-132), which is responsible for recognizing the viral DNA replication origin, and (ii) the endonuclease active site which contains signature motif HUH and performs strand-specific cleavage at Ori (152). The HUH motif of HBoV1 OBD contains two histidine residues (H115/H117) separated by cysteine C116, followed by the three hydrophobic residues I118, L119, and V120 (152). However, these active sites are only predicted from superposition of the HBoV1 OBD structure into the AAV5 OBD structure (72). Here, we confirmed that R193 and R194 in the surface hairpin of the OBD and K127 and R128 in the loop region are critical to terminal resolution, and, by contrast, the neighboring 123EGL125 residues are not. Mutation of the two histidine residues (H115 and H117) confirmed their nicking function. Structure study of the MVM NS1 OBD also revealed conserved residues of DNA binding and nicking activities (150), highlighting the importance of the confirmed DNA binding and nicking residues of the HBoV1 NS1 OBD.

NP1 function: We have previously shown that bocaparvovirus NP1 plays an important role in the replication of viral duplex DNA (69,145). HBoV1 NP1 or BPV1 NP1 can complement replication of a mutant MVC infectious clone that does not express MVC NP1 (145). Three other newly identified HBoV1 small NS proteins NS2-4 are not required for replication of HBoV1 duplex DNA genome in HEK293 cells (134). Since NS2-4 all contain the NS1C terminus, the anti-NS1C antibody reacts with all these isoforms (134). Thus, we demonstrated that all NS1-4 proteins and NP1 colocalize within APAR bodies. Nevertheless, it is unlikely that NS2-4 recruit NP1 to the APAR bodies. Direct interactions between NS1-4 and NP1 were not confirmed (**Fig. 3-6**). NP1 contains a non-classical nuclear localization signal (ncNLS) at aa7-50 (92), and is able to complement the functions of the MVM NS2 in viral DNA replication during an early

phase of infection (106). In fact, during MVM infection of NP1-expressing A9 cells, NP1 was progressively lost from its nucleolus-localization and began to be colocalized with MVM NS1 in APAR bodies. Moreover, NP1 expression rescues APAR body maturation in cells infected with an NS2null mutant of MVMp (106). Additionally, NP1 is involved in viral pre-mRNA processing (53,143,173). HBoV1 NP1 is required for viral mRNA splicing at the A3 splice site and read-through of the viral mRNA through the (pA)p site (173). Taken together, we hypothesize that during infection or viral DNA replication, NP1 is critical in the development of viral DNA replication centers (APAR bodies) together with NS1, in which cellular DNA replication factors are enriched, however, after the formation of the APAR bodies, NP1 could be relocated to the cellular compartment for viral RNA processing. On the other hand, NP1 could possibly be recruited by cellular DNA replication factors to the APAR bodies, in response to the efforts of NS1 in interacting with the viral Ori and cellular DNA replication factors (29,71,112).

Identification of the HBoV1 OriR.

For a homotelomeric parvovirus whose replication depends on a helper virus, a 43-nt DNA sequence, was identified as the AAV Ori, containing the Rep binding element (RBE) and nicking site (128). For homotelomeric parvoviruses that replicate autonomously, a specific 38-nt DNA sequence has been identified as the Ori of goose parvovirus (GPV) (135), and a 67-nt DNA was identified as B19V Ori that contains a nicking site and four GC-rich NSBEs that are required for optimal virus replication (63). The B19V ITR resembles that of GPV in that both have an arrow-like hairpin structure (36,170). For heterotelomeric parvoviruses that replicate autonomously, there are two replication origins located at the LEH and REH, respectively. The active form of MVM LEH Ori ($OriL_{TC}$) is ~50-nt in length, composed of a transcription factor PIF binding site, the $(ACCA)_2$ NSBEs, and the nicking site (33,35). It functions as a template for junction resolution that generates ssDNA genome. By contrast, the MVM REH Ori (OriR) is around 125-nt in length, and contains a region composed a nicking site and two closely

contacted $(ACCA)_2$ NSBEs, a degenerate NSBE (CGGT) at the tip of the hairpin, and a cis sequence that is non-specifically bound by HMG1/2 family DNA binding proteins (30). Therefore, the MVM OriR includes almost the entire sequence of the REH (30,35).

In this study, we identified a 46-nt sequence (OriR) at the REH of the HBoV1 genome is responsible for the replication of duplex HBoV1 genome in HEK293 cells. This OriR represents the first Ori in members of heterotelomeric parvoviruses that functions as a template of terminal resolution in a short closely contacted DNA sequence (46-nt), containing the NSBEs and nicking site. We speculate that cis-acting sequences surrounding the nicking site and NSBEs are required for interacting with cellular factors, e.g., HMG1/2 with MVM OriR (30) and PIF with MVM OriL (26).

Characterization of the nicking site and NSBEs.

The nicking site at which Rep78/68 or NS1 nicks is specific to each parvovirus (36). The nicking site (5'-GAGT/TGG-3') is conserved only in AAV1-4 and 6, but AAV5 uses 5'-AGTG/TGGC-3' (19). For autonomous parvoviruses, GPV uses (5'TGAG/TCT3') (135), B19V Ori uses a unique nicking site (5'-GACA/CCA-3') (63), and MVM uses a nicking site (5'-CTWW/TCA-3', W=A/T) (135). Thus, the nicking sites of autonomous parvoviruses differ from each other. The HBoV1 nicking site (5'-CTA/TATCT-3') identified in this study closely resembles the MVM TRS with an A/T-rich sequence in the center. Of note, such a similar nicking site is not found at the LEH of the HBoV1 genome, therefore. However, one unique nicking site of AAV2 Rep78/68 (5'-CTCCA/TTT-3') has been identified in the minimal replication origin present within the AAV2 P5 promoter (56,163). The nicking of the AAV2 Rep78/68 at the nicking site in the P5 promoter involves the TATA box in cis and the TATA-binding protein in trans (56). We hypothesize that HBoV1 NS1 must employ a different nicking site to perform junction resolution at the OriL of the LEH, and that cellular transcriptional factors or DNA binding proteins should facilitate nicking of the NS1 at the nicking site at the OriL.

Several Rep78/68 and NS1 binding elements have been characterized, and confirmed by in vitro binding assay. The AAV RBE consists of three tetramer repeats $(GCTC)_3$ plus a degenerate GCGC (128). Similar three tetramer repeats $(GTTC)_3$ plus GAAC were found in the ITR of GPV (135). Two hexamer repeats $(GCCGCCGG)_2$ were confirmed to bind B19V NS1 OBD in an in vitro binding assay (151). MVM NSBE in either the OriL or OriR, comprise 2-3 tandem copies of the tetranucleotide $(TGGT)_{2-3}$. Densoparvovirus GmDNV NS1 binds a $(GAC)_4$ trimer repeated sequence in its ITR (153). A consensus NSBE for HBoV1 NS1 binding cannot be found in the LEH and REH of HBoV1 genome (69). In the HBoV1 OriR identified in this study, at ~12 nt downstream of the nicking site, a tetramer tri-nucleotide $[(TGT)_4]$ was proved critical to viral duplex DNA replication at the OriR. However, we were not able to confirm a specific binding between HBoV1 NS1 and OriR in vitro. We believe that our in vitro binding assay is capable of revealing the specific binding. We adapted the in vitro binding buffer which has been successfully used to confirm MVM NS1 binding to its NSBE (24,29). We also demonstrate B19V NS1 binding to the B19V Ori in side-by-side studies assessing HBoV1 NS1 binding of the HBoV1 OriR. Although a strong and specific binding between B19V NS1 and its Ori was observed and confirmed, we did not observe any specific binding between HBoV1 NS1 and OriR. We had further used a more sensitive in vitro binding assay, in which an anti-NS1 antibody was used to pull down any bound OriR (29), to observe the interaction between NS1 and OriR. Again, we did not observe any positive binding (data not shown). Therefore, we speculate that HBoV1 NS1 and OriR binding may require the involvement of viral and cellular proteins. However, in a subsequent in vitro pull-down assay, the biotinylated HBoV1 OriR did not pull down any HBoV1 NS1 from the lysate of the cells expressing HBoV1 NS1. As a control, B19V Ori pulled down NS1 at a significantly higher level than the mutant Ori, which can be competed by the wild–type B19V Ori but not the mutant Ori. A further experiment using nuclear extract prepared from NS1- and NP1-coexpressing cells also did not show any binding between HBoV1 NS1 and OriR. We hypothesize that in vivo oligomerization of the NS1 may be

necessary to the recognition of the NSBEs, as Rep78 is oligomerized in recognition the RBEs (67).

Nevertheless, based on the model of rolling circle replication in which Rep78/68 or NS1 has to bind the origin and melt the duplex viral DNA, and performs nicking of the ssDNA at the nicking site of ~20-nt upstream of the NSBEs (35), we believe that the $(TGT)_4$ repeat in HBoV1 OriR should be the NSBEs. The $(TGT)_4$ repeat closely resembles the $(GAC)_4$ repeat of GmDNV NSBE (153). Since the $(TGT)_4$ repeat contains the $(TGTT)_2$ repeat, the HBoV1 NSBEs also resemble MVM NSBEs $(TGGT)_{2-3}$ (29). Considering no cognate binding sequence can be found in the origins at both the LEH and REH of HBoV1 genome, we hypothesize that contrary to what has been observed, HBoV1 NS1 must bind the origins at a low affinity and requires the help of other viral components and cellular proteins to do so.

Function of the 3' NCR of HBoV1.

Identification of a role of the 3' NCR between VP-coding region and the REH in HBoV1 DNA replication is important. In other parvoviruses, various cis-sequences that are outside of the terminal hairpins have been identified to be important for DNA replication, e.g., an additional AAV2 minimal DNA replication origin at the P5 promoter (5' NCR) (115,156,163). In MVM, it has been shown that specific elements inboard of the REH between nt 4,489-4,636 and nt 4,636-4,695 are necessary for efficient replication of MVM duplex DNA (146). In the development of recombinant MVMp vector (rMVMp), the rMVMp genome, a large portion of cis-element was remained at the 3' end (nt 4,631-5,149) (65). However, how these cis-elements outside of the hairpins facilitate viral DNA replication has not been studied.

We have previously developed a recombinant HBoV1 vector, in which both the rAAV2 genome and rHBoV1 genome were used. However, large portions were retained at the 3' and 5' end in the rHBoV1 genome, in order to ensure efficient replication in the presence of a packaging plasmid (168). Unfortunately, the cis-sequences that remained resulted in a high rate

of recombination that generated wild-type virus in the rHBoV1 preparations (168). Therefore, to define the cis minimal requirement for HBoV1 DNA replication is important to develop a better rHBoV1 vector that may hold benefits for gene targeting in human airways, since 95% of the HBoV1 genome is negative sense, while the AAV genome has equal polarity (10,145). We plan to further define the cis element at the left end in order to construct an rHBoV1 genome that has a minimal sequence of HBoV1 (to avoid homology recombination with the HBoV1 packaging plasmid).

Chapter IV:

Hairpin-independent HBoV1 DNA replication

Abstract

Parvoviruses are ssDNA viruses with duplex hairpin structures at the ends. The hairpin sequences on both ends are indispensable to viral DNA replication. Here we provide evidence that the duplex genome of human bocavirus 1(HBoV) replicates in HEK293 cells independent on the hairpin structure. We propose a model of HBoV1 DNA replication in that the large nonstructural protein NS1 may guide the direction of the strand-displacement, which is previously called “hairpin-transfer” step in parvovirus DNA replication. Thus, our study extends our understanding of parvovirus DNA replication in general.

Introduction

Parvovirus has a single stranded DNA (ssDNA) genome. Both termini of the genome harbor partially inverted repeat sequences, which are predicted to be hairpin structure. A ‘rolling-hairpin model’ of parvoviral DNA replication has been proposed, which was essentially derived from the ‘rolling-circle replication model’ utilized by bacterial phages (148). Based on the hairpin structures, parvoviruses can be categorized into two groups: homotelomeric parvoviruses that contain inverted terminal repeats (identical repeats at both termini), and heterotelomeric parvoviruses that has disparity terminal sequences and structures at ends. All the dependoparvovirus are homotelomeric, including adeno-associated viruses (AAVs). Most of the autonomous parvoviruses, which replicate in cells independent of a helper virus, belongs to heterotelomeric parvoviruses, except for members of the genera *Erythroparvovirus* and *Dependoparvovirus*. For autonomous parvoviruses, the viral DNA replication mechanism has been largely studied for protoparvoviruses, e.g., minute virus of mice (MVM). To be notified, as

most of the heterotelomeric virus genome isolated are negative in sense, the left-end hairpin (LEH) is designated to be at 3’ end, while the right-end hairpin (REH) at 5’ end.

Human bocavirus1 (HBoV1) is a human pathogen identified in 2005 (1). It associates with lower respiratory tract infections worldwide, especially to infants under 2 years old (2,13,23,50,59,61,73,74,104,105,111,132). Death cases were also reported due to high virus loads (23,85,158). HBoV1 belongs to genus *Bocaparvovirus* of the *Parvoviridae* family. It infects and replicates the well-differentiated human airway epithelial cells but not the highly dividing cells (41). Although HBoV1 does not infect HEK293 cells, the HBoV1 duplex genome replicates in HEK293 cells (69). The HBoV1 genome structure is quite unique, compared with other parvoviruses. It is heterotrimeric, but the REH is a perfect palindromic hairpin (69).

Other representative members of bocaparvoviruses are minute virus of canines (MVC) and bovine parvovirus 1 (BPV1) (145). Although they were isolated decades ago, little is known about the DNA replication of bocaparvoviruses. Moreover, HBoV1 has been explored to produce recombinant HBoV1 vector that packages rHBoV1 genome, which has been shown promising in the application of gene delivery in human airway (168).

In this study, we attempted to examine the replication model of bocaparvovirus using the HBoV1 reverse genetics system in HEK293 cells. We observed novel replication patterns of HBoV1 genome, whose replication is independent of the hairpin structures at ends. We confirmed this fact by using different approaches, and proposed a potential HBoV1 DNA replication model. This study not only improves our understanding of parvovirus DNA replication in general, but also helps to develop better strategies to generate rHBoV1 vector in HEK239 cells.

Material and Methods

Plasmids construction.

pIHBoV1, pHBoV1Ori, pHBoVΔREH2 were previously described. pHBoV1OriRλm1 were constructed by inserting Lambda (λ) DNA sequences of 250 bp (nt 10,030-10,280) immediately after the Ori in pHBoV1Ori. Similarly, λ DNA sequences of 500, 750, 1000, 1500 bp were inserted just after the Ori in pHBoV1-Ori to construct pHBoV1OriRλm2, pHBoV1OriRλm3, pHBoV1OriRλm4, and pHBoV1OriRλm5. In addition, λ DNA sequences of 500 bp (nt 10,030-10,530) and 1,000 bb (nt 10,030-11,030) were introduced at the 5' end (nt 141) of the HBoV1 sequence in pHBoV1Ori to construct pHBoV1OriLλm1 and pHBoV1OriLλm2.

Cell culture, transfection, and virus infection.

HEK 293 cells were cultured in HyClone™ Dulbecco's Modified Eagle Medium (DMEM, GE Healthcare Bio-Sciences, Piscataway, NJ) with 10% fetal calf serum (FCS, #F0926, Sigma-Aldrich, St Louis, MO). HEK293 cells grown in 60-mm dishes were transfected with 3 µg of plasmid as indicated in the figures, LipoD293 transfection reagent (SignaGen, Rockville, MD) was used following manufacturer's instructions. HAE-ALI cultures were generated following previously publications (69,134). HAE-ALI cultures were infected with HBoV1 at an MOI=10 from the apical side of the ALI culture.

Low-molecular-weight (Hirt) DNA extraction and Southern blotting.

Hirt DNA extraction and Southern blotting were performed exactly as previously described (134). After hybridization, the membrane was exposed to a phosphor screen, which was finally scanned on a phosphor imager (GE Typhoon FLA 9000, Fuji). The developed image was processed analyzed using ImageQuant TL8.1 software (GE healthcare, Marlborough, MA).

Two-dimensional (2D) gel electrophoresis (57,94,113).

Hirt DNA samples were extracted and digested by DpnI as described in Southern blotting (134). The treated samples (~ 500 ng) were first loaded onto the first dimensional gel of 0.7 % agarose gel (prepared in TAE buffer) with a molecular size marker ranged from 3-20 kb, supplemented with 10 ng/ml ethidium bromide, and were electrophoresed for 36 hr at 15 volts. Then, the sample lane was excised out of the gel and was rotated 90° before heading to the

edge of the second dimension gel. The excision edge was fused with the second dimension gel by heated 0.7% agarose. The second dimension gel was prepared of 1% agarose in deionized water. After forming firm fusion, the fused gel was emerged in alkaline running buffer (30 mM NaOH, 2 mM EDTA) for an hour before electrophoresis. The second dimension gel was run for 24 hr at 20 volts. Then, the alkaline buffer was exchanged by deionized water and washed three times (each for an hour) with slightly shaking. The following steps were performed the same as those in Southern blotting, including buffer exchanging, membrane transferring, hybridization and signal exposure.

Result

HBoV1 duplex genome replicates in HEK293 cells without hairpin structures.

Previously, we identified the minimal replication origin (OriR) at the REH of HBoV1 genome. This is a 46-nt sequence, including NS1 binding and nicking sites. OriR replicates independent of the LEH in the context of NS1 and NP1 gene expression. Notably, OriR does not harbor hairpined sequence within itself. To further confirm replication of the OriR independent of any hairpin sequence, we constructed various mutants by extending OriR with different length of non-specific λ DNA sequence. In the context of pHBoVOri, 0.25, 0.5, 0.75, 1, or 1.5 kb λ DNA were added beyond of the right end of the OriR (**Fig. 4-1A**). Constructs with 0.5 or 1kb λ DNA inserted at the left end of genome in the context of pHBoV1Ori were made as controls. We transfected linearized DNA of the constructs and performed Southern blotting to examine viral DNA replication. We observed that OriR still replicated with non-specific DNA inserted into either the left end (**Fig. 4-1B**, lane 1, 2) or the right end (**Fig. 4-1B**, lane 3-7) of the duplex DNA of the HBoV1OriR. The increased size of the replicative DNA (RF DNA) represented the length of the DNA fragments with an extended sequence (insertion).

Resolution of the replicative intermediates by 2-dimentinal gel electrophoresis.

Figure 4-1. HBoV1-Ori replicated with extended non-specific sequence on either of the terminals.

(A) Diagram of HBoV1Ori and its mutants with various λ phage sequence insertions. Based on the HBoV1Ori, 0.25, 0.5, 0.75, 1, or 1.5 kb of λ DNA sequence was inserted at the right end of HBoV1 sequence (OriR). In comparison, 0.5 or 1 kb of λ DNA sequence was inserted at the left-end of HBoV1 sequence (in which the REH was already deleted). **(B) Southern blot analysis of HBoV1Ori mutants with λ sequence insertion.** Linearized constructs as indicated were transfected into HEK293 cells. 2 days post transfection, Hirt DNA were extracted and applied to southern blot as mentioned.

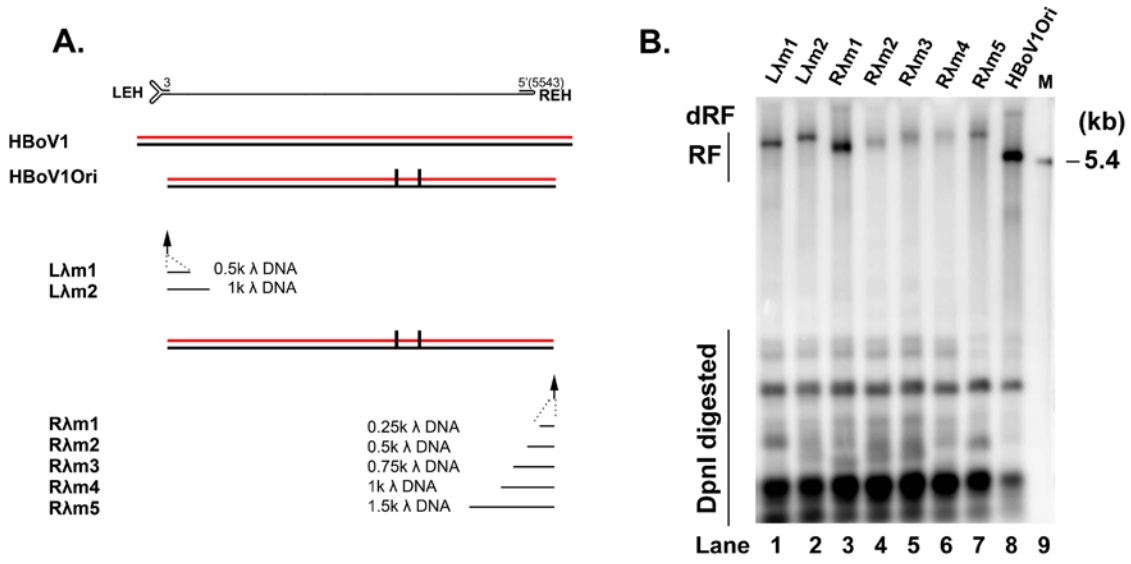
A.
LEH
3
5'(5543)
REH
HBoV1
HBoV1Ori
LΛm1
LΛm2
0.5k λ DNA
1k λ DNA
RΛm1
RΛm2
RΛm3
RΛm4
RΛm5
0.25k λ DNA
0.5k λ DNA
0.75k λ DNA
1k λ DNA
1.5k λ DNA
B.
LΛm1
LΛm2
RΛm1
RΛm2
RΛm3
RΛm4
RΛm5
HBoV1Ori
M
dRF
RF
(kb)
5.4
DpnI digested
Lane 1 2 3 4 5 6 7 8 9

Two possible mechanisms could explain how the viral DNA is synthesized without the hairpin ends. One possibility is that a free molecule attached at the 3' end of the viral DNA, which acts as a primer and providing free 3'–OH for the second strand DNA synthesis. Another possibility is that the 3' end of the viral DNA could be turn around by itself to form a hairpin structure even without a sequence that has complementary nucleotides.

To explore which strategy is utilized during the replication of the OriR, we used 2-D gel electrophoresis to analyze small molecular weight (Hirt) DNA extracted during OriR replication of HBoV1Ori-transfected HEK293 cells. In 2-D gel electrophoresis, vertical dimension separates DNA by sizes, while the horizontal dimension differentiates DNA by structure, so that the DNA molecules with the same size but in different structure will be revealed on the 2D. Previously, we constructed ΔREH2 based on pHBoV1 (LEH-VP1/3-), whose replication level is comparable with that from the infectious clone pIHBoV1 in HEK293 cells. ΔREH2 does not hold any hairpin sequences at the ends. By 2-D gel electrophoresis, ΔREH2 replication revealed 4 dominant replication intermediates (**Fig. 4-2B**). Dot A and Dot B are closed monomer replicative form (c-mRF) and opened monomer replicative form (o-mRF), respectively. Dot C and Dot D are obviously dimeric size of closed and open replication form (c-dRF & o-dRF), respectively. Single stranded DNA could derived from either strand displacement (very minor) or the product of nicking dRF DNA (dot E). The appearance of Dot A and Dot C proved hairpin (or turn-round) structure is formed during replication of ΔREH2. More importantly, replication of HBoV1Ori or HBoV1Ori-0.25kλ showed a highly accumulated Dot A (**Fig. 4-2**, C&D), suggesting that the hairpin (or turn-round) structure is formed during the replication of these hairpin-less HBoV1 DNA.

To supplement the 'rolling hairpin replication model' derived from the study of MVM, we proposed the HBoV1 DNA replication model independent of hairpin sequence, based on the above observations (**Fig. 4-2**). After NS1 nicking at OriR and DNA synthesizing to the end of the right terminus (**Fig. 4-3**, Steps 1-2), the newly synthesized 3' end turns around towards itself.

Figure 4-2. HBoV1 Ori replicates independent of hairpin structure at the right-end, which still reveals hairpin structure (turn-around) replicative intermediates.

(A) Diagram of putative replicative intermediates on a 2-D gel. The vertical dimension is a low concentration agarose gel electrophoresed at a low voltage. Based on molecular weight, ssDNA, RF DNA and dRF DNA are separated as indicated. Transferring clockwise for 90 ºC, the second dimension is a high concentration agarose gel electrophoresed in an alkaline buffer. Covalently linked duplex from intermediates (c-mRF and c-dRF DNA) are separated with open ended duplex (o-mRF, o-dRF) as indicated. Single stranded DNA (ssDNA) is either nicked from c-dRF DNA or derived from strand displacement as indicated. **(B-D) 2-D gel electrophoresis analysis of DNA replication.** The lower MW DNA samples extracted from HEK293 cells transfected with HBoV1ΔREH2 (A), HBoV1Ori (B), and HBoV1Ori-Rλm1 (C) were resolved by 2-D. Sizes of molecular markers are shown to each dimensions.

A.

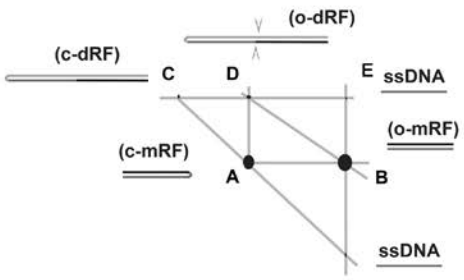
(o-dRF)
(c-dRF)
C
D
E
ssDNA
(o-mRF)
(c-mRF)
A
B
ssDNA

B.

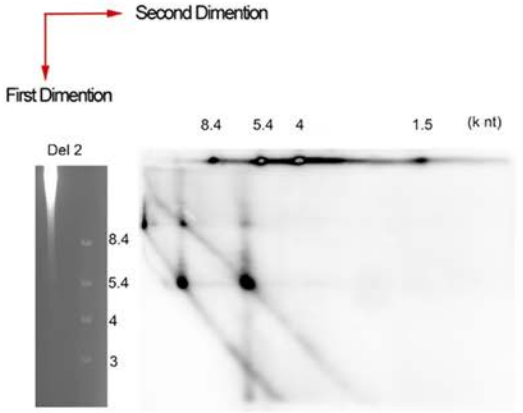
Second Dimention
First Dimention
8.4
5.4
4
1.5
(k nt)
Del 2
8.4
5.4
4
3

C.

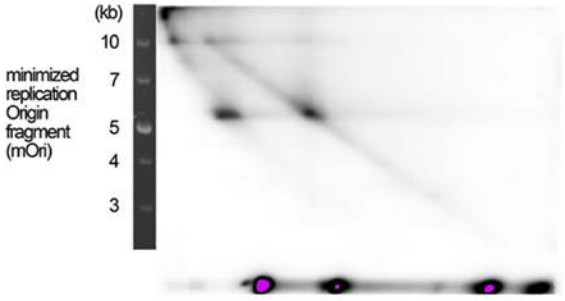
(kb)
10
7
5
4
3
minimized
replication
Origin
fragment
(mOri)

D.

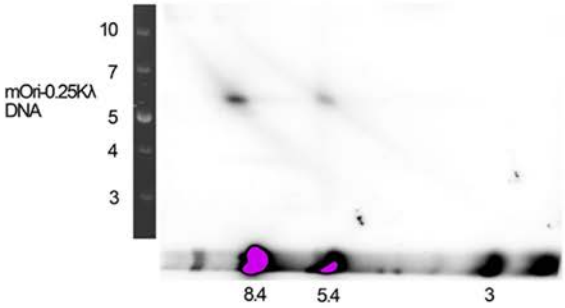
10
7
5
4
3
mOri-0.25Kλ
DNA
8.4
5.4
3

Figure 4-3. Proposed model of hairpin sequence-independent HBoV1 DNA replication.

Similar as the hairpin-transfer model, NS1 binds to a duplex DNA sequence harboring an Ori. With potential cellular factors involved, NS1 binds Ori at the NS1-binding site, and nicks the top strand (5’ to 3’) of the Ori at the nicking site upstream of the NS1-binidng site, and covalently linked to 5’ end of the nicked strand. In the second step, NS1 in combination with cellular replication machinery extend the free 3’ nicked site to end of the genome. In the following, NS1 unwinds the end duplex by the helicase activity meanwhile helping 3’ free-OH folded back to match somewhere within the same molecule. NP1 and other cellular components may directly involve in this step. Further DNA synthesis and strand displacement processes with the cellular DNA replication machinery, and the bottom strand is replaced with newly synthesized DNA. The product is the right-end closed DNA in the length of a monomer replicative form (c-mRF). In the same manner, the NS1 and related factors could refold and base-match the 3’ end to the inboard DNA within itself, initiating the second round of strand displacement. The product will be the left-end closed DNA in length of double replicative form (c-dRF). Intermediates such as RF DNA and dRF DNA could be resolved by terminal resolution (Step 7’, 9), resulting in open RF DNA or dRF DNA (o-mRF, o-dRF). The corresponding structures for the named dots are labeled aside.

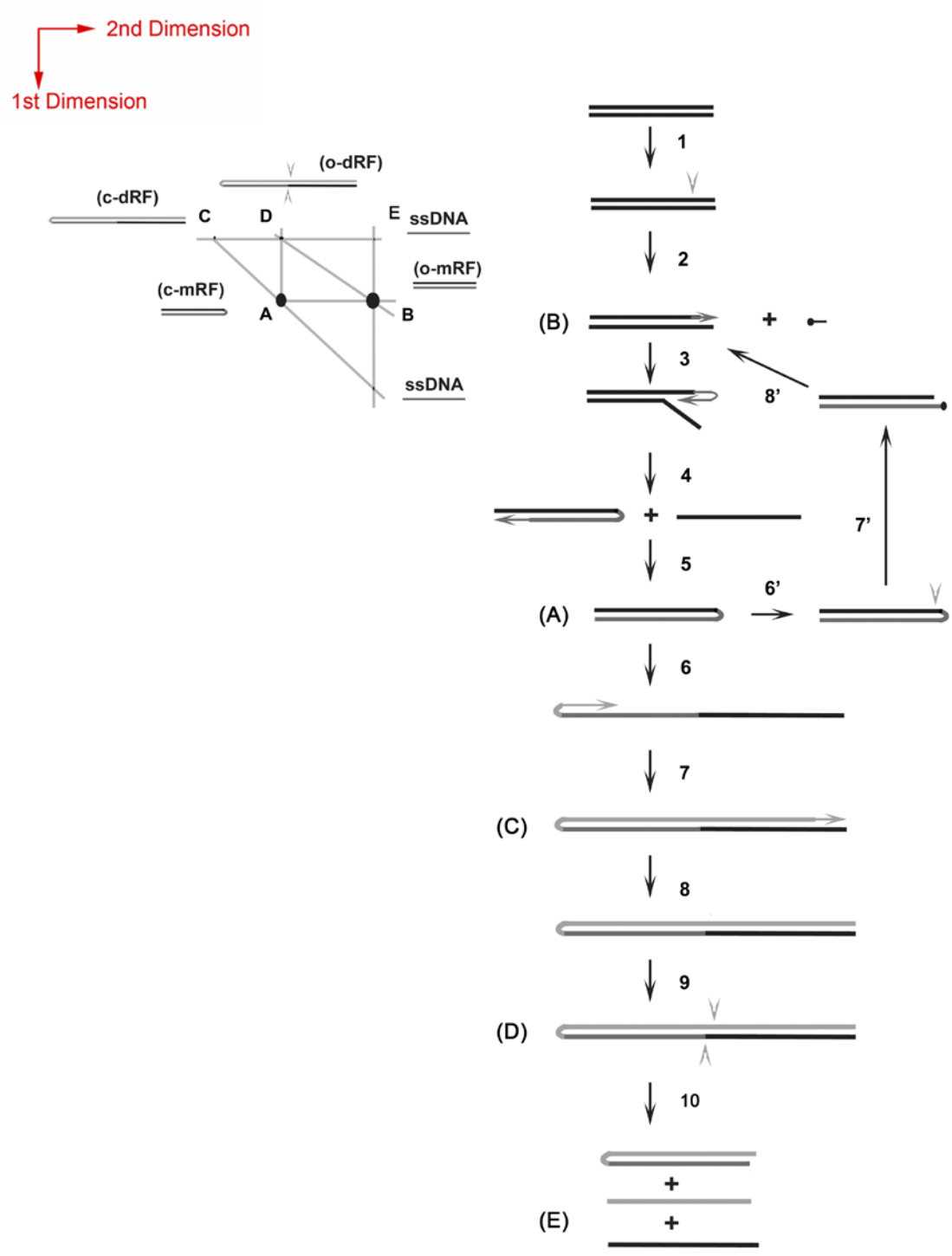
2nd Dimension
1st Dimension
(o-dRF)
(c-dRF)
C
D
E
ssDNA
(o-mRF)
(c-mRF)
A
B
ssDNA
1
2
(B)
3
8'
4
7'
5
6'
(A)
6
7
(C)
8
9
(D)
10
(E)

We hypothesize that NS1 protein is involved in the self-turning-round process with potential help from cellular factors (**Fig. 4-3**, Step 3). Similarly, the replication folk could fold back the 3' end of mRF to further the strand-displacement to produce dRF DNA (**Fig. 4-3**, step 6). Different from the MVM replication model, tetrameric DNA replicative form (tRF DNA) was not obviously detected during HBoV1 DNA replication (**Fig. 4-3**, step 9), suggesting that viral ssDNA genome could be directly resolved from dRF DNA.

2-D gel electrophoresis analysis of DNA replication of full-length duplex HBoV1 DNA and during virus infection.

To further look into the replication of the viral DNA that has hairpin sutures, we resolved the replication intermediates from pIHBoV1-transfected HEK293 cells by 2-D gel electrophoresis (**Fig. 4-4A**). We observed that, besides the four dots accumulated in the ΔREH2-transfected sample, 3 additional dots appeared around Dot A (c-mRF) and two additional dots around Dot C (c-dRF) (**Fig. 4-4A**). Comparing with ΔREH2, pIHBoV1 has the LEH sequence. Those new dots may reflect the replicative intermediates from resolution of the Ori at the LEH. Moreover, we resolved the replicative intermediates during HBoV1 infection of HAE cells. Surprisingly, the replication pattern of virus-infection of HAE cells didn't reveal apparent accumulations of dRF DNAs (**Fig. 4-4, B**). Similarly to the transfection with duplex HBoV1 genome and its mutants, HBoV1 infection accumulated largely the c-mRF (Dot A) and o-mRF (Dot B) intermediates, except for a dominant accumulation of ssDNA. The shortage of dRF and accumulation of ssDNA strongly suggests that either in transfection of the duplex HBoV1 genome or during virus infection, dRF DNA is generating rapidly and therefore becomes a transient step that is a template to generate ssDNA genome, or the (junction) resolution process from RF DNA to ssDNA is highly efficient.

Figure 4-4. Analysis of replication of the full-length HBoV1 duplex genome and of HBoV1 infection using 2-D gel electrophoresis.

(A) 2-D gel analysis of transfection of HBoV1 infectious clone. pIHBoV1 was linearized and transfected into HEK293 cells. Hirt DNA extraction and 2-D gel analysis were performed as mentioned above. **(B) 2-D gel analysis of HAE cells infected by HBoV1 virus.** Well differentiated HAE cells cultured on air-liquid interface were infected with HBoV1 in a MOI of 10. Hirt DNA was extracted at 14 days post-infection and was subjected to 2-D gel electrophoresis analysis.

A.

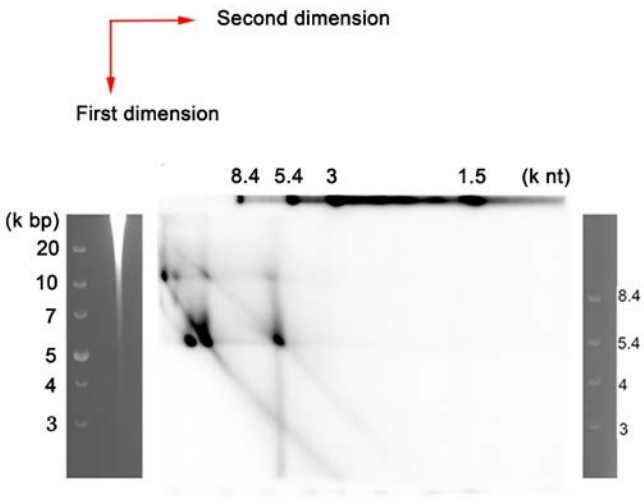

pIHBoV1 transfection/HEK293

B.

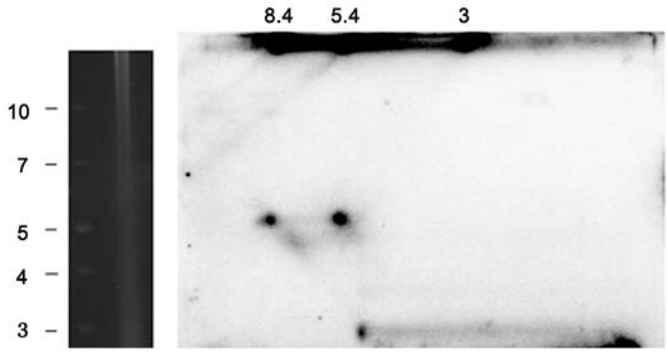

HBoV1 infection/HAE-ALI

Discussion

The replication mechanism of autonomous parvovirus has been mainly studied in MVM. It is not clear whether other heterotelomeric parvoviruses take a similar strategy for replication. With the discovery of HBoV1 and many more other parvoviruses that are distinct from protoparvoviruses in hairpin sequence and structure (18,69,77). We believe that it is significant to understand how these viruses replicate, especially for these ones that cause diseases in humans, e.g., parvovirus B19 (B19V) and HBoV1.

Previously, we observed a mutant B19V infectious clone, which has large deletions on ITRs and was excluded of the hairpin sequence, replicated in both HEK293 cells and B19V-permisive cells, UT7/Epo-S1 cells (63). In the previous study of the identification of the HBoV1 OriR, we defined the OriR to be a 46-nt sequence on the REH (134). In this study, we prove that HBoV1 DNAs only containing the OriR replicate in HEK 293 cells by turning round itself at end of the OriR. Further analysis of the replicative intermediates in transfection of duplex HBoV1 genome and HBoV1 infection reveals that the monomer replicative form DNA is the dominant replicative intermediates of HBoV1 DNA replication. Thus, our study highlights a new model of autonomous parvovirus DNA replication in that NS1 plays a more important role in directing hairpin-switch and strand-displacement than the hairpin structure *per se*. HBoV1 may use a unique mechanism to carry out junction resolution that results in the production of ssDNA genome, awaiting further investigation.

Chapter IV:

Conclusions

The studies presented in this thesis for my PhD degree are composed of three parts. For the first part, we proved by different approaches that the transcription and expression profile of HBoV1 is much more complex than its sibling viruses in the genus *Bocaparvovirus*, especially, during infection. In this study, not only the expression of NS2, NS3, NS4 and NS1-70 was confirmed but also NS2 or NS3 related proteins were largely expressed during infection. As the HBoV1 is the only reported parvovirus that infects well-differentiated/non-proliferating cells, those novel proteins may help HBoV1 to replicate in this unique cell type. For the second part, we disclosed many details underlying the basic HBoV1 DNA replication mechanism. Thus, this study facilitates the understanding of HBoV pathogenesis and further development of antiviral strategies to combat HBoV1-associated diseases. For the third part, we promoted a new bocavirus replication model, which may also fit the replication mechanism of parvoviruses in other genera. These following points are derived from these studies.

Functions of HBoV1 small NS proteins. Firstly, it is clear that NS2 protein is significant, as knocking out NS2 prevented airway epithelial cells from cilia loss and tight junction disruption caused by HBoV1 infection. Secondly, NS2-4 ORFs locate wholly within the ORF of NS1, and are expressed in redundant forms, like the NS2 or NS3-related proteins (**Fig. 2-8C**). The virus replication and production is more disrupted if all NS-related proteins are knocked out. Last but not least, the cultured airway epithelial cells do not fully reflect the immune cellular networking in human airways. An HBoV1 infection animal model is needed for further study on the virus and its host interaction.

HBoV1 pre-mRNA processing: Importantly, alignment of all 4 HBoV sequences showed that all splicing sites are reserved, including the newly confirmed D1’ and A1’ sites (**Fig. 1-2**). Moreover, the new RNA splicing donor site in minute virus of canines (MVC) was identified and MVC NS2 expression was confirmed. In bovine parvovirus, there was also viral mRNAs

detected on Northern blot but without known origin (119). From an evolutionary perspective, those splicing sites may be conserved in bocaviruses. As HBoV is a new virus and evolved quite recently, It is also possible that those small NS proteins were highly expressed by the virus in adapting to the host (non-dividing cells) (78).

Function of viral non-coding sequences: Alignment of the REH among HBoV1, BPV and MVC showed several conserved sequences, suggesting these sequences may bind the same cellular factors that facilitate viral DNA replication. In addition, the (pA)d signal of both BPV and MVC locates within the REH, whereas HBoV1 has it (pA) signal located in the VP1-coding sequence. Therefore, HBoV1 leaves a large space downstream of the REH, referred as 3' NCR. Together with the evidence that HBoV1 NS1 does not specifically bind OriR, it is suggested that viruses from the same genus are evolving quite uniquely, in order to adapt to their residing host, proliferating vs. non-proliferating (differentiated) cells.

Notably, previous studies speculated the NS1 could only specifically bind to the replication as in dimer or oligomer forms (116,169). We essentially followed this protocol but still failed to detect any specific HBoV1 NS1-OriR binding (Figure or data not shown). Considering the importance of the 3' NCR in HBoV1 DNA replication, it is possible that the 3' NCR may function in the recognition of the NS1 with the OriR.

Hairpin-independent DNA replication: Similar to the observation with B19 replication, we proved that HBoV1 replicates independent on the hairpin structure at the REH in our study. Further results showed that even mature virions were produced from a pIHBoV1-based clone that has more than half of the REH truncated, although at a titer of 1-2 log decrease, compared with the wild type counterpart.

The functions of NP1, small NS proteins and 3' NCR in HBoV1 DNA replication need further investigation, and much information will be revealed on HBoV1 NS1 binding, NP1 involvement, hairpin-independent DNA replication in the future.

Reference List

1. **ABINANTI FR and WARFIELD MS**. 1961. Recovery of a hemadsorbing virus (HADEN) from the gastrointestinal tract of calves. Virology **14**:288-289.

2. **Allander, T., T. Jartti, S. Gupta, H. G. Niesters, P. Lehtinen, R. Osterback, T. Vuorinen, M. Waris, A. Bjerkner, A. Tiveljung-Lindell, B. G. van den Hoogen, T. Hyypiä, and O. Ruuskanen**. 2007. Human bocavirus and acute wheezing in children. Clin.Infect.Dis. **44**:904-910.

3. **Allander, T., M. T. Tammi, M. Eriksson, A. Bjerkner, A. Tiveljung-Lindell, and B. Andersson**. 2005. Cloning of a human parvovirus by molecular screening of respiratory tract samples. Proc.Natl.Acad.Sci.U.S.A **102**:12891-12896.

4. **Arnold, J. C., K. K. Singh, S. A. Spector, and M. H. Sawyer**. 2006. Human bocavirus: prevalence and clinical spectrum at a children's hospital. Clin.Infect.Dis. **43**:283-288.

5. **Arthur, J. L., G. D. Higgins, G. P. Davidson, R. C. Givney, and R. M. Ratcliff**. 2009. A novel bocavirus associated with acute gastroenteritis in Australian children. PLoS.Pathog. **5**:e1000391.

6. **Astell, C. R., M. B. Chow, and D. C. Ward**. 1985. Sequence analysis of the termini of virion and replicative forms of minute virus of mice DNA suggests a modified rolling hairpin model for autonomous parvovirus DNA replication. J.Virol. **54**:171-177.

7. **Astell, C. R., M. Thomson, M. B. Chow, and D. C. Ward**. 1983. Structure and replication of minute virus of mice DNA. Cold Spring Harb.Symp.Quant.Biol. **47 Pt 2:751-62.**:751-762.

8. **Bartlett, J. S., R. Wilcher, and R. J. Samulski**. 2000. Infectious entry pathway of adeno-associated virus and adeno-associated virus vectors. J.Virol. **74**:2777-2785.

9. **Bashir, T., J. Rommelaere, and C. Cziepluch**. 2001. In vivo accumulation of cyclin A and cellular replication factors in autonomous parvovirus minute virus of mice-associated replication bodies. J.Virol. **75**:4394-4398.

10. **Berns, K. I.** 1990. Parvovirus replication. Microbiol.Rev. **54**:316-329.

11. **Blessing, K., F. Neske, U. Herre, H. W. Kreth, and B. Weissbrich**. 2009. Prolonged detection of human bocavirus DNA in nasopharyngeal aspirates of children with respiratory tract disease. Pediatr.Infect.Dis.J. **28**:1018-1019.

12. **Brieu, N., G. Guyon, M. Rodiere, M. Segondy, and V. Foulongne**. 2008. Human bocavirus infection in children with respiratory tract disease. Pediatr.Infect.Dis.J. **27**:969-973.

13. **Brodzinski, H. and R. M. Ruddy**. 2009. Review of new and newly discovered respiratory tract viruses in children. Pediatr.Emerg.Care. **25**:352-360.

14. **Calvo, C., M. L. Garcia-Garcia, F. Pozo, O. Carvajal, P. Perez-Brena, and I. Casas**. 2008. Clinical characteristics of human bocavirus infections compared with other respiratory viruses in Spanish children. Pediatr.Infect.Dis.J. **27**:677-680.

15. **Chejanovsky, N. and B. J. Carter**. 1989. Mutagenesis of an AUG codon in the adeno-associated virus rep gene: effects on viral DNA replication. Virology **173**:120-128.

16. **Chen, A. Y., F. Cheng, S. Lou, Y. Luo, Z. Liu, E. Delwart, D. Pintel, and J. Qiu**. 2010. Characterization of the gene expression profile of human bocavirus. Virology. **403**:145-154.

17. **Chen, K. C., B. C. Shull, E. A. Moses, M. Lederman, E. R. Stout, and R. C. Bates**. 1986. Complete nucleotide sequence and genome organization of bovine parvovirus. J.Virol. **60**:1085-1097.

18. **Cheng, W. X., J. S. Li, C. P. Huang, D. P. Yao, N. Liu, S. X. Cui, Y. Jin, and Z. J. Duan**. 2010. Identification and nearly full-length genome characterization of novel porcine bocaviruses. PLoS.ONE. **5**:e13583.

19. **Chiorini, J. A., S. Afione, and R. M. Kotin**. 1999. Adeno-associated virus (AAV) type 5 Rep protein cleaves a unique terminal resolution site compared with other AAV serotypes. J Virol. **73**:4293-4298.

20. **Choi, E. H., H. J. Lee, S. J. Kim, B. W. Eun, N. H. Kim, J. A. Lee, J. H. Lee, E. K. Song, S. H. Kim, J. Y. Park, and J. Y. Sung**. 2006. The association of newly identified respiratory viruses with lower respiratory tract infections in Korean children, 2000-2005. Clin.Infect.Dis. **43**:585-592.

21. **Christensen, A., H. Døllner, L. H. Shanke, S. Krokstad, N. Moe, and S. A. Nordbø**. 2013. Detection of spliced mRNA from human bocavirus 1 in clinical samples from children with respiratory tract infections. Emerg.Infect.Dis. **19**:574-580.

22. **Christensen, A., S. A. Nordbo, S. Krokstad, A. G. Rognlien, and H. Dollner**. 2008. Human bocavirus commonly involved in multiple viral airway infections. J Clin.Virol. **41**:34-37.

23. **Christensen, A., S. A. Nordbø, S. Krokstad, A. G. Rognlien, and H. Døllner**. 2010. Human bocavirus in children: mono-detection, high viral load and viraemia are associated with respiratory tract infection. J.Clin.Virol. **49**:158-162.

24. **Christensen, J., S. F. Cotmore, and P. Tattersall**. 1995. Minute virus of mice transcriptional activator protein NS1 binds directly to the transactivation region of the viral P38 promoter in a strictly ATP-dependent manner. J.Virol. **69**:5422-5430.

25. **Christensen, J., S. F. Cotmore, and P. Tattersall**. 1997. A novel cellular site-specific DNA-binding protein cooperates with the viral NS1 polypeptide to initiate parvovirus DNA replication. J.Virol. **71**:1405-1416.

26. **Christensen, J., S. F. Cotmore, and P. Tattersall**. 1997. Parvovirus initiation factor PIF: a novel human DNA-binding factor which coordinately recognizes two ACGT motifs. J.Virol. **71**:5733-5741.

27. **Cohen, S., A. K. Marr, P. Garcin, and N. Pante**. 2011. Nuclear envelope disruption involving host caspases plays a role in the parvovirus replication cycle. J.Virol. **85**:4863-4874. doi:JVI.01999-10 [pii];10.1128/JVI.01999-10 [doi].

28. **Cotmore, S. F., M. Agbandje-McKenna, J. A. Chiorini, D. V. Mukha, D. J. Pintel, J. Qiu, M. Söderlund-Venermo, P. Tattersall, P. Tijssen, D. Gatherer, and A. J. Davison**. 2014. The family Parvoviridae. Arch.Virol. **159**:1239-1247.

29. **Cotmore, S. F., J. Christensen, J. P. Nuesch, and P. Tattersall**. 1995. The NS1 polypeptide of the murine parvovirus minute virus of mice binds to DNA sequences containing the motif [ACCA]2-3. J.Virol. **69**:1652-1660.

30. **Cotmore, S. F., J. Christensen, and P. Tattersall**. 2000. Two widely spaced initiator binding sites create an HMG1-dependent parvovirus rolling-hairpin replication origin. J.Virol. **74**:1332-1341.

31. **Cotmore, S. F., R. L. Gottlieb, and P. Tattersall**. 2007. Replication initiator protein NS1 of the parvovirus minute virus of mice binds to modular divergent sites distributed throughout duplex viral DNA. J.Virol. **81**:13015-13027.

32. **Cotmore, S. F. and P. Tattersall**. 1989. A genome-linked copy of the NS-1 polypeptide is located on the outside of infectious parvovirus particles. J.Virol. **63**:3902-3911.

33. **Cotmore, S. F. and P. Tattersall**. 1994. An asymmetric nucleotide in the parvoviral 3' hairpin directs segregation of a single active origin of DNA replication. EMBO J. **13**:4145-4152.

34. **Cotmore, S. F. and P. Tattersall**. 1998. High-mobility group 1/2 proteins are essential for initiating rolling-circle-type DNA replication at a parvovirus hairpin origin. J.Virol. **72**:8477-8484.

35. **Cotmore, S. F. and P. Tattersall**. 2005. A rolling-haipin strategy: basic mechanisms of DNA replication in the parvoviruses, p. 171-181. *In*: J. Kerr, S. F. Cotmore, M. E. Bloom, R. M. Linden, and C. R. Parrish (eds.), Parvoviruses. Hoddler Arond, London.

36. **Cotmore, S. F. and P. Tattersall**. 2005. Structure and Organization of the Viral Genome, p. 73-94. *In*: J. Kerr, S. F. Cotmore, M. E. Bloom, R. M. Linden, and C. R. Parrish (eds.), Parvoviruses. Hodder Arnold, London.

37. **Cotmore, S. F. and P. Tattersall**. 2014. Parvoviruses: Small Does Not Mean Simple. Annu.Rev.Virol **1**:517-537.

38. **Cziepluch, C., S. Lampel, A. Grewenig, C. Grund, P. Lichter, and J. Rommelaere**. 2000. H-1 parvovirus-associated replication bodies: a distinct virus-induced nuclear structure. J.Virol. **74**:4807-4815.

39. **Del Rosal, T., M. L. Garcia-Garcia, C. Calvo, F. Gozalo, F. Pozo, and I. Casas**. 2015. Recurrent wheezing and asthma after bocavirus bronchiolitis. Allergol.Immunopathol.(Madr.). **pii: S0301-0546(15)00126-3**:doi: 10.1016/j.aller.2015.07.004. [Epub ahead of print].

40. **Deng, X., Y. Li, and J. Qiu**. 2014. Human bocavirus 1 infects commercially available primary human airway epithelium cultures productively. J.Virol Methods. **195**:112-119.

41. **Deng, X., Z. Yan, F. Cheng, J. F. Engelhardt, and J. Qiu**. 2016. Replication of an Autonomous Human Parvovirus in Non-dividing Human Airway Epithelium Is Facilitated through the DNA Damage and Repair Pathways. PLoS.Pathog. **12**:e1005399.

42. **Deng, X., Z. Yan, Y. Luo, J. Xu, Y. Cheng, Y. Li, J. Engelhardt, and J. Qiu**. 2013. In vitro modeling of human bocavirus 1 infection of polarized primary human airway epithelia. J.Virol. **87**:4097-4102.

43. **Deng, Y., X. Gu, X. Zhao, J. Luo, Z. Luo, L. Wang, Z. Fu, X. Yang, and E. Liu**. 2012. High viral load of human bocavirus correlates with duration of wheezing in children with severe lower respiratory tract infection. PLoS.ONE. **7**:e34353.

44. **Dignam, J. D., R. M. Lebovitz, and R. G. Roeder**. 1983. Accurate transcription initiation by RNA polymerase II in a soluble extract from isolated mammalian nuclei. Nucleic Acids Res. **11**:1475-1489.

45. **Dijkman, R., S. M. Koekkoek, R. Molenkamp, O. Schildgen, and L. van der Hoek**. 2009. Human bocavirus can be cultured in differentiated human airway epithelial cells. J.Virol. **83**:7739-7748.

46. **Ding, C., M. Urabe, M. Bergoin, and R. M. Kotin**. 2002. Biochemical characterization of Junonia coenia densovirus nonstructural protein NS-1. J Virol. **76**:338-345.

47. **Ding, W., L. Zhang, Z. Yan, and J. F. Engelhardt**. 2005. Intracellular trafficking of adeno-associated viral vectors. Gene Ther. **12**:873-880.

48. **do Amaral de, L. C., S. L. Amantea, D. A. Pilger, and V. Cantarelli**. 2013. Clinical and epidemiologic profile of lower respiratory tract infections associated with human bocavirus. Pediatr.Pulmonol. **48**:1112-1118.

49. **Don, M., M. Söderlund-Venermo, K. Hedman, O. Ruuskanen, T. Allander, and M. Korppi**. 2011. Don't forget serum in the diagnosis of human bocavirus infection. J.Infect.Dis. **203**:1031-1032.

50. **Don, M., M. Söderlund-Venermo, F. Valent, A. Lahtinen, L. Hedman, M. Canciani, K. Hedman, and M. Korppi**. 2010. Serologically verified human bocavirus pneumonia in children. Pediatr.Pulmonol. **45**:120-126.

51. **Dubielzig, R., J. A. King, S. Weger, A. Kern, and J. A. Kleinschmidt**. 1999. Adeno-associated virus type 2 protein interactions: formation of pre-encapsidation complexes. J.Virol. **73**:8989-8998.

52. **Edner, N., P. Castillo-Rodas, L. Falk, K. Hedman, M. Soderlund-Venermo, and T. Allander**. 2011. Life-threatening respiratory tract disease with human bocavirus-1 infection in a four-year-old child. J.Clin.Microbiol. **50**:531-532.

53. **Fasina, O. O., Y. Dong, and D. J. Pintel**. 2015. NP1 Protein of the Bocaparvovirus Minute Virus of Canines Controls Access to the Viral Capsid Genes via Its Role in RNA Processing. J.Virol. **90**:1718-1728.

54. **Fauquet, C. M., M. A. Mayo, U. Desselberger, and L. A. Ball**. 2005. Virus Taxonomy: VIIIth report of the International Committee on Taxonomy of Viruses. Academic Press.

55. **Fediere, G., Y. Li, Z. Zadori, J. Szelei, and P. Tijssen**. 2002. Genome organization of Casphalia extranea densovirus, a new iteravirus. Virology **292**:299-308. doi:10.1006/viro.2001.1257 [doi];S0042682201912577 [pii].

56. **Francois, A., M. Guilbaud, R. Awedikian, G. Chadeuf, P. Moullier, and A. Salvetti**. 2005. The cellular TATA binding protein is required for rep-dependent replication of a minimal adeno-associated virus type 2 p5 element. J Virol. **79**:11082-11094.

57. **Friedman, K. L. and B. J. Brewer**. 1995. Analysis of replication intermediates by two-dimensional agarose gel electrophoresis. Methods Enzymol. **262**:613-627. doi:0076-6879(95)62048-6 [pii].

58. **Fry, A. M., X. Lu, M. Chittaganpitch, T. Peret, J. Fischer, S. F. Dowell, L. J. Anderson, D. Erdman, and S. J. Olsen**. 2007. Human bocavirus: a novel parvovirus epidemiologically associated with pneumonia requiring hospitalization in Thailand. J.Infect.Dis. **195**:1038-1045.

59. **Garcia-Garcia, M. L., C. Calvo, A. Falcon, F. Pozo, P. Perez-Brena, J. M. De Cea, and I. Casas**. 2010. Role of emerging respiratory viruses in children with severe acute wheezing. Pediatr.Pulmonol. **45**:585-591.

60. **gbandje-McKenna, M., A. L. Llamas-Saiz, F. Wang, P. Tattersall, and M. G. Rossmann**. 1998. Functional implications of the structure of the murine parvovirus, minute virus of mice. Structure. **6**:1369-1381.

61. **Gendrel, D., R. Guedj, C. Pons-Catalano, A. Emirian, J. Raymond, F. Rozenberg, and P. Lebon**. 2007. Human bocavirus in children with acute asthma. Clin.Infect.Dis. **45**:404-405.

62. **Goldman, M. J., P. S. Lee, J. S. Yang, and J. M. Wilson**. 1997. Lentiviral vectors for gene therapy of cystic fibrosis. Hum.Gene Ther. **8**:2261-2268.

63. **Guan, W., S. Wong, N. Zhi, and J. Qiu**. 2009. The genome of human parvovirus B19 virus can replicate in non-permissive cells with the help of adenovirus genes and produces infectious virus. J.Virol. **83**:9541-9553.

64. **Gurda, B. L., K. N. Parent, H. Bladek, R. S. Sinkovits, M. A. DiMattia, C. Rence, A. Castro, R. McKenna, N. Olson, K. Brown, T. S. Baker, and M. Agbandje-McKenna**. 2010. Human bocavirus capsid structure: insights into the structural repertoire of the parvoviridae. J.Virol. **84**:5880-5889.

65. **Hendrie, P. C., R. K. Hirata, and D. W. Russell**. 2003. Chromosomal integration and homologous gene targeting by replication-incompetent vectors based on the autonomous parvovirus minute virus of mice. J Virol. **77**:13136-13145.

66. **Hickman, A. B., D. R. Ronning, R. M. Kotin, and F. Dyda**. 2002. Structural unity among viral origin binding proteins: crystal structure of the nuclease domain of adeno-associated virus Rep. Mol.Cell. **10**:327-337.

67. **Hickman, A. B., D. R. Ronning, Z. N. Perez, R. M. Kotin, and F. Dyda**. 2004. The nuclease domain of adeno-associated virus rep coordinates replication initiation using two distinct DNA recognition interfaces. Mol.Cell. **13**:403-414.

68. **Hoque, M., K. Ishizu, A. Matsumoto, S. I. Han, F. Arisaka, M. Takayama, K. Suzuki, K. Kato, T. Kanda, H. Watanabe, and H. Handa**. 1999. Nuclear transport of the major capsid protein is essential for adeno-associated virus capsid formation. J.Virol. **73**:7912-7915.

69. **Huang, Q., X. Deng, Z. Yan, F. Cheng, Y. Luo, W. Shen, D. C. Lei-Butters, A. Y. Chen, Y. Li, L. Tang, M. Söderlund-Venermo, J. F. Engelhardt, and J. Qiu**.

2012. Establishment of a reverse genetics system for studying human bocavirus in human airway epithelia. PLoS.Pathog. **8**:e1002899.

70. **Huang, Q., Y. Luo, F. Cheng, S. M. Best, M. E. Bloom, and J. Qiu**. 2014. Molecular characterization of the small nonstructural proteins of parvovirus Aleutian mink disease virus (AMDV) during infection. Virology. **452-453**:23-31.

71. **Ihalainen, T. O., E. A. Niskanen, J. Jylhava, T. Turpeinen, J. Rinne, J. Timonen, and M. Vihinen-Ranta**. 2007. Dynamics and interactions of parvoviral NS1 protein in the nucleus. Cell Microbiol. **9**:1946-1959.

72. **James, J. A., C. R. Escalante, M. Yoon-Robarts, T. A. Edwards, R. M. Linden, and A. K. Aggarwal**. 2003. Crystal structure of the SF3 helicase from adeno-associated virus type 2. Structure. **11**:1025-1035.

73. **Jartti, T., K. Hedman, L. Jartti, O. Ruuskanen, T. Allander, and M. Söderlund-Venermo**. 2011. Human bocavirus-the first 5 years. Rev.Med.Virol. **22**:46-64.

74. **Kahn, J.** 2008. Human bocavirus: clinical significance and implications. Curr.Opin.Pediatr. **20**:62-66.

75. **Kailasan, S., S. Halder, B. Gurda, H. Bladek, P. R. Chipman, R. McKenna, K. Brown, and M. Agbandje-McKenna**. 2015. Structure of an enteric pathogen, bovine parvovirus. J.Virol. **89**:2603-2614.

76. **Kantola, K., L. Hedman, T. Allander, T. Jartti, P. Lehtinen, O. Ruuskanen, K. Hedman, and M. Söderlund-Venermo**. 2008. Serodiagnosis of human bocavirus infection. Clin.Infect.Dis. **46**:540-546.

77. **Kapoor, A., N. Mehta, F. Esper, M. Poljsak-Prijatelj, P. L. Quan, N. Qaisar, E. Delwart, and W. I. Lipkin**. 2010. Identification and characterization of a new bocavirus species in gorillas. PLoS.ONE. **5**:e11948.

78. **Kapoor, A., P. Simmonds, E. Slikas, L. Li, L. Bodhidatta, O. Sethabutr, H. Triki, O. Bahri, B. S. Oderinde, M. M. Baba, D. N. Bukbuk, J. Besser, J. Bartkus, and E. Delwart**. 2010. Human bocaviruses are highly diverse, dispersed, recombination prone, and prevalent in enteric infections. J.Infect.Dis. **201**:1633-1643.

79. **Kapoor, A., E. Slikas, P. Simmonds, T. Chieochansin, A. Naeem, S. Shaukat, M. M. Alam, S. Sharif, M. Angez, S. Zaidi, and E. Delwart**. 2009. A newly identified bocavirus species in human stool. J.Infect.Dis. **199**:196-200.

80. **Karalar, L., J. Lindner, S. Schimanski, M. Kertai, H. Segerer, and S. Modrow**. 2010. Prevalence and clinical aspects of human bocavirus infection in children. Clin.Microbiol.Infect. **16**:633-639.

81. **Kaufmann, B., A. A. Simpson, and M. G. Rossmann**. 2004. The structure of human parvovirus B19. Proc.Natl.Acad.Sci.U.S.A. **101**:11628-11633.

82. **Kesebir, D., M. Vazquez, C. Weibel, E. D. Shapiro, D. Ferguson, M. L. Landry, and J. S. Kahn**. 2006. Human bocavirus infection in young children in the United States: molecular epidemiological profile and clinical characteristics of a newly emerging respiratory virus. J.Infect.Dis. **194**:1276-1282.

83. **King, J. A., R. Dubielzig, D. Grimm, and J. A. Kleinschmidt**. 2001. DNA helicase-mediated packaging of adeno-associated virus type 2 genomes into preformed capsids. EMBO J. **20**:3282-3291.

84. **Koonin, E. V.** 1993. A common set of conserved motifs in a vast variety of putative nucleic acid-dependent ATPases including MCM proteins involved in the initiation of eukaryotic DNA replication. Nucleic Acids Res. **21**:2541-2547.

85. **Korner, R. W., M. Soderlund-Venermo, S. van Koningsbruggen-Rietschel, R. Kaiser, M. Malecki, and O. Schildgen**. 2011. Severe human bocavirus infection, Germany. Emerg.Infect.Dis. **17**:2303-2305.

86. **Lau, S. K., P. C. Woo, H. C. Yeung, J. L. Teng, Y. Wu, R. Bai, R. Y. Fan, K. H. Chan, and K. Y. Yuen**. 2012. Identification and characterization of bocaviruses in cats and dogs reveals a novel feline bocavirus and a novel genetic group of canine bocavirus. J.Gen.Virol. **93**:1573-1582. doi:vir.0.042531-0 [pii];10.1099/vir.0.042531-0 [doi].

87. **Lederman, M., S. F. Cotmore, E. R. Stout, and R. C. Bates**. 1987. Detection of bovine parvovirus proteins homologous to the nonstructural NS-1 proteins of other autonomous parvoviruses. J.Virol. **61**:3612-3616.

88. **Legendre, D. and J. Rommelaere**. 1994. Targeting of promoters for trans activation by a carboxy-terminal domain of the NS-1 protein of the parvovirus minute virus of mice. J.Virol. **68**:7974-7985.

89. **Li, L., S. F. Cotmore, and P. Tattersall**. 2013. Parvoviral left-end hairpin ears are essential during infection for establishing a functional intra-nuclear transcription template and for efficient progeny genome encapsidation. J.Virol.

90. **Li, L. and D. J. Pintel**. 2012. Splicing of goose parvovirus pre-mRNA influences cytoplasmic translation of the processed mRNA. Virology. **426**:60-65.

91. **Li, L., T. Shan, C. Wang, C. Cote, J. Kolman, D. Onions, F. M. Gulland, and E. Delwart**. 2011. The fecal viral flora of California sea lions. J.Virol. **85**:9909-9917. doi:JVI.05026-11 [pii];10.1128/JVI.05026-11 [doi].

92. **Li, Q., Z. Zhang, Z. Zheng, X. Ke, H. Luo, Q. Hu, and H. Wang**. 2013. Identification and characterization of complex dual nuclear localization signals in

human bocavirus NP1: identification and characterization of complex dual nuclear localization signals in human bocavirus NP1. J Gen.Virol. **94**:1335-1342.

93. **Li, Y., Z. Zadori, H. Bando, R. Dubuc, G. Fediere, J. Szelei, and P. Tijssen**. 2001. Genome organization of the densovirus from Bombyx mori (BmDNV-1) and enzyme activity of its capsid. J.Gen.Virol. **82**:2821-2825. doi:10.1099/0022-1317-82-11-2821 [doi].

94. **Linskens, M. H. and J. A. Huberman**. 1990. Ambiguities in results obtained with 2D gel replicon mapping techniques. Nucleic Acids Res. **18**:647-652.

95. **Lombardo, E., J. C. Ramirez, M. Agbandje-McKenna, and J. M. Almendral**. 2000. A beta-stranded motif drives capsid protein oligomers of the parvovirus minute virus of mice into the nucleus for viral assembly. J.Virol. **74**:3804-3814.

96. **Longtin, J., M. Bastien, R. Gilca, E. Leblanc, G. de Serres, M. G. Bergeron, and G. Boivin**. 2008. Human bocavirus infections in hospitalized children and adults. Emerg.Infect.Dis. **14**:217-221.

97. **Lorson, C., L. R. Burger, M. Mouw, and D. J. Pintel**. 1996. Efficient transactivation of the minute virus of mice P38 promoter requires upstream binding of NS1. J.Virol. **70**:834-842.

98. **Lu, X., M. Chittaganpitch, S. J. Olsen, I. M. Mackay, T. P. Sloots, A. M. Fry, and D. D. Erdman**. 2006. Real-time PCR assays for detection of bocavirus in human specimens. J Clin.Microbiol. **44**:3231-3235.

99. **Luo, Y., X. Deng, F. Cheng, Y. Li, and J. Qiu**. 2013. SMC1-mediated intra-S phase arrest facilitates Bocavirus DNA replication. J.Virol. **87**:4017-4032.

100. **Luo, Y., S. Lou, X. Deng, Z. Liu, Y. Li, S. Kleiboeker, and J. Qiu**. 2011. Parvovirus B19 infection of human primary erythroid progenitor cells triggers ATR-Chk1 signaling, which promotes B19 virus replication. J.Virol. **85**:8046-8055.

101. **Maiti, R., G. H. Van Domselaar, H. Zhang, and D. S. Wishart**. 2004. SuperPose: a simple server for sophisticated structural superposition. Nucleic Acids Res. **32**:W590-W594.

102. **Manning, A., V. Russell, K. Eastick, G. H. Leadbetter, N. Hallam, K. Templeton, and P. Simmonds**. 2006. Epidemiological profile and clinical associations of human bocavirus and other human parvoviruses. J.Infect.Dis. **194**:1283-1290.

103. **Martin, E. T., M. P. Fairchok, J. Kuypers, A. Magaret, D. M. Zerr, A. Wald, and J. A. Englund**. 2010. Frequent and prolonged shedding of bocavirus in young children attending daycare. J.Infect.Dis. **201**:1625-1632.

104. **Martin, E. T., J. Kuypers, J. P. McRoberts, J. A. Englund, and D. M. Zerr**. 2015. Human Bocavirus-1 Primary Infection and Shedding in Infants. J.Infect.Dis. **212**:516-524.

105. **Meriluoto, M., L. Hedman, L. Tanner, V. Simell, M. Mäkinen, S. Simell, J. Mykkänen, J. Korpelainen, O. Ruuskanen, J. Ilonen, M. Knip, O. Simell, K. Hedman, and M. Söderlund-Venermo**. 2012. Association of Human Bocavirus 1 Infection with Respiratory Disease in Childhood Follow-up Study, Finland. Emerg.Infect.Dis. **18**:264-271.

106. **Mihaylov, I. S., S. F. Cotmore, and P. Tattersall**. 2014. Complementation for an essential ancillary non-structural protein function across parvovirus genera. Virology. **468-470**:226-237.

107. **Moesker, F. M., J. J. van Kampen, A. A. van der Eijk, A. M. van Rossum, H. M. de, M. Schutten, S. L. Smits, R. Bodewes, A. D. Osterhaus, and P. L. Fraaij**. 2015. Human bocavirus infection as a cause of severe acute respiratory tract infection in children. Clin.Microbiol Infect. **21**:964-968.

108. **Monteny, M., H. G. Niesters, H. A. Moll, and M. Y. Berger**. 2007. Human bocavirus in febrile children, The Netherlands. Emerg.Infect.Dis. **13**:180-182.

109. **Moriyama, Y., H. Hamada, M. Okada, N. Tsuchiya, H. Maru, Y. Shirato, Y. Maeda, Y. Hirose, M. Yoshida, Y. Omura, T. Honda, A. Muto, K. Hayashi, and M. Terai**. 2010. Distinctive clinical features of human bocavirus in children younger than 2 years. Eur.J Pediatr. **169**:1087-1092.

110. **Naeger, L. K., J. Cater, and D. J. Pintel**. 1990. The small nonstructural protein (NS2) of the parvovirus minute virus of mice is required for efficient DNA replication and infectious virus production in a cell-type-specific manner. J.Virol. **64**:6166-6175.

111. **Nascimento-Carvalho, C. M., M. R. Cardoso, M. Meriluoto, K. Kemppainen, K. Kantola, O. Ruuskanen, K. Hedman, and M. Söderlund-Venermo**. 2012. Human bocavirus infection diagnosed serologically among children admitted to hospital with community-acquired pneumonia in a tropical region. J.Med.Virol. **84**:253-258.

112. **Nash, K., W. Chen, M. Salganik, and N. Muzyczka**. 2009. Identification of cellular proteins that interact with the adeno-associated virus rep protein. J.Virol. **83**:454-469.

113. **Nawotka, K. A. and J. A. Huberman**. 1988. Two-dimensional gel electrophoretic method for mapping DNA replicons. Mol.Cell Biol. **8**:1408-1413.

114. **Neske, F., K. Blessing, F. Tollmann, J. Schubert, A. Rethwilm, H. W. Kreth, and B. Weissbrich**. 2007. Real-time PCR for diagnosis of human bocavirus infections and phylogenetic analysis. J Clin.Microbiol. **45**:2116-2122.

115. **Nony, P., J. Tessier, G. Chadeuf, P. Ward, A. Giraud, M. Dugast, R. M. Linden, P. Moullier, and A. Salvetti**. 2001. Novel cis-acting replication element in the adeno-associated virus type 2 genome is involved in amplification of integrated rep-cap sequences. J Virol. **75**:9991-9994.

116. **Nuesch, J. P., S. F. Cotmore, and P. Tattersall**. 1995. Sequence motifs in the replicator protein of parvovirus MVM essential for nicking and covalent attachment to the viral origin: identification of the linking tyrosine. Virology. **209**:122-135.

117. **Pozo, F., M. L. Garcia-Garcia, C. Calvo, I. Cuesta, P. Perez-Brena, and I. Casas**. 2007. High incidence of human bocavirus infection in children in Spain. J.Clin.Virol. **40**:224-228.

118. **Qiu, J., F. Cheng, L. R. Burger, and D. Pintel**. 2006. The transcription profile of Aleutian Mink Disease Virus (AMDV) in CRFK cells is generated by alternative processing of pre-mRNAs produced from a single promoter. J.Virol. **80**:654-662.

119. **Qiu, J., F. Cheng, F. B. Johnson, and D. Pintel**. 2007. The transcription profile of the bocavirus bovine parvovirus is unlike those of previously characterized parvoviruses. J.Virol. **81**:12080-12085.

120. **Qiu, J., F. Cheng, Y. Yoto, Z. Zadori, and D. Pintel**. 2005. The expression strategy of goose parvovirus exhibits features of both the Dependovirus and Parvovirus genera. J.Virol. **79**:11035-11044.

121. **Qiu, J., R. Nayak, G. E. Tullis, and D. J. Pintel**. 2002. Characterization of the transcription profile of adeno-associated virus type 5 reveals a number of unique features compared to previously characterized adeno-associated viruses. J.Virol. **76**:12435-12447.

122. **Qiu, J. and D. J. Pintel**. 2002. The adeno-associated virus type 2 Rep protein regulates RNA processing via interaction with the transcription template. Mol.Cell Biol. **22**:3639-3652.

123. **Qiu, J., Y. Yoto, G. E. Tullis, and D. Pintel**. 2006. Parvovirus RNA processing strategies, p. 253-274. *In*: J. R. Kerr, S. F. Cotmore, M. E. Bloom, M. E. Linden, and C. R. Parish (eds.), Parvoviruses. Hodder Arnold, London, UK.

124. **Rezes, S., M. Soderlund-Venermo, M. Roivainen, K. Kemppainen, Z. Szabo, I. Sziklai, and A. Pitkaranta**. 2009. Human bocavirus and rhino-enteroviruses in childhood otitis media with effusion. J Clin.Virol. **46**:234-237.

125. **Ros, C., C. J. Burckhardt, and C. Kempf**. 2002. Cytoplasmic trafficking of minute virus of mice: low-pH requirement, routing to late endosomes, and proteasome interaction. J.Virol. **76**:12634-12645.

126. **Ruiz, Z., A. D'Abramo, Jr., and P. Tattersall**. 2006. Differential roles for the C-terminal hexapeptide domains of NS2 splice variants during MVM infection of murine cells. Virology. **349**:382-395.

127. **Ruohola, A., M. Waris, T. Allander, T. Ziegler, T. Heikkinen, and O. Ruuskanen**. 2009. Viral etiology of common cold in children, Finland. Emerg.Infect.Dis. **15**:344-346.

128. **Ryan, J. H., S. Zolotukhin, and N. Muzyczka**. 1996. Sequence requirements for binding of Rep68 to the adeno-associated virus terminal repeats. J Virol. **70**:1542-1553.

129. **Samulski, R. J. and N. Muzyczka**. 2014. AAV-Mediated Gene Therapy for Research and Therapeutic Purposes. Annu.Rev.Virol. **1**:427-451.

130. **Sanlioglu, S., P. K. Benson, J. Yang, E. M. Atkinson, T. Reynolds, and J. F. Engelhardt**. 2000. Endocytosis and nuclear trafficking of adeno-associated virus type 2 are controlled by rac1 and phosphatidylinositol-3 kinase activation. J.Virol. **74**:9184-9196.

131. **Schildgen, O.** 2010. Human bocavirus: increasing evidence for virulence. Pediatr.Pulmonol. **45**:118-119.

132. **Schildgen, O., A. Muller, T. Allander, I. M. Mackay, S. Volz, B. Kupfer, and A. Simon**. 2008. Human bocavirus: passenger or pathogen in acute respiratory tract infections? Clin.Microbiol.Rev. **21**:291-304.

133. **Schwartz, D., B. Green, L. E. Carmichael, and C. R. Parrish**. 2002. The canine minute virus (minute virus of canines) is a distinct parvovirus that is most similar to bovine parvovirus. Virology. **302**:219-223.

134. **Shen, W., X. Deng, W. Zou, F. Cheng, J. F. Engelhardt, Z. Yan, and J. Qiu**. 2015. Identification and Functional Analysis of Novel Non-structural Proteins of Human Bocavirus 1. J.Virol. **89**:10097-10109.

135. **Smith, D. H., P. Ward, and R. M. Linden**. 1999. Comparative characterization of rep proteins from the helper-dependent adeno-associated virus type 2 and the autonomous goose parvovirus. J Virol. **73**:2930-2937.

136. **Smith, R. H. and R. M. Kotin**. 1998. The Rep52 gene product of adeno-associated virus is a DNA helicase with 3'-to-5' polarity. J.Virol. **72**:4874-4881.

137. **Smith, R. H., A. J. Spano, and R. M. Kotin**. 1997. The Rep78 gene product of adeno-associated virus (AAV) self-associates to form a hexameric complex in the presence of AAV ori sequences. J.Virol. **71**:4461-4471.

138. **Soderberg, O., M. Gullberg, M. Jarvius, K. Ridderstrale, K. J. Leuchowius, J. Jarvius, K. Wester, P. Hydbring, F. Bahram, L. G. Larsson, and U.**

Landegren. 2006. Direct observation of individual endogenous protein complexes in situ by proximity ligation. Nat.Methods. **3**:995-1000.

139. **Söderlund-Venermo, M., A. Lahtinen, T. Jartti, L. Hedman, K. Kemppainen, P. Lehtinen, T. Allander, O. Ruuskanen, and K. Hedman**. 2009. Clinical assessment and improved diagnosis of bocavirus-induced wheezing in children, Finland. Emerg.Infect.Dis. **15**:1423-1430.

140. **Sonntag, F., K. Kother, K. Schmidt, M. Weghofer, C. Raupp, K. Nieto, A. Kuck, B. Gerlach, B. Bottcher, O. J. Muller, K. Lux, M. Horer, and J. A. Kleinschmidt**. 2011. The assembly-activating protein promotes capsid assembly of different adeno-associated virus serotypes. J.Virol. **85**:12686-12697.

141. **Sowd, G. A., N. Y. Li, and E. Fanning**. 2013. ATM and ATR activities maintain replication fork integrity during SV40 chromatin replication. PLoS.Pathog. **9**:e1003283.

142. **Stracker, T. H., G. D. Cassell, P. Ward, Y. M. Loo, B. B. van, S. D. Carrington-Lawrence, R. K. Hamatake, P. C. van der Vliet, S. K. Weller, T. Melendy, and M. D. Weitzman**. 2004. The Rep protein of adeno-associated virus type 2 interacts with single-stranded DNA-binding proteins that enhance viral replication. J.Virol. **78**:441-453.

143. **Sukhu, L., O. Fasina, L. Burger, A. Rai, J. Qiu, and D. J. Pintel**. 2013. Characterization of the nonstructural proteins of the bocavirus minute virus of canines. J Virol. **87**:1098-1104.

144. **Sukhu, L., O. Fasina, L. Burger, A. Rai, J. Qiu, and D. J. Pintel**. 2013. Characterization of the nonstructural proteins of the bocavirus minute virus of canines. J Virol. **87**:1098-1104.

145. **Sun, Y., A. Y. Chen, F. Cheng, W. Guan, F. B. Johnson, and J. Qiu**. 2009. Molecular characterization of infectious clones of the minute virus of canines reveals unique features of bocaviruses. J.Virol. **83**:3956-3967.

146. **Tam, P. and C. R. Astell**. 1993. Replication of minute virus of mice minigenomes: novel replication elements required for MVM DNA replication. Virology. **193**:812-824.

147. **Tattersall, P., L. V. Crawford, and A. J. Shatkin**. 1973. Replication of the parvovirus MVM. II. Isolation and characterization of intermediates in the replication of the viral deoxyribonucleic acid. J.Virol. **12**:1446-1456.

148. **Tattersall, P. and D. C. Ward**. 1976. Rolling hairpin model for replication of parvovirus and linear chromosomal DNA. Nature. **263**:106-109.

149. **Terrosi, C., M. Fabbiani, C. Cellesi, and M. G. Cusi**. 2007. Human bocavirus detection in an atopic child affected by pneumonia associated with wheezing. J.Clin.Virol. **40**:43-45.

150. **Tewary, S. K., L. Liang, Z. Lin, A. Lynn, S. F. Cotmore, P. Tattersall, H. Zhao, and L. Tang**. 2015. Structures of minute virus of mice replication initiator protein N-terminal domain: Insights into DNA nicking and origin binding. Virology. **476**:61-71.

151. **Tewary, S. K., H. Zhao, X. Deng, J. Qiu, and L. Tang**. 2014. The human parvovirus B19 non-structural protein 1 N-terminal domain specifically binds to the origin of replication in the viral DNA. Virology. **449**:297-303.

152. **Tewary, S. K., H. Zhao, W. Shen, J. Qiu, and L. Tang**. 2013. Structure of the NS1 protein N-terminal origin-recognition/nickase domain from the emerging human bocavirus. J.Virol. **87**:11487-11494.

153. **Tijssen, P., Y. Li, M. El-Far, J. Szelei, M. Letarte, and Z. Zadori**. 2003. Organization and expression strategy of the ambisense genome of densonucleosis virus of Galleria mellonella. J.Virol. **77**:10357-10365.

154. **Tozer, S. J., S. B. Lambert, D. M. Whiley, S. Bialasiewicz, M. J. Lyon, M. D. Nissen, and T. P. Sloots**. 2009. Detection of human bocavirus in respiratory, fecal, and blood samples by real-time PCR. J.Med.Virol. **81**:488-493.

155. **Tullis, G., R. V. Schoborg, and D. J. Pintel**. 1994. Characterization of the temporal accumulation of minute virus of mice replicative intermediates. J.Gen.Virol. **75**:1633-1646.

156. **Tullis, G. E. and T. Shenk**. 2000. Efficient replication of adeno-associated virus type 2 vectors: a cis-acting element outside of the terminal repeats and a minimal size. J Virol. **74**:11511-11521.

157. **Ursic, T., M. Jevsnik, N. Zigon, U. Krivec, A. B. Beden, M. Praprotnik, and M. Petrovec**. 2012. Human bocavirus and other respiratory viral infections in a 2-year cohort of hospitalized children. J.Med.Virol. **84**:99-108.

158. **Ursic, T., A. Steyer, S. Kopriva, G. Kalan, U. Krivec, and M. Petrovec**. 2011. Human bocavirus as the cause of a life-threatening infection. J.Clin.Microbiol. **49**:1179-1181.

159. **Vihinen-Ranta, M., A. Kalela, P. Makinen, L. Kakkola, V. Marjomaki, and M. Vuento**. 1998. Intracellular route of canine parvovirus entry. J.Virol. **72**:802-806.

160. **von Linstow, M. L., M. Hogh, and B. Høgh**. 2008. Clinical and epidemiologic characteristics of human bocavirus in Danish infants: results from a prospective birth cohort study. Pediatr.Infect.Dis.J. **27**:897-902.

161. **Walters, R. W., M. gbandje-McKenna, V. D. Bowman, T. O. Moninger, N. H. Olson, M. Seiler, J. A. Chiorini, T. S. Baker, and J. Zabner**. 2004. Structure of adeno-associated virus serotype 5. J.Virol. **78**:3361-3371.

162. **Wang, K., W. Wang, H. Yan, P. Ren, J. Zhang, J. Shen, and V. Deubel**. 2010. Correlation between bocavirus infection and humoral response, and co-infection with other respiratory viruses in children with acute respiratory infection. J.Clin.Virol. **47**:148-155.

163. **Wang, X. S. and A. Srivastava**. 1997. A novel terminal resolution-like site in the adeno-associated virus type 2 genome. J Virol. **71**:1140-1146.

164. **Ward, P.** 2006. Replication of adeno-associated virus DNA, p. 189-211. *In*: J. Kerr, Cotmore SF, M. E. Bloom, M. E. Linden, and C. R. Parrish (eds.), The parvoviruses. Hodder Arnold, London.

165. **Weitzman, M. D., S. R. Kyostio, B. J. Carter, and R. A. Owens**. 1996. Interaction of wild-type and mutant adeno-associated virus (AAV) Rep proteins on AAV hairpin DNA. J.Virol. **70**:2440-2448.

166. **Weitzman, M. D., S. R. Kyostio, R. M. Kotin, and R. A. Owens**. 1994. Adeno-associated virus (AAV) Rep proteins mediate complex formation between AAV DNA and its integration site in human DNA. Proc.Natl.Acad.Sci.U.S.A **91**:5808-5812.

167. **Wistuba, A., A. Kern, S. Weger, D. Grimm, and J. A. Kleinschmidt**. 1997. Subcellular compartmentalization of adeno-associated virus type 2 assembly. J.Virol. **71**:1341-1352.

168. **Yan, Z., N. W. Keiser, Y. Song, X. Deng, F. Cheng, J. Qiu, and J. F. Engelhardt**. 2013. A novel chimeric adenoassociated virus 2/human bocavirus 1 parvovirus vector efficiently transduces human airway epithelia. Mol.Ther. **21**:2181-2194.

169. **Young, P. J., K. T. Jensen, L. R. Burger, D. J. Pintel, and C. L. Lorson**. 2002. Minute virus of mice NS1 interacts with the SMN protein, and they colocalize in novel nuclear bodies induced by parvovirus infection. J.Virol. **76**:3892-3904.

170. **Zadori, Z., R. Stefancsik, T. Rauch, and J. Kisary**. 1995. Analysis of the complete nucleotide sequences of goose and muscovy duck parvoviruses indicates common ancestral origin with adeno-associated virus 2. Virology. **212**:562-573.

171. **Zadori, Z., J. Szelei, M. C. Lacoste, Y. Li, S. Gariepy, P. Raymond, M. Allaire, I. R. Nabi, and P. Tijssen**. 2001. A viral phospholipase A2 is required for parvovirus infectivity. Dev.Cell. **1**:291-302.

172. **Zhang, Y.** 2008. I-TASSER server for protein 3D structure prediction. BMC.Bioinformatics. **9:40. doi: 10.1186/1471-2105-9-40.**:40-49.

173. **Zou, W., F. Cheng, W. Shen, J. F. Engelhardt, Z. Yan, and J. Qiu**. 2016. Nonstructural Protein NP1 of Human Bocavirus 1 Plays a Critical Role in the Expression of Viral Capsid Proteins. J.Virol. **90**:4658-4669.